STATIC AND DYNAMIC STUDIES ON FG POROUS SANDWICH STRUCTURES WITH VISCOELASTIC BOUNDARY CONDITIONS IN THERMAL ENVIRONMENT

Thesis
Submitted in partial fulfillment of the requirement for the degree
of

DOCTOR OF PHILOSOPHY
by

RAKESH PATIL
(Reg. No. 177131ME014)

DEPARTMENT OF MECHANICAL ENGINEERING
NATIONAL INSTITUTE OF TECHNOLOGY
KARNATAKA, SURATHKAL, MANGALORE – 575025,
INDIA
MAY 2023

This dissertation is dedicated to my Father and Mother, who instilled in me the virtues of perseverance and commitment and relentlessly encouraged me to strive for excellence.

DECLARATION

I hereby *declare* that the Research Thesis entitled **STATIC AND DYNAMIC STUDIES ON FG POROUS SANDWICH STRUCTURES WITH VISCOELASTIC BOUNDARY CONDITIONS IN THERMAL ENVIRONMENT,** which is being submitted to the ***National Institute of Technology Karnataka, Surathkal*** in partial fulfillment of the requirements for the award of the Degree of ***Doctor of Philosophy*** is a ***bonafide report of the research work carried out by me.*** The material contained in this thesis has not been submitted to any University or Institution for the award of any degree.

Register Number: **177131ME014**
Name of the Research Scholar: **RAKESH PATIL**
Signature of the Research Scholar: R.B.Patil

Department of Mechanical Engineering

Place: NITK, Surathkal

Date: 25/05/2023

CERTIFICATE

This is to *certify* that the Research Thesis entitled **STATIC AND DYNAMIC STUDIES ON FG POROUS SANDWICH STRUCTURES WITH VISCOELASTIC BOUNDARY CONDITIONS IN THERMAL ENVIRONMENT,** submitted by **RAKESH PATIL** (Register Number: 177131ME014) as the record of the research work carried out by him, is *accepted* as the *Research Thesis submission* in partial fulfilment of the requirements for the award of the degree of **Doctor of Philosophy.**

Research Guide

25/05/2023

Dr. Sharnappa Joladarashi
Associate Professor
Department of Mechanical Engineering

25/5/2023

Chairman-DRPC
Department of Mechanical Engineering
National Institute of Technology Karnataka
Surathkal, Mangalore - 575025

ACKNOWLEDGEMENTS

First and foremost, I would like to express my sincere gratitude and profound thanks to my research guide **Dr. Sharnappa Joladarashi**, Associate Professor, Department of Mechanical Engineering, National Institute of Technology Karnataka, Surathkal, for his exemplary guidance and encouragement throughout my research work. His eternal supervision helped me understand the subject better and completion of this thesis. The time I have spent with him will be remembered and cherished all my life.

I would like to express my sincere gratitude and profound thanks to **Dr. Ravikiran Kadoli**, Professor and Head, Department of Mechanical Engineering, National Institute of Technology Karnataka, Surathkal, for guiding me throughout my research journey. He has been an ideal teacher, mentor, and well-wisher for me.

I sincerely thank the RPAC members, Dr. V. Murugan, Department of Civil Engineering, and Dr. P. Jeyaraj, Department of Mechanical Engineering, for providing valuable suggestions and support extended to me on all occasions.

I am immensely grateful for the unending help and support received from my fellow research scholars, Mr. Mukund Patil, Mr. Vasista Ademane, and Mr. Surya Rao, in the course of my research work.

I also would like to thank my co-researchers Mr. Ritwik Sohgaura, Mr. Nirmal Kumar, Mr. Hari Tej, Ms. Snehal Chandurkar, and Mr. Ashwani Kumar, for their support in carrying out my research work. I would like to thank all my lab mates for their encouragement and moral support during the downhearted time in research.

I am grateful to my friends Mr. Mohammed Sohail Bakshi, Mr. Vinayak Kallannavar, Mr. Sachin Hirannaiah, Mr. Antonio Dylan Carvalho, Mr. Purna Chandra Tanti, Mr. Arunkumar D. S., Ms. Aswathy T., Mr. Chetan H. C., Dr. Gangadhar Kanaginahal, and Dr. Satish Kanakannavar for their encouragement and moral support during my research work. The days I spent with them in NITK was unforgettable.

I would like to thank God for giving me the strength, knowledge, ability, and opportunity to understand this research study and to persevere and complete it satisfactorily.

I would like to thank my father, **Basanagouda Patil**, mother, **Daxayani Goudar,** and brother **Prashanth Patil**, for their immense love and support throughout my life. Without them, achieving this goal would not have been possible.

(RAKESH PATIL)

ABSTRACT

The present study investigates the static bending, buckling, and vibration behavior of functionally graded (FG) sandwich beams and plates with a viscoelastic interlayer. Finite element (FE) and analytical methods are used for the formulations. The metal-ceramic gradation of FG stiff layers along the thickness is governed by the rule of mixture and power law index. The kinematics of the sandwich beam stiff layers are based on the Euler-Bernoulli beam theory. The viscoelastic interlayer is assumed to undergo only shear. Lagrange density functions for sandwich beams have been deduced, taking into account the effect of strain energies of the stiff and core layers along with the corresponding translational energies and work done by external forces. Static and dynamic equilibrium equations of sandwich beams are derived using Euler-Lagrange equations.

FE solutions are developed to solve equilibrium equations. The developed FE sandwich beam model is validated with an analytical model. Navier's solution method is used to solve simply supported sandwich beams. Further porosity models and viscoelastic boundary conditions (VBCs) are incorporated into the study; bending, buckling, and vibration studies are carried out. A complex stiffness model is adopted for VBCs. Various types of porosity patterns, such as H, O, V, and X, across the thickness directions are assumed. The effect of porosities and VBCs on transverse deflection, natural frequency (NF), and loss factor (LF) of the FG sandwich beam is investigated. The results convey that VBCs contribution to vibration damping is more predominant when the supports are less stiff (more viscous). In addition, the effect of temperature on buckling and free vibration of FG porous sandwich beams with VBCs is discussed.

The study also addresses the geometric nonlinearity of sandwich beams due to thermal stresses. Accordingly, temperature-dependent material properties are considered for FG stiff layers and viscoelastic interlayers. The study investigates the sandwich beam's critical buckling temperature (CBT), natural frequency, and loss factors in thermal environment.

Further, the proposed sandwich beam model is used to study the vibration and damping behavior of the disc brake pad. In the first case, only the back plate with brake insulator is considered as a sandwich beam.

A comparison study is presented in terms of the free and forced vibration characteristics of different back plate-brake insulator sandwich beams such as Steel-Acrylic-Steel, FGM-Acrylic-Steel, FGM-Acrylic-Aluminium, and Steel-Acrylic-Aluminium. The study reveals that the natural frequency, loss factor, and with regard to dynamic loading, the imaginary part of transverse deflection, axial displacement, stress, and strain of FGM-Acrylic-Steel are higher. As a result, FGM-Acrylic-Steel is a suitable combination for back plate and brake insulator assembly that enhances the overall disc brake system's damping capacity and helps to reduce brake squeal problems associated with the operation of the disc brake system.

In the second case, a complete brake pad (including friction material) is considered as a sandwich plate. Free and forced vibration studies are carried out on the brake pad for simply supported case (SSSS) using an analytical sandwich plate model. A comparative examination is provided among the brake pads with conventional steel and Al-Al_2O_3 FG back plates. The influence of several parameters on fundamental frequency and loss factors is also discussed. In addition, transient and steady-state analysis is carried out for the brake pad subjected to uniformly distributive transverse load (UDL) using the Newmark method. The results and analysis reveal that the brake pad with an Al-Al_2O_3 FG back plate having 0 to 100% Al_2O_3 variation is as stiff as a pad with a steel back plate and withstands the transverse load (brake load) effectively. The replacement of the steel back plate with an Al-Al_2O_3 FG enhances energy dissipation in the brake pad and is more efficient in vibration reduction.

TABLE OF CONTENTS

ACKNOWLEDGEMENTS .... **i**

ABSTRACT .... **iii**

LIST OF TABLES .... **ix**

LIST OF FIGURES .... **xi**

NOMENCLATURE .... **xvii**

LIST OF ABBREVIATIONS .... **xix**

1 INTRODUCTION **1**

- 1.1 FUNCTIONALLY GRADED MATERIALS (FGMs) 1
  - 1.1.1 Applications of Functionally graded materials 1
- 1.2 VISCOELASTIC MATERIALS 2
  - 1.2.1 Creep and stress relaxation 3
  - 1.2.2 Dynamic response of viscoelastic materials 3
- 1.3 POROSITY AND VISCOELASTIC BOUNDARY CONDITIONS 4
- 1.4 ORGANIZATION OF THE DISSERTATION 6

2 LITERATURE REVIEW **9**

- 2.1 INTRODUCTION 9
- 2.2 STATIC BENDING AND VIBRATION STUDIES ON SANDWICH BEAMS AND PLATES 9
- 2.3 BUCKLING AND VIBRATION OF SANDWICH BEAMS AND PLATES IN THERMAL ENVIRONMENT 12
- 2.4 EFFECT OF POROSITY AND VISCOELASTIC BOUNDARY CONDITIONS ON BEAMS AND PLATES 14
- 2.5 BRAKE PAD AND BRAKE INSULATORS OF DISC BRAKE SYSTEM15
- 2.6 MOTIVATION AND RESEARCH GAP 17
- 2.7 OBJECTIVES OF RESEARCH WORK 18

3 METHODOLOGY **19**

- 3.1 INTRODUCTION 19
- 3.2 FE MODEL FOR STATIC AND DYNAMIC STUDIES OF FG SANDWICH BEAM 20
  - 3.2.1 Geometric stiffness matrix 26

3.2.2 Thermal buckling 26
3.2.3 Free and forced vibration 27
3.2.4 Functional gradation of FG Stiff layers 27
3.3 ANALYTICAL MODEL FOR FG SANDWICH BEAM 28
3.3.1 Analytical solution for simply supported sandwich beam 30
3.4 Validation study for sandwich beam models 32
3.4.1 Example-1: Sandwich beam with isotropic stiff layer and viscoelastic core 32
3.4.2 Example-2: Sandwich beam with FG stiff layer and viscoelastic core 34
3.5 Porosity models and viscoelastic boundary conditions 35
3.5.1 Porosity patterns 35
3.5.2 FE formulation for viscoelastic boundary conditions for beam 36
3.5.3 Validation and convergence study of viscoelastic boundary conditions 38
3.6 ANALYTICAL MODEL FOR FG SANDWICH PLATE 41
3.6.1 Static and dynamic equilibrium equations of sandwich plate 42
3.6.2 Analytical solution for the sandwich plate with simple support 45
3.6.3 Validation of analytical sandwich plate model 47
3.7 SUMMARY 49
4 RESULTS AND DISCUSSION 51
4.1 INTRODUCTION 51
4.2 STATIC BENDING AND FREE VIBRATION OF FG SANDWICH BEAM (ROOM TEMPERATURE) 51
4.2.1 Static bending studies 55
4.2.2 Vibration studies 59
4.3 BUCKLING AND FREE VIBRATION OF FG SANDWICH BEAM IN UNDER THERMAL ENVIRONMENT 66
4.3.1 Thermal buckling 66
4.3.2 Free vibration 71
4.4 SUMMARY 76
5 STUDIES ON DISC BRAKE PAD WITH Al-Al_2O_3 FG BACK PLATE AND BRAKE INSULATOR 77
5.1 INTRODUCTION 77
5.2 CASE-1: VIBRATION OF STEEL AND AL-AL_2O_3 FG BACK PLATE WITH BRAKE INSULATOR 79
5.2.1 Free Vibration results 80

5.3 CASE-2: VIBRATION OF COMPLETE BRAKE PAD (STEEL/AL-AL_2O_3 FG BACK PLATE AND FRICTION MATERIAL) WITH BRAKE INSULATOR........86
  5.3.1 Free vibration........87
  5.3.2 Transient response and steady state response........91
5.4 SUMMARY........94

6 SUMMARY AND CONCLUSIONS........95

6.1 SUMMARY........95
6.2 CONCLUSIONS........95
  6.2.1 Studies on FG porous sandwich beam with viscoelastic boundary conditions in thermal environment........96
  6.2.2 Studies on disc brake pad with Al-Al_2O_3 functionally graded back plate and brake insulator of a disc brake system........97
6.3 SCOPE FOR FUTURE STUDIES........99

REFERENCE........101

CURRICULUM VITAE........107

LIST OF PUBLICATIONS BASED ON THESIS........109

LIST OF TABLES

Table 3.1: Material properties and dimensions of example 1. 33

Table 3.2: Natural frequencies of example 1 (rad/sec). 33

Table 3.3: System loss factor values (%) of example 1. 34

Table 3.4: Properties of example 2. 34

Table 3.5: Natural frequency and loss factors of example 2......................................35

Table 3.6: Material properties and dimensions of case 1...38

Table 3.7: Natural frequency of case 1 (rad/sec). 39

Table 3.8: System loss factor values (%) of case 1..39

Table 3.9: Material properties and dimension of case 2 (Bhangale and Ganesan 2006). 40

Table 3.10: Convergence of CBT of the sandwich beam. 40

Table 3.11: Properties of sandwich plate materials of example 1. 48

Table 3.12: Non-dimensional natural frequency of example 1...................................48

Table 3.13: Dimensions and material properties of example 2. 48

Table 3.14: Natural frequency (Hz) of example 2 in different modes of vibration. 49

Table 3.15: Loss factor of example 2 in different modes of vibration. 49

Table 4.1: Temperature coefficients of FG constituents (Reddy and Chin 1998) 53

Table 4.2: Support stiffness values (SSVs) for various boundary conditions of Ti-6Al-4V/ZrO_2 FG sandwich beam 56

Table 4.3: Support stiffness values for various conditions (BCs) of SUS304/Si_3N_4 FG sandwich beam. 68

Table 4.4: CBT for various boundary conditions (β=0.3, p=1, and η_{sp}=0.0). 70

Table 4.5: Natural frequency and loss factor for various boundary conditions at ΔT=10 ^{0}C (β=0.3, p=1, and η_{sp}=0.2). 76

Table 5.1: Material properties and dimensions of sandwich beams. 79

Table 5.2: Rigidity and inertia coefficients of sandwich beams for different material combinations. 81

Table 5.3: Material properties of brake insulator and friction materials. 87

Table 5.4: Stiffness coefficients of brake pad with steel/FGM back plates. 88

Table 5.5 Inertia coefficients of brake pad with steel/FGM back plates. 88

Table 5.6: Damped transverse deflection of FGM-NBR-Steel and Steel-NBR-Steel at different points of time..92

Table 5.7: Percentage damping of transverse deflection in FGM-NBR-Steel and Steel-NBR-Steel in 0.2 sec..92

LIST OF FIGURES

Figure 1.1: FG beam with continuous gradation. 1

Figure 1.2: FG beam with stepwise gradation. 1

Figure 1.3: Transient phenomena: i) Creep and ii) Stress relaxation (Lakes 2009). 3

Figure 1.4: Stress and strain plot of viscoelastic material under dynamic loading (Lakes 2009). 4

Figure 1.5: Turbine and compressor blades with viscoelastic blocking pads: i) Blade disc with pad ii) Schematic diagram of blade (Wang et al. 2018). 5

Figure 1.6: Schematic diagram of fluidlastic damper in helicopter rotor blade (Han et al. 2013). 5

Figure 3.1: Flow chart of project work. 19

Figure 3.2: Two-noded FG Sandwich beam. 21

Figure 3.3: Kinematics of sandwich beam subjected to transverse deflection. 21

Figure 3.4: Functional gradation along the thickness: a) Ceramic volume fraction along the thickness and b) metal and ceramic contents along the thickness of beam. 28

Figure 3.5: Porosity distribution models. 35

Figure 3.6: Two-noded beam element with viscoelastic boundary condition. 36

Figure 3.7: The natural frequency of case 1 (P-R). 39

Figure 3.8: The loss factor of case 1 (P-R). 39

Figure 3.9: CBP of the case 2. 40

Figure 3.10: CBT of the case 2. 40

Figure 3.11: FG Sandwich plate. 41

Figure 3.12: Kinematics of sandwich plate subjected to transverse load. 41

Figure 4.1: Temperature-dependent shear modulus of DYAD 606 core. 52

Figure 4.2: Temperature-dependent loss factor of DYAD 606 core. 52

Figure 4.3: Young's modulus of Ti-6Al-4V/ZrO_2 FG stiff layers with various porosity patterns at β=0.2 (i) p=0.5, ii) p=1 and iii) p=3) 52

Figure 4.4: Density of Ti-6Al-4V/ZrO_2 FG stiff with various porosity patterns at β=0.2 (i) p=0.5, ii) p=1 and iii) p=3) 53

Figure 4.5 Transverse deflection (w_{max}) of sandwich beam under varying support stiffness: i) C-F, ii) C-C (2D). iii) C-C (3D) iv) P-R (p=1, F=10N, β=0.0). 56

Figure 4.6 Transverse deflection (w_{max}) of sandwich beam under varying point loads: i) C-F, ii) C-C. iii) P-R (β=0.0). 57

Figure 4.7: Transverse deflection (w_{max}) of C-C sandwich beam for various porosity distribution models: i) p=0.5, ii) p=1. iii) p=3 (F=10N). 58

Figure 4.8: Transverse deflection of sandwich beam for varying x/l ratio: i) C-F, ii) C-C. iii) P-R (p=1, F=10N, β=0.2). 59

Figure 4.9 Natural frequency of sandwich beam under varying C-F support stiffness (p=1, β=0.0, η_{sp}=0.0). 60

Figure 4.10 Loss factor of sandwich beam under varying C-F support stiffness (p=1, β=0.0, η_{sp}=0.0). 60

Figure 4.11: Natural frequency of sandwich beam under varying C-C support stiffness (p=1, β=0.0, η_{sp}=0.0). 61

Figure 4.12: Loss factor of sandwich beam under varying C-C support stiffness (p=1, β=0.0, η_{sp}=0.0). 61

Figure 4.13: Natural frequency of sandwich beam under varying P-R support stiffness (p=1, β=0.0, η_{sp}=0.0). 61

Figure 4.14: Loss factor of sandwich beam under varying P-R support stiffness (p=1, β=0.0, η_{sp}=0.0). 61

Figure 4.15: Mode shapes of sandwich beam under varying support stiffness: i) C-F, ii) C-C. iii) P-R (p=1, β=0.0, η_{sp}=0.0). 62

Figure 4.16: Sandwich beam loss factor under varying viscoelastic support stiffness: i) C-F, ii) C-C. iii) P-R (p=1, β=0.0). 63

Figure 4.17: Natural frequency of C-C sandwich beam for various porosity distribution models: i) p=0.5, ii) p=1. iii) p=3 (η_{sp}=0.1). 64

Figure 4.18: Loss factor of C-C sandwich beam for various porosity distribution models: i) p=0.5, ii) p=1. iii) p=3 (η_{sp}=0.1). 65

Figure 4.19: Loss factor of C-C sandwich beam for various VES loss factors (η_{sp}): i) p=0.5, ii) p=1. iii) p=3 (β=0.3, η_v=0.388). 66

Figure 4.20: CBT of sandwich beam: i) C-C, ii) C-P, iii) P-P, and iv) P-R (p=1, β =0.0, ΔT=50 ^{0}C and η_{sp}=0.0). 67

Figure 4.21: Buckling mode shape of sandwich beam: i) C-C, ii) C-P, iii) P-P, and iv) P-R (p=1, β=0.0, ΔT=50 ^{0}C and η_{sp}=0.0). 68

Figure 4.22: CBT of C-C sandwich beam at different temperature rise (p=1, β=0.3, and η_{sp}=0.0)......69

Figure 4.23: CBT of C-C sandwich beam at different porosity (p=1, ΔT=50 ^{0}C, and η_{sp}=0.0)......69

Figure 4.24: CBT of C-C sandwich beam at different power law index (β=0.3, ΔT=50 ^{0}C, and η_{sp}=0.0)......70

Figure 4.25: Natural frequency of sandwich beam: i) C-C, ii) C-P, iii) P-P, and iv) P-R (p=1, β=0.0, ΔT=10 ^{0}C and η_{sp}=0.0)......71

Figure 4.26: Loss factor of sandwich beam: i) C-C, ii) C-P, iii) P-P, and iv) P-R (p=1, β=0.0, ΔT=10 ^{0}C and η_{sp}=0.0)......72

Figure 4.27: Transverse mode shape of sandwich beam in vibration: i) C-C, ii) C-P, iii) P-P, and iv) P-R (p=1, β=0.0, ΔT=10 ^{0}C and η_{sp}=0.0)......73

Figure 4.28: Natural frequency of C-C sandwich beam at different temperatures (p=1, β=0.3, and η_{sp}=0.2)......73

Figure 4.29: Loss factor of C-C sandwich beam at different temperatures (p=1, β=0.3, and η_{sp}=0.2)......73

Figure 4.30: Natural frequency of C-C sandwich beam at different porosity (p=1, and η_{sp}=0.2)......74

Figure 4.31: Loss factor of C-C sandwich beam at different porosity (p=1, and η_{sp}=0.2). 74

Figure 4.32: Natural frequency of C-C sandwich beam at different power law index (β=0.3 and η_{sp} =0.2)......74

Figure 4.33: Loss factor of C-C sandwich beam at different power law index (β=0.3 and η_{sp} =0.2)......74

Figure 4.34: Natural frequency of C-C sandwich beam at CBT (p=1, β=0.3, and η_{sp}=0.2)......75

Figure 4.35: Loss factor of C-C sandwich beam at CBT (p=1, β=0.3, and η_{sp}=0.2)...75

Figure 4.36: Loss factor of C-C sandwich beam with change in support damping (η_{sp}) (p=1, β=0.3)......75

Figure 5.1: Disc brake system......78

Figure 5.2: Back plate with brake insulator......79

Figure 5.3: Natural frequency of sandwich beams......80

Figure 5.4: Loss factor of sandwich beams. 80
Figure 5.5:Variation in frequency with beam length. 81
Figure 5.6: Variation in loss factor with beam length. 81
Figure 5.7: Variation in natural frequency with core thickness (*l*=400mm)...............82
Figure 5.8: Variation in loss factor with core thickness (*l* =400mm). 82
Figure 5.9: Real part of transverse deflection of sandwich beams (*x/l*=0.5). 83
Figure 5.10: Imaginary part of transverse deflection of sandwich beams (*x/l*=0.5). ...83
Figure 5.11: Real part of axial displacement of back plate at neutral axis of back plates (*x/l*=0.5)...84
Figure 5.12: Imaginary part of axial displacement of back plate at neutral axis of back plates (*x/l*=0.5). 84
Figure 5.13: Real part of axial strain at neutral axis of back plates (*x/l*=0.5). 84
Figure 5.14: Imaginary part of axial strain at neutral axis of back plates (*x/l* =0.5). ...84
Figure 5.15: Real part of axial stress at neutral axis of back plates (*x/l* =0.5). 84
Figure 5.16: Imaginary part of axial stress at neutral axis of back plates (*x/l* =0.5). ...84
Figure 5.17: Axial displacement along the thickness direction *z* (*x/l* =0.25, *t*=0.157sec). 85
Figure 5.18: Axial strain along the thickness direction *z* (*x/l* =0.25, *t*=0.157sec). 85
Figure 5.19: Axial stress along the thickness direction *z* (*x/l* =0.25, *t*=0.157sec). 85
Figure 5.20: Shear strain in core along the length of beam (*t*=0.157sec). 86
Figure 5.21: Shear stress in core along the length of beam (*t*=0.157sec). 86
Figure 5.22: Brake pad with brake insulator. 87
Figure 5.23: Natural frequency of brake pad assembly. 88
Figure 5.24: Loss factor of the brake pad assembly. 88
Figure 5.25: Effect of *b/l* ratio on natural frequency (*l* =400mm). 89
Figure 5.26: Effect of *b/l* ratio on loss factor (*l* =400mm). 89
Figure 5.27: Influence of core thickness on natural frequency. 89
Figure 5.28: Influence of core thickness on loss factor. 89
Figure 5.29: Influence of constraining layer thickness on the natural frequency. 90
Figure 5.30: Influence of constraining layer thickness on loss factor. 90
Figure 5.31: Influence of core loss factor on natural frequency. 90
Figure 5.32: Influence of core loss factor on sandwich plate loss factor. 90

Figure 5.33: Influence of power law index on natural frequency. 91

Figure 5.34: Influence of power law index on loss factor. 91

Figure 5.35: Damped and undamped transverse deflection of Steel-NBR-Steel at the center of plate (η_v=0.126).. 92

Figure 5.36: Damped and undamped transverse deflection of FGM-NBR-Steel at the center of plate (η_v=0.126).. 92

Figure 5.37: Influence of core loss factor on damping of central transverse deflection of FGM-NBR-Steel (η_v= 0.05, 0.1, 0.2, 0.3)... 93

Figure 5.38: Transverse deflection of brake pad under UDL harmonic loading. 94

NOMENCLATURE

l : Length of beam and plate (m)

b : Breadth of beam and plate (mm)

h_f : Thickness of stiff layers (mm)

h_v : Thickness of viscoelastic core (mm)

z_1: Distance of neutral axis of upper stiff layer (mm)

z_2 : Distance of neutral axis of lower stiff layer (mm)

H : Distance between neutral axis of stiff layers (mm)

H_T : Total thickness of sandwich beam and plate (mm)

E : Young's modulus (N/m^2)

ρ : Density (kg/m^3)

G_v : Shear modulus of core (N/m^2)

η : Loss factor

u : Axial displacement (mm)

w : Transverse deflection (mm)

θ : Rotaion

q : Displacement vector

N_{ax} : Lagrange shape function for axial displacement

N_b : Hermite shape function for transverse displacement and rotation

σ : Axial stress (N/m^2)

ε : Axial strain

τ : Shear stress (N/m^2)

γ : Shera strain

α : Coefficient of thermal expansion (1/K)

β : Porosity volume fraction

K : Stiffness matrix (N/m)

K_{geo} : Geometric stiffness matrix (N/m)

K_{sp} Support stiffness matrix (N/m)

σ_0 : Initial stress due to temperature effect (N/m^2)

M : Mass matrix (kg)

F	Force vector
λ	Critical buckling parameter
T_b	Critical buckling temperature
ω	Natural frequency (Hz)
φ	Eigen vector

LIST OF ABBREVIATIONS

FGMs : Functionally Graded Materials
FEM : Finite Element Method
BCs : Boundary Conditions
VBCs : Viscoelastic Boundary Conditions
1D : 1 Dimensional
2D : 2 Dimensional
MT : Metal
CM : Ceramic
CBP : Critical Buckling Parameter
CBT : Critical Buckling Temperature
NF : Natural Frequency
LF : Loss Factor
ESS : Elastic Support Stiffness
VSS : Viscoelastic Support Stiffness
SSV Support Stiffness Value
BSS Beam Stiffness Value
NBR : Nitrile butadiene Rubber
C-C Clamped-Clamped
C-F Clamped-Free
P-P Pinned-Pinned
C-P Clamped-Pinned
P-R Pinned-Roller

CHAPTER 1

INTRODUCTION

1.1 FUNCTIONALLY GRADED MATERIALS (FGMs)

Functionally graded materials (FGMs) are developed as a replacement for conventional metals and alloys. FGMs exhibit non-homogenous properties along the dimensions because of which, FGMs have potential use in automobile, aerospace, marine, and biomedical applications (Mahamood et al. 2012), (Miyamoto et al. 2013), (Pompe et al. 2003), (Sayyad and Ghugal 2019). FGMs can be fabricated in two different ways: continuous gradation and stepwise gradation, as shown in Figure. 1.1 and Figure. 1.2, respectively.

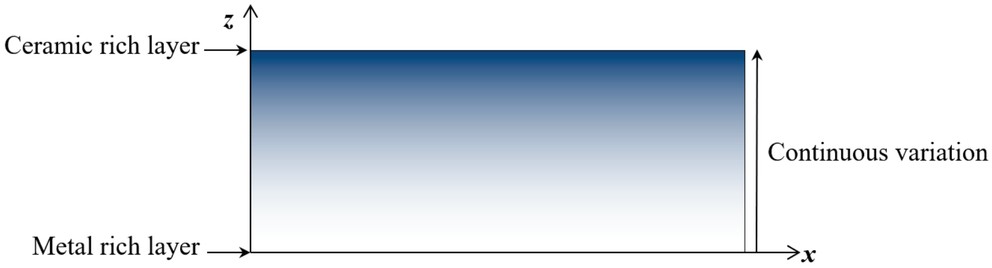

Figure 1.1: FG beam with continuous gradation.

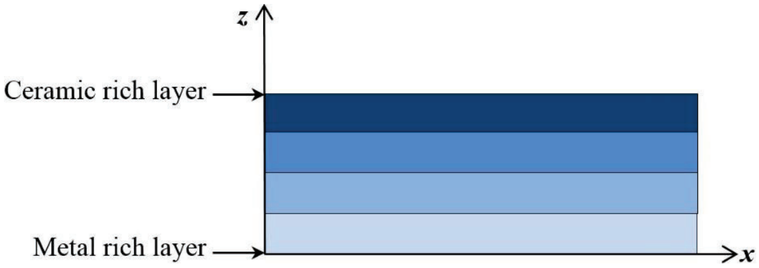

Figure 1.2: FG beam with stepwise gradation.

1.1.1 Applications of Functionally graded materials

In the year 1984, a class of new composite materials called FGMs was developed by Japanese scientists for the structural application of spacecraft. The main reason for this new invention was to sustain high temperatures and strength.

As time went on, the area of application expanded, now the FGMs are being used in many of the applications (Mahamood et al. 2012):

- **Aerospace:** FGM can sustain a very high thermal gradient of loading, making it suitable for structures and re-entry space plane bodies, rocket engine parts, etc.
- **Medicine:** Living human tissues like bones and teeth can be modeled as FGM. To replace these tissues, a well-matched material will serve the original bio-tissue's purpose.
- **Defense:** One of the essential properties of FGM is the ability to restrain crack propagation. This property makes it useful in defense as a penetration-resistant material for armor plates and bullet-proof vests.
- **Optoelectronics:** FGM also finds its application in optoelectronics as graded refractive index materials, highly efficient photodetectors, lenses, and audio-video disc magnetic storage media.
- **Energy:** FGM is applicable in energy conversion devices. They provide thermal barriers and are used as a protective coating on turbine blades used in gas turbine engines.

Other prospective areas of application are cutting tool insert coating, nuclear reactor components, heat exchangers, sensors, fire retardant doors, etc.

1.2 VISCOELASTIC MATERIALS

Viscoelastic materials are a special type of material comprising viscous and elastic properties. The relationship between stress and strain in viscoelastic materials depends on time (time domain) and frequency (frequency domain)(Lakes 2009). Viscoelastic materials include amorphous polymers, semi-crystalline polymers, biopolymers, metals at very high temperatures, and bitumen materials. Some of the phenomena of viscoelastic materials are listed as follows:

- The strain increases with time even though the stress is constant (creep).
- The stress decreases with time even though the strain is constant (relaxation).
- The material stiffness changes with the rate of the applied load.
- Viscoelastic material undergoes hysteresis in cyclic loading, which leads to energy dissipation.

Viscoelastic materials are used in aircraft and automobiles to reduce interior noise and vibration. These are also utilized as mechanical energy dissipaters in machines.

1.2.1 Creep and stress relaxation

Viscoelastic materials exhibit unique characteristics called creep and relaxation. When the constant load is applied to viscoelastic materials, the instantaneous strain will develop upon loading, including elastic and plastic strain. The strain increases with decreasing strain rate over time even though the load is constant. This time-dependent response is known as creep. As the loading time is prolonged, a constant strain rate is achieved. A part of the strain accumulated during creep will be recovered instantly (elastic strain) when the load is removed, and some parts will recover over a certain period (anelastic). Finally, some strain remains permanent, called plastic strain or creep strain. Figure 1.3 (i) shows the creep behavior of viscoelastic material. If the constant strain is applied to viscoelastic materials, decreasing stress is observed over time, as shown in Figure 1.3 (ii), which is stress relaxation.

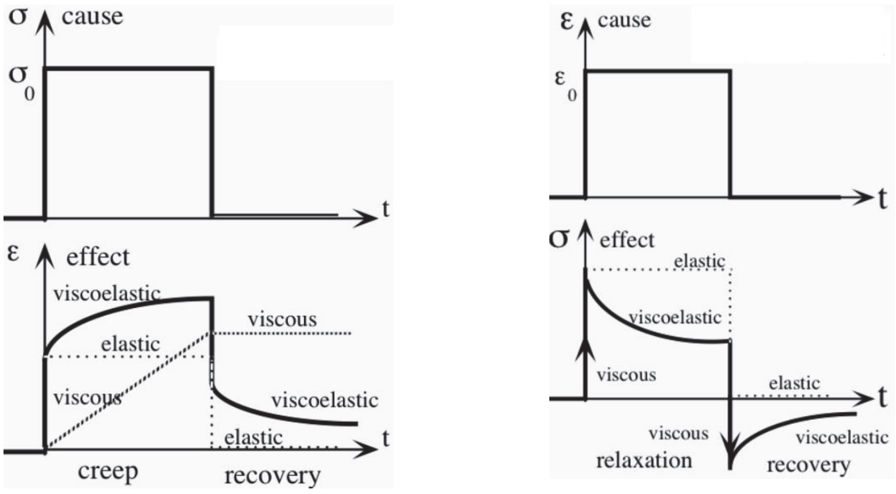
σ
cause
σ0
t
ε
effect
viscoelastic
viscous
elastic
viscous
viscoelastic
elastic
t
creep
recovery
ε
cause
ε0
t
σ
effect
elastic
viscoelastic
viscous
elastic
t
viscous
viscoelastic
relaxation
recovery

i) ii)

Figure 1.3: Transient phenomena: i) Creep and ii) Stress relaxation (Lakes 2009).

1.2.2 Dynamic response of viscoelastic materials

When the periodic sinusoidal load ($\sigma(t)$) is applied to a viscoelastic material, the strain ($\varepsilon(t)$) induced in the material is also sinusoidal, but the strain response lags by a certain phase angle (δ), as shown in Figure 1.4.

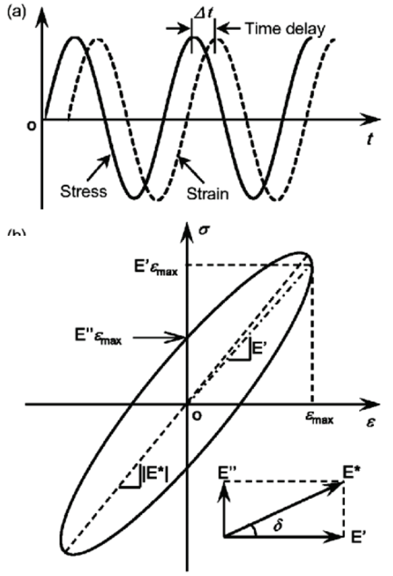

Figure 1.4: Stress and strain plot of viscoelastic material under dynamic loading (Lakes 2009).

The phase lag between stress and strain leads to complex dynamic stiffness (E^*).

$$E^* = \frac{\sigma}{\varepsilon} = E' + iE'' \tag{1.1}$$

where E' is storage modulus and E'' is loss modulus.

The phase angle is also called the loss angle (δ), and the tangent of 'δ' is called the loss tangent or loss factor (η). The loss factor is given as,

$$\eta = \tan\delta = \frac{E'}{E''} \tag{1.2}$$

1.3 POROSITY AND VISCOELASTIC BOUNDARY CONDITIONS

Porosity is the most common defect affecting the structure's mechanical properties (Al-Maharma et al. 2020).

Usually, in any fabrication process, there is every possibility of existing fabrication defects in the structures, such as porosity, due to the significant difference in the solidification temperature of constituents. The percentage of porosity is higher at the surface in some cases due to the difference in temperature of the die and pouring material; in others, the porosity distribution is higher at the center of samples due to the higher solidification time (Vynnycky 2020), (Xu et al. 2017). Both phenomena are possible in the case of FGMs, so it is essential to carry out studies on FGM considering porosity. Various components need to be assembled to develop any engineering equipment or machines. Fasteners, rivets, and various viscoelastic components such as washers, gaskets, and seals are used in the assembly process. In many instances, fasteners fail to constrain the component firmly, which causes slack in the assembly and affects a component's static and dynamic behavior. In applications like aeronautical and aerospace, a minute error may lead to failure. Therefore, studying the behavior of structures constrained by supports with varying stiffness is essential. Turbine and compressor blades with viscoelastic blocking pads (Wang et al. 2018), as shown in Figure 1.5, and Fluidlastic dampers used in vibration reduction in helicopter rotor blades (Han et al. 2013), as shown in Figure 1.6 are the engineering examples for structures with viscoelastic boundary conditions.

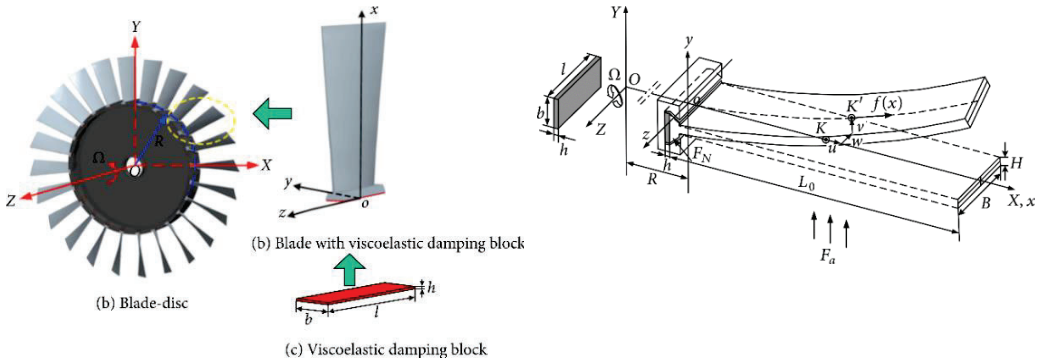
Y
Ω
R
X
Z
(b) Blade-disc
x
y
z
o
(b) Blade with viscoelastic damping block
h
b
l
(c) Viscoelastic damping block
Y
l
b
h
Ω
O
Z
y
z
K′
f(x)
K
v
u
w
F_N
h
R
L_0
H
B
X, x
F_a

i) ii)

Figure 1.5: Turbine and compressor blades with viscoelastic blocking pads: i) Blade disc with pad ii) Schematic diagram of blade (Wang et al. 2018).

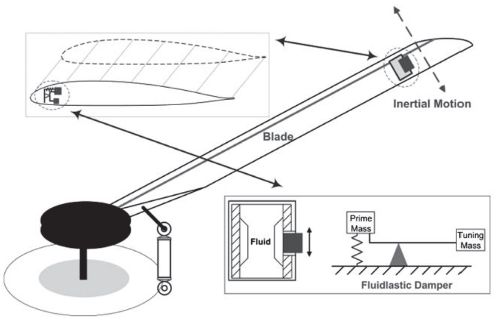
Inertial Motion
Blade
Fluid
Prime Mass
Tuning Mass
Fluidlastic Damper

Figure 1.6: Schematic diagram of fluidlastic damper in helicopter rotor blade (Han et al. 2013).

1.4 ORGANIZATION OF THE DISSERTATION

The thesis presents static and dynamic studies of FG porous sandwich beams with viscoelastic boundary conditions (VBCs). The static analysis comprises transverse bending and buckling, and dynamic studies include free and forced vibration. The rule of mixture and power law index governs the variation of FG properties. A complex shear modulus is considered for the viscoelastic core.

Further, FG stiff layers with temperature-dependent material properties are presumed imperfect due to various porosities. The effect of porosity and temperature on the bending, buckling, and vibration characteristics of FG sandwich beams with viscoelastic boundary conditions is discussed. Finally, the developed sandwich beam and plate formulations are incorporated to study the vibration behavior of brake pad assembly of a disc brake system akin to a sandwich beam and plate. The study proposes an Al–Al_2O_3 metal-ceramic functionally graded stiff layer as a back plate, with conventional steel being the constraining layer for brake insulators that enhances the damping characteristics of the brake pad. In initial studies, the Al–Al_2O_3 FG back plate, brake insulator, and constraining steel layer are presumed to be a three-layered sandwich beam, and then the complete brake pad is considered as a sandwich plate. The free and forced vibration of the brake pad is examined in both cases. The results conclude that the damping behavior of the brake pad is improved by replacing the steel back plate with Al–Al_2O_3 FG back plate. The whole thesis is divided into six chapters, and the contents of each chapter are summarized as follows:

Chapter-1: In this chapter, a brief introduction of functionally graded materials and viscoelastic materials is given with their applications. The chapter also described porosity, VBCs, and engineering examples for VBCs.

Chapter-2: The chapter thoroughly explains the literature review carried out for the present work. Further, the motivation, research gap, and research objectives are also discussed.

Chapter-3: The finite element (FE) formulations for static bending, buckling, and vibration behavior of FG sandwich beams in a thermal environment are explained in this chapter. Further, an analytical solution is developed for the FG sandwich beam to validate the FE model. Further, the porosity models and viscoelastic boundary conditions (VBCs) are incorporated into the formulation to study the effect of porosity and VBCs on the bending and vibration characteristics of FG sandwich beams. Finally, an analytical model is developed for the sandwich plate to study the vibration and damping response of the disc brake pad with the FG back plate and brake insulator.

Chapter-4: In this chapter, the effect of porosity and VBCs on static bending, buckling, and vibration studies of FG sandwich beams in a thermal environment is investigated. The impact of several parameters, such as support stiffness, loss factor, porosity dispersion, and power-law variation, on the static and dynamic behavior of sandwich beams is also discussed in this chapter.

Chapter-5: This chapter discusses the vibration and damping studies of FG back plates with brake insulators of a disc brake pad. In this chapter, comparison studies are presented between steel back plate and Al-Al_2O_3 FG back plate with brake insulator using sandwich beam and sandwich plate models.

Chapter-6: This chapter summarizes the overall research work carried out. The important findings and conclusions are presented, and the scope for future work is also discussed in this chapter.

CHAPTER 2

LITERATURE REVIEW

2.1 INTRODUCTION

Many research works have been carried out on sandwich structures over the years. Different types of stiff layers, such as metals, alloys, and composites; core materials, such as honeycomb and viscoelastic materials, are used to develop sandwich structures. The literature review mainly focuses on theoretical studies, including static bending, buckling, and vibration of sandwich beams and plates. The literature is studied in which the effect of temperature, porosity models, and viscoelastic boundary conditions on the static and dynamic behavior of beams and plates are discussed. The literature review also extends to study vibration characteristics of disc brake pads with brake insulators.

2.2 STATIC BENDING AND VIBRATION STUDIES ON SANDWICH BEAMS AND PLATES

A lot of research work has been done on static bending and vibration studies of sandwich beams and plates. The authors did experimental and numerical studies to determine transverse deflection and natural frequencies of sandwich beams and plates. Kao (1968) studied the static deflection of a simply supported sandwich beam. The minimization of energy approach was used to derive the governing differential equations (GDE), and trigonometric displacement fields were used to solve GDEs. The results were compared with results obtained by Liaw and Little (1967).

Mead and Markus (1969) derived the sixth-order differential equation of motion to analyze the transverse deflection of a beam under forced vibration. The authors extended the forced vibration field analysis based on DiTaranto's (1965) formulation. Three layered sandwich beam with two stiff layers and a viscoelastic core in between was considered for the study. The governing differential equations were derived, and the derived differential equations were solved for various boundary conditions. The axial displacements obtained in the upper and lower stiff layers were equal and opposite in direction because of zero axial loads on the beam.

The schematic representation of the kinematics of the viscoelastic beam after deformation was presented. The total transverse load on the beam was assumed to be a summation of inertia and external loads. The viscoelastic layer was assumed to have a complex shear modulus. The study concludes with the remark that modes, resonate frequency, and loss factors are identifiable with DiTaranto and Blasingame (1967) discussions.

Khatua and Cheung (1973) derived the stiffness and mass matrix of multilayer sandwich beams and plates using the finite element method. The study considered different rigidities such as coupling, bending, and extensional rigidities for stiff layers. Some of the assumptions were considered to derive the governing differential equations of motions. For example, the stiff layers experience only tensile and compressive stresses, whereas the cores are subjected to pure shear. The authors considered a common shear angle for all cores, which Kao (1968) neglected. For the study, a five-layered simply supported sandwich beam is considered as defined in Azar (1968).

Johnson and Kienholz (1982) developed finite element (FE) models for the vibration of three-layered sandwich beams, rings, and plates with a viscoelastic core. The author used the modal strain energy method (MSE) to determine the modal damping ratios and implemented the MSE method in commercially available finite element software (NASTRAN). Finally, the obtained results are validated with analytical solutions and experimental results.

Lall et al. (1987) studied partially covered sandwich beams using three methods: two numerical methods (one developed by Markus (1974) and the other using a Rayleigh–Ritz formulation) and one exact method. The mode shapes satisfying the boundary conditions are assumed in forms with unknown coefficients, leading to the complex eigenvalues defining the resonance frequencies and the associated modal system loss factors.

Kung and Singh (1997) performed the vibration analysis of multiple patched constrained layer damping beams. Since all deformation variables in various layers, only flexural shape functions are incorporated in the complex eigenvalue problem in the developed model.

Galucio et al. (2004) studied transient dynamic analysis of sandwich beams with viscoelastic core material using fractional derivative constitutive equations. Euler-Bernoulli's theory is used for stiff layers, and Timoshenko's theory was used for the viscoelastic core. The author used the finite element method and Newmark scheme to solve the equation of motion.

Gao and Liao (2005) studied the vibration of simply supported beams with enhanced self-sensing active constrained layer damping. Rayleigh-Ritz method was used to solve the equilibrium equations. The effects of several key parameters such as control gain, location and coverage of the self-sensing actuators on the system performance are also studied.

Tang et al. (2008) performed an analysis on the partially covered beam configurations with a constrained damping layer including the normal strain effects

Arikoglu and Ozkol (2010) investigated the vibration behavior of three-layered composite beams with a viscoelastic core. Governing differential equations (GDEs) were derived using Hamilton's principle, and GDEs were solved using the differential transform method.

The authors considered hypothetical problems from other literature for simply supported and clamped-free conditions. Studies were carried out on composite beams with glass fiber reinforced polymer (GFRP) stiff layers and VIB 12 (commercial name) viscoelastic interlayer. The effect of different parameters like the orientation of laminates, beam length, viscoelastic core location, and core thickness on loss factors was discussed.

Galuppi and Royer-Carfagni (2012) conducted analytical studies on the time-dependent behavior of a three-layered sandwich beam with polymeric film as core material. Prony's series of Maxwell elements were used to model viscoelastic structures. An interlayer was considered linear elastic, assuming its equivalent elastic moduli (E^*) to be stored (E') and relaxed moduli (E'') under constant strain using a secant stiffness solution (SSS). The author compared the results with a full viscoelastic FE solution (FVS). The comparison of results showed a considerable difference in the characteristic curves obtained from FVS and SSS methods.

Li et al. (2014) developed an analytical model to study the time-dependent behavior of sandwich beams with laminated functionally graded beams (FGM) as stiff layers and viscoelastic material as interlayers. The formulation of the sandwich beam's governing differential equations (GDEs) was obtained using Euler-Lagrange equations, and further GDEs were solved by the Fourier series method.

After studying all the literature regarding the bending and vibration of sandwich beams and plates, it is observed that various solution methods, such as the finite element method, analytical method, and differential quadrature, are used to solve the equation of motion of sandwich beams and plates. Various materials, such as metals and fiber-reinforced composites, are used as stiff layers with flexible cores. Still, the researchers have less explored sandwich structures with FG stiff layers and viscoelastic cores.

2.3 BUCKLING AND VIBRATION OF SANDWICH BEAMS AND PLATES IN THERMAL ENVIRONMENT

The metal-ceramic FG structures are used in high-temperature applications. Therefore, studying the static and dynamic behavior of FG sandwich structures in a thermal environment is important.

Ganesan and Pradeep (2005) studied the buckling and vibration behavior of sandwich beams under a thermal environment. The author used Khatua and Cheung formulations for the study. Temperature-dependent and independent shear modulus is considered for the core. 2D steady-state Fourier heat conduction equations are used to define the variation of temperature across the thickness and along the length.

Bhangale and Ganesan (2006) discussed the buckling and vibration behavior of functionally graded (FG) sandwich beams with a constrained viscoelastic layer in a thermal environment using finite element formulation. The FG sandwich beam was assumed to be clamped on both edges. The material properties of the stiff layer were functionally graded in the thickness direction according to power law distribution.

Sharnappa et al. (2007) carried out a vibration analysis of active constrained layer damped (ACLD) composite beams under a thermal environment. The author discussed the effect of core thickness, fiber angle, and temperature on the sandwich beam's natural frequency and loss factor. The behavior of natural frequency and loss factor at buckling temperature is also discussed in this work.

Vangipuram and Ganesan (2007) investigated the buckling and vibration of composite sandwich plates with a viscoelastic core. Temperature-dependent shear modulus and loss factor are considered for the core material, and inherent damping is considered for composite stiff layers. Parametric studies are also carried out by changing fiber angle, ply layup, and core thickness. The results reveal a shift in vibration modes with temperature rise.

Jeyaraj et al. (2011) studied the vibroacoustic behavior of sandwich plates with viscoelastic cores in a thermal environment.

The author obtained critical buckling temperature, natural frequency, and loss factor of sandwich beam for thermally pre-stressed sandwich beam using the finite element method. Further sound radiation characteristic study is also conducted using the boundary element method. From the results, the author concluded that vibroacoustic response decreases with a rise in temperature.

Joseph and Mohanty (2019) investigated buckling and free vibration of sandwich plates with FG stiff layers and viscoelastic core in high temperatures. The author used first-order shear deformation theory and FE formulation to derive static and dynamic equilibrium equations. The author concludes that a temperature rise reduces critical buckling temperature and natural frequency but enhances the loss factor.

The literature study on the buckling and vibration of sandwich beams and plates in a thermal environment reveals that geometric nonlinearity due to thermal stresses is a crucial parameter that changes a structure’s static and dynamic behavior.

2.4 EFFECT OF POROSITY AND VISCOELASTIC BOUNDARY CONDITIONS ON BEAMS AND PLATES

Porosity and boundary conditions are two important parameters that can change any structure's static and dynamic behavior. Porosity is a defect that occurs during the fabrication processes, such as casting, welding, powder metallurgy, coating, etc. Viscoelastic boundary conditions (VBCs) exist when a structure is supported by viscoelastic material. Viscoelastic supports contribute to the damping of the structure along with stiffness, so incorporating these two parameters is essential. There are few literature studies in which porosity and boundary conditions with varying stiffness are discussed.

Lin (1962) investigated the vibration behavior of continuous beams on equally spaced elastic supports. The author modeled the support with displacement and torsional springs and obtained the beam's natural frequency and mode shapes.

Wattanasakulpong and Ungbhakorn (2014) used the differential transform method (DTM) to discuss linear and nonlinear vibration of functionally graded (FG) beams having porosity restrained by elastic supports.

The authors addressed the effect of parameters such as volume fraction distribution, spring constant variation, and property distribution on nonlinear frequencies.

Demir and Oz (2014) studied the free vibration of FG beams supported by viscoelastic supports. The author modeled viscoelastic supports using springs and dampers. The study concludes that resonance frequencies increase with increasing elastic moduli ratio between the top and bottom surface of the FG beam and power law index. Still, the increasing trend can be seen at higher modes of low stiffness values and all modes of high stiffness values.

Singh et al. (2015) discussed the dynamic characteristics of axially vibrating rods and transversely vibrating beams with viscoelastic supports analytically in the article. The author modified the location and material parameters to get the desired vibration level.

Fazzolari (2018) discussed free vibration and elastic stability of 3D FG sandwich beams with porosity resting on an elastic foundation. The author used the Ritz method to solve governing equations and orthogonalized the Ritz functions to enhance accuracy. The effect of various parameters such as slenderness ratio, beam typology, boundary conditions, and elastic foundation coefficients on vibration and stability of FG sandwich beam.

Daikh and Zenkour (2019) studied the effect of porosity on the static deflection of FG sandwich plates. The author used the variable kinematic method to apply the properties of functionally graded carbon nanotubes (FG-CNTs). The authors proposed a new higher-order deformation theory for simply supported FG sandwich plates.

Zhang et al. (2020) studied the vibration behavior of FG porous sandwich plates for different boundary conditions. The author used a modified Fourier-Ritz method to derive governing equations; even and uneven porosities are considered for the study. The author concludes that porosity plays a vital role in the vibration and damping performance of the FG sandwich plate.

Hadji and Avcar (2021) investigated the free vibration behavior of FG porous sandwich plates having a ceramic core layer.

The authors considered various patterns of porosity distributions. The natural frequencies are calculated for different boundary conditions by varying the viscoelastic stiffness values. The study concludes that the natural frequency reduces with increased porosity volume fraction. The porosity effect will be maximum for the sandwich plate with higher side-to-thickness ratios.

The extensive literature study on porosity and viscoelastic boundary conditions in beam and plate structures exhibit that very few works have discussed the effect of viscoelastic boundary conditions (VBCs) on the damping of beam and plate structures. The combined effect of porosity and VBCs on the static and dynamic behavior of FG sandwich beams and plates is the area to be explored.

2.5 BRAKE PAD AND BRAKE INSULATORS OF DISC BRAKE SYSTEM

New inventions and innovations are happening in the automobile sector to improve the performance of vehicles. Drum brakes are replaced with disc brakes to improve the braking operation. There are some ongoing problems with the disc brake system, and brake squeal or brake noise is one among them. Research works are going on worldwide to address the brake squeal issue. Brake insulators are being used to suppress the squeal. Many theoretical and experimental studies are documented by researchers on vibration analysis of disc brake systems and the influence of brake insulators on the braking operation.

Triches Jr et al. (2004) studied the reduction in squeal noise of disc brake systems using constrained layer damping. The author conducted experiments on inertial dynamometers. Modal analysis of brake pads is also discussed in the article. The study concludes that low-frequency squeal occurs due to the coupling of out-of-plane rotor modes and brake pad bending modes.

Glisovic and Miloradovic (2010) discussed the brake system's noise, vibration, and harshness (NVH). The authors discussed the brake insulator types: single-layer, constrained-layer, multilayer constrained, double-sticky, and clip-on insulators.

The study concludes that brake pad damping is a vital parameter in suppressing squeal compared to material damping.

Wang et al. (2011) investigated the root cause of brake squeal of the disc brake of a car and illustrated a few methods to avoid or reduce the noise problem from brake system design. The author did both experimental and numerical studies on the disc brake system. The study concludes that disc surface finish, quality of installation, contaminations, and weather conditions contribute to noise.

Festjens et al. (2012) did a numerical study on the effectiveness of multilayer viscoelastic insulators in preventing brake squeals. The author used Abaqus for the simulation of the braking mechanism. The study concludes that the brake insulator attached to the back plate of the disc brake pad reduces brake squeal by dissipating the vibration energy

Abdullah et al. (2017) investigated the effectiveness of brake insulators in suppressing brake noise using Abaqus. The author considered various configurations of insulators and insulation materials for the study and predicted the brake system's modal frequencies and mode shapes.

The literature survey reveals that the vibration and passive damping of sandwich structures with the viscoelastic core is an important area of research. The replacement of conventional stiff layers with functionally graded materials (FGMs) in the sandwich structures adds supplementary properties to the base material.

2.6 MOTIVATION AND RESEARCH GAP

After the literature review, it is found that static and dynamic studies on FG sandwich structures with the viscoelastic core have been a hot research topic in recent years. Most of the literary works are focused on analytical and numerical studies on bending, buckling, and vibration of sandwich beams having different cores with conventional or ideal boundary conditions such as simply supported or pinned-roller (P-R), clamped-clamped (C-C), and clamped-free (C-F), etc. In many cases, due to the slack in the assembly of the structure, machine, or mechanism, ideal boundary conditions are not able to achieve (C-F, C-C, and P-R).

A small slack can vary the structure's overall stiffness, leading to a change in the dynamic behavior of components. Moreover, porosity is a common defect that can be seen in any fabrication method, such as casting, powder metallurgy, coating, layups, etc. The difference in melting points of graded components in FG structures leads to porosities. Most of the previous studies considered FG stiff layers to be perfect. Few works address the effect of temperature on static buckling and vibration characteristics of FG porous sandwich structures with varying support stiffness. Keeping these things in mind, the finite element (FE) model is developed for FG sandwich beams with the viscoelastic core. The static and dynamic behavior of sandwich beams is studied with porous and non-porous FG stiff layers. Also, the effect of temperature on buckling and free vibration of the FG sandwich beam is investigated. Finally, the Al-Al_2O_3 FG back plate is proposed as a replacement for the steel back plate based on vibration and damping studies on the brake pad of the disc brake system.

2.7 OBJECTIVES OF RESEARCH WORK

- To develop finite element formulation for static deflection and vibration response of FG sandwich beams with the viscoelastic core.
- To study the effect of porosity on static deflection and vibration characteristics of FG sandwich beams with the viscoelastic core.
- To investigate the effect of viscoelastic boundary conditions on static deflection and vibration response of FG sandwich beams with the viscoelastic core.
- To investigate the influence of the thermal environment on buckling and vibration response of FG porous sandwich beams under viscoelastic boundary conditions.
- To study the vibration and damping characteristics of disc brake pad with FG back plate and brake insulator.

CHAPTER 3

METHODOLOGY

3.1 INTRODUCTION

In this chapter, theoretical models are discussed to study the static and dynamic behavior of FG sandwich beams and plates with a viscoelastic core. The energy equations are derived for FG sandwich beams, and equilibrium equations are obtained for static bending, free, and forced vibrations. The derived equilibrium equations are solved using the FE approach. The accuracy of the developed FE model is validated with an analytical model. Further, the study incorporates porosity, viscoelastic boundary conditions (VBCs), temperature, and geometric nonlinearity due to thermal stresses. The developed model discusses the bending, buckling, and free vibration of FG porous sandwich beam with viscoelastic boundary conditions (VBCs) in a thermal environment. Finally, the analytical sandwich plate model is discussed, which is used to study vibration and damping characteristics of disc brake pads with FG back plate and brake insulator. Figure 3.1 shows the flow chart of the project work carried out.

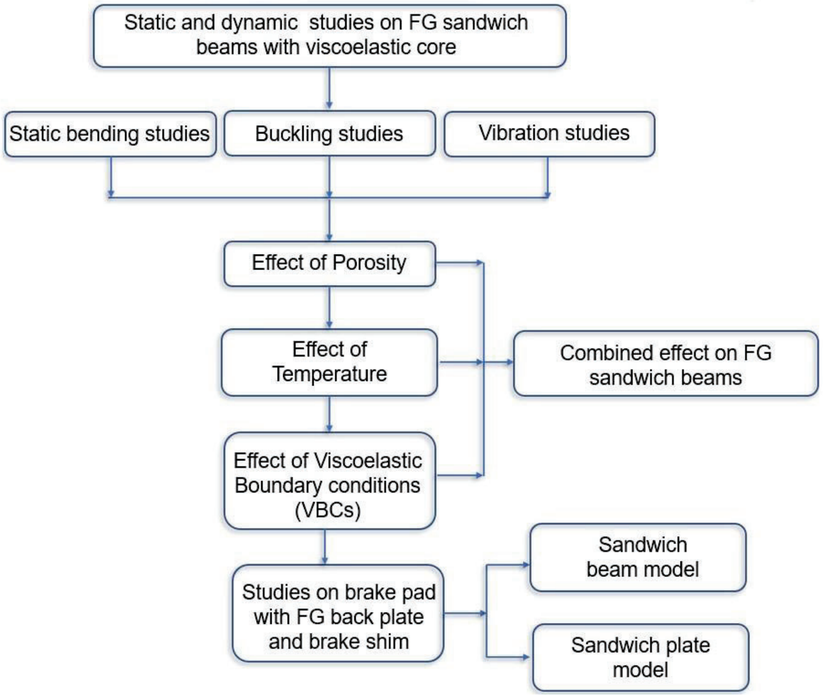
Static and dynamic studies on FG sandwich beams with viscoelastic core
Static bending studies
Buckling studies
Vibration studies
Effect of Porosity
Effect of Temperature
Combined effect on FG sandwich beams
Effect of Viscoelastic Boundary conditions (VBCs)
Studies on brake pad with FG back plate and brake shim
Sandwich beam model
Sandwich plate model

Figure 3.1: Flow chart of project work.

3.2 FE MODEL FOR STATIC AND DYNAMIC STUDIES OF FG SANDWICH BEAM

Consider a three-layered sandwich beam with two stiff and a viscoelastic core of length l and breadth b, as shown in Figure 3.2. The upper, lower stiff layer and core thickness are h_{f1}, h_{f2}, and h_v, respectively. The overall thickness of the sandwich beam is H_T. The neutral axis of the upper and lower stiff layers is at the distance z_1 and z_2, respectively, from the center of the core. H is the distance between the neutral axis of stiff layers. E_1 and E_2 are Young's modulus of upper and lower stiff layers, respectively. h_1, h_2, h_3, and h_4 are measured from the center of the core. Complex shear modulus G_v is considered for the viscoelastic core. When the beam vibrates, the stress and strain in the beam vary sinusoidally with respect to time, but there will be a phase lag between stress and strain, which leads to the dissipation of mechanical energy, due to which damping occurs. Therefore, properties like Young's modulus and shear modulus of the viscoelastic core are represented in the complex form (Lakes 2009). For FG stiff layers, Young's modulus and density vary with the z coordinate (Thickness). Some of the assumptions are made in order to get equilibrium equations (Li et al. 2014), such as:

- The upper and lower stiff layers behave according to the Euler-Bernoulli beam theory.
- Equal transverse deflection and rotation are considered for the two stiff layers; however, axial displacements for both layers differ along the neutral axis.
- Viscoelastic core undergoes only shear deformation due to axial displacements of stiff layers, and its normal stress and strain are neglected.
- There is no slip between the layers.

A two-noded 1D beam element with four degrees of freedom is taken for FE formulation, as shown in Figure 3.2. Temperature (T in kelvin) dependent properties in FG stiff layers can be defined as

$$P(T) = P_0(P_{-1}T^{-1} + 1 + P_1T + P_2T^2 + P_3T^3), \tag{3.1}$$

where P_{-1} to P_3 are temperature coefficients.

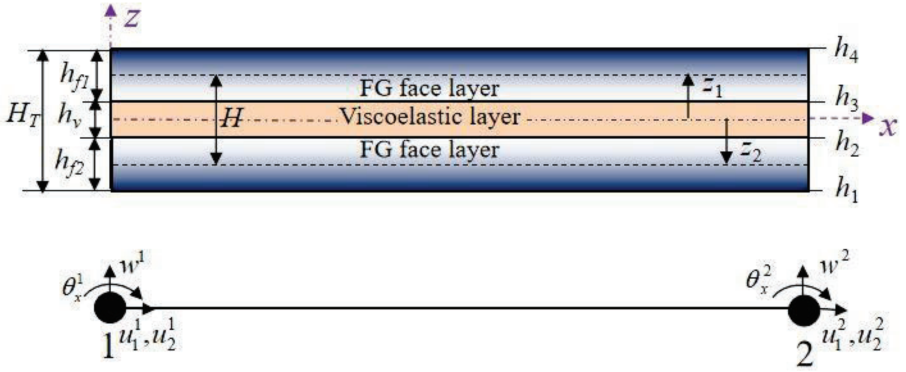
z
h_{f1}
H_T
h_v
h_{f2}
H
FG face layer
Viscoelastic layer
FG face layer
z_1
z_2
h_4
h_3
x
h_2
h_1
θ_x^1
w^1
1
u_1^1, u_2^1
θ_x^2
w^2
2
u_1^2, u_2^2

Figure 3.2: Two-noded FG Sandwich beam.

Eq. (3.2) shows the nodal parameter of an element where the numbers in subscripts and superscripts represent layers and nodes, respectively.

$$\{q\} = \begin{Bmatrix} u_t \\ u_b \\ w \end{Bmatrix} = \begin{Bmatrix} u_1^1 & u_2^1 & w^1 & \theta_x^{\,1} & u_1^2 & u_2^2 & w^2 & \theta_x^{\,2} \end{Bmatrix}^T, \tag{3.2}$$

where u_1, u_2, w, and θ_x are displacement of the neutral axis in the upper and lower stiff layers along the x-axis, displacement along the z-axis, and rotation of normal, respectively.

The kinematics of the sandwich beam subjected to transverse loading is shown in Figure 3.3, according to which the kinematic relations are derived as follows:

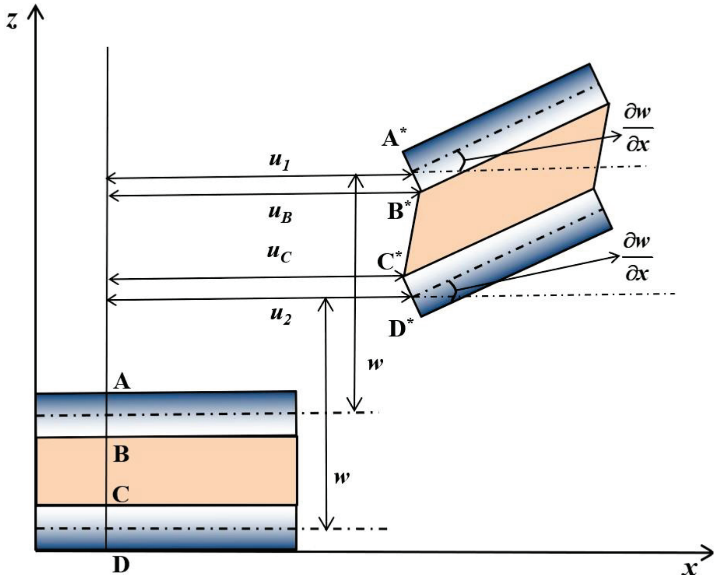
z
x
A^*
B^*
C^*
D^*
$\frac{\partial w}{\partial x}$
$\frac{\partial w}{\partial x}$
u_1
u_B
u_C
u_2
w
w
A
B
C
D

Figure 3.3: Kinematics of sandwich beam subjected to transverse deflection.

The axial and transverse displacements of a sandwich beam element at each node can be written as:

$$\{u_1\} = \begin{bmatrix} N^1_{ax1} & N^2_{ax1} \end{bmatrix} \begin{Bmatrix} u_1^1 \\ u_1^2 \end{Bmatrix} \tag{3.3}$$

$$\{u_2\} = \begin{bmatrix} N^1_{ax2} & N^2_{ax2} \end{bmatrix} \begin{Bmatrix} u_2^1 \\ u_2^2 \end{Bmatrix} \tag{3.4}$$

$$\{w\} = \begin{bmatrix} N_{b1} & N_{b2} & N_{b3} & N_{b4} \end{bmatrix} \begin{Bmatrix} w^1 \\ \theta^1 \\ w^2 \\ \theta^2 \end{Bmatrix} \tag{3.5}$$

where $\left[N^1_{ax1}\right]$ and $\left[N^1_{ax2}\right]$ are the Lagrange shape functions and $[N_b]$ is the Hermit shape function for axial and transverse displacements of upper and lower stiff layers, respectively, for node one. The Hermite interpolation is used if the curve needs to be fit for ordinate (variable) and its slope (derivative of variable) whereas Lagrange interpolation is used if the curve needs to be fit only for ordinate (variable) without concerning its derivatives. In the study, only axial displacement is considered and its slope is not considered at the nodes, so, the Lagrange shape functions satisfy the variable (displacement) condition, whereas both transverse displacement and its slope are considered at the nodes and the Hermite shape functions satisfy the variable (displacement) as well as slope at the nodes.

The Lagrange shape functions and Hermit shape functions are given by,

$$\begin{bmatrix} N^1_{ax1} & N^2_{ax1} \end{bmatrix} = \begin{bmatrix} 1-\frac{x}{L} & \frac{x}{L} \end{bmatrix} \tag{3.6}$$

$$\begin{bmatrix} N_{b1} & N_{b2} & N_{b3} & N_{b4} \end{bmatrix} = \begin{bmatrix} \frac{2x^3}{L^3}-\frac{3x^2}{L^2}+1 & \frac{x^3}{L^2}-\frac{2x^2}{L}+x & -\frac{2x^3}{L^3}+\frac{3x^2}{L^2} & \frac{x^3}{L^2}-\frac{2x^2}{L} \end{bmatrix} \tag{3.7}$$

Hence global displacements are written in the form:

$$\{u_1\} = [N_{ax1}]\{\bar{u}_1\} \tag{3.8}$$

$$\{u_2\} = [N_{ax2}]\{\bar{u}_2\} \tag{3.9}$$

$$\{w\} = [N_b]\{\bar{w}\} \tag{3.10}$$

where $\bar{u}_1, \bar{u}_2$ and $\bar{w}$ are elemental displacements

The displacement fields for the sandwich beam are written as follows:

$$u = \begin{cases} u_1 - (z - z_1)\theta_x & (h_3 \le z \le h_4) \\ u_2 - (z - z_2)\theta_x & (h_1 \le z \le h_2) \end{cases}, \tag{3.11}$$

$$w_1 = w_2 = w \cdot \tag{3.12}$$

Strain associated with FG stiff layers is given by,

$$\begin{Bmatrix} \varepsilon_{xx} \\ \varepsilon_{yy} \\ \gamma_{xy} \end{Bmatrix}_{(i)} = \begin{Bmatrix} \varepsilon_{0xx} \\ \varepsilon_{0yy} \\ \gamma_{0xy} \end{Bmatrix}_{(i)} - (z - z_{(i)}) \begin{Bmatrix} \kappa_{xx} \\ \kappa_{yy} \\ \kappa_{xy} \end{Bmatrix}_{(i)}, \tag{3.13}$$

where subscript i=1, 2 represents the upper and lower FG stiff layers. Constitutive relations of stress and strains are given as:

$$\begin{Bmatrix} \sigma_{xx} \\ \sigma_{yy} \\ \tau_{xy} \end{Bmatrix}_{(i)} = \begin{bmatrix} C_{11} & C_{12} & 0 \\ C_{12} & C_{22} & 0 \\ 0 & 0 & C_{66} \end{bmatrix} \begin{Bmatrix} \varepsilon_{xx} - \alpha_{xx}(\Delta T) \\ \varepsilon_{yy} - \alpha_{yy}(\Delta T) \\ \gamma_{xy} - \alpha_{xy}(\Delta T) \end{Bmatrix}_{(i)}, \tag{3.14}$$

where $C_{11} = C_{22} = \dfrac{E(z,T)}{1-(\nu^2)}, C_{12} = \nu C_{11}, C_{66} = \dfrac{E(z,T)}{2(1+\nu)}$, $E(z,T)$ is temperature-dependent Young's modulus varies across the thickness, and 'v' is poison's ratio. ΔT and $\alpha(z,T)$ are the temperature rise and coefficient of thermal expansion, respectively.

Integration of stresses over thickness results in in-plane stress and moment resultants:

$$\begin{Bmatrix} N_{xx} \\ N_{yy} \\ N_{xy} \end{Bmatrix}_{(i)} = \int_{h_{st(i)}} \begin{Bmatrix} \sigma_{xx} \\ \sigma_{yy} \\ \tau_{xy} \end{Bmatrix}_{(i)} dz, \quad \begin{Bmatrix} M_{xx} \\ M_{yy} \\ M_{xy} \end{Bmatrix}_{(i)} = \int_{h_{st(i)}} \begin{Bmatrix} \sigma_{xx} \\ \sigma_{yy} \\ \tau_{xy} \end{Bmatrix}_{(i)} zdz, \tag{3.15}$$

$$\begin{Bmatrix} N_{xx} \\ N_{yy} \\ N_{xy} \\ M_{xx} \\ M_{yy} \\ M_{xy} \end{Bmatrix}_{(i)} = \begin{bmatrix} A_{11} & A_{12} & 0 & B_{11} & B_{12} & 0 \\ A_{21} & A_{22} & 0 & B_{21} & B_{22} & 0 \\ 0 & 0 & A_{66} & 0 & 0 & B_{66} \\ B_{11} & B_{12} & 0 & D_{11} & D_{12} & 0 \\ B_{21} & B_{22} & 0 & D_{21} & D_{22} & 0 \\ 0 & 0 & B_{66} & 0 & 0 & D_{66} \end{bmatrix} \begin{Bmatrix} \varepsilon^0_{xx} \\ \varepsilon^0_{yy} \\ \gamma^0_{xy} \\ \kappa_{xx} \\ \kappa_{yy} \\ \kappa_{xy} \end{Bmatrix}_{(i)} - \begin{Bmatrix} N_{Txx} \\ N_{Tyy} \\ N_{Txy} \\ M_{Txx} \\ M_{Tyy} \\ M_{Txy} \end{Bmatrix}_{(i)}, \tag{3.16}$$

where A_{jk}, B_{jk}, and D_{jk} are stiffness coefficients for extension, coupling, and bending, respectively, which are given as:

$$(A_{kl}, B_{kl}, D_{kl})_{(i)} = \int_{h_i}^{h_{i+1}} C_{kl}(1,(z-z_i),(z-z_i)^2 dz \quad k,l = 1,2,6\,, \tag{3.17}$$

$$\begin{bmatrix} N_{Txx} \\ N_{Tyy} \\ N_{Txy} \end{bmatrix}_{(i)} = \int_{h_i}^{h_{i+1}} \left(\begin{bmatrix} C_{11} & C_{12} & 0 \\ C_{12} & C_{22} & 0 \\ 0 & 0 & C_{66} \end{bmatrix} \begin{bmatrix} \alpha_{xx} \\ \alpha_{yy} \\ 0 \end{bmatrix}_{(i)} \left(\Delta T\right) dz \right), \tag{3.18}$$

$$\begin{bmatrix} M_{Txx} \\ M_{Tyy} \\ M_{Txy} \end{bmatrix}_{(i)} = \int_{h_i}^{h_{i+1}} \left(\begin{bmatrix} C_{11} & C_{12} & 0 \\ C_{12} & C_{22} & 0 \\ 0 & 0 & C_{66} \end{bmatrix} \begin{bmatrix} \alpha_{xx} \\ \alpha_{yy} \\ 0 \end{bmatrix}_{(i)} \left(\Delta T\right) zdz \right). \tag{3.19}$$

Eq. (3.16) is divided into two parts: Eq. (3.20) and Eq. (3.21),

$$\begin{Bmatrix} N_{xx} \\ M_{xx} \end{Bmatrix} = \begin{bmatrix} A_{11} & B_{11} \\ B_{11} & D_{11} \end{bmatrix} \begin{Bmatrix} \varepsilon^0_{xx} \\ \kappa_{xx} \end{Bmatrix} + \begin{bmatrix} A_{12} & B_{12} \\ B_{12} & D_{12} \end{bmatrix} \begin{Bmatrix} \varepsilon^0_{yy} \\ \kappa_{yy} \end{Bmatrix} - \begin{Bmatrix} N_{Txx} \\ M_{Txx} \end{Bmatrix}, \tag{3.20}$$

$$\begin{Bmatrix} N_{yy} \\ M_{yy} \end{Bmatrix} = \begin{bmatrix} A_{12} & B_{12} \\ B_{12} & D_{12} \end{bmatrix} \begin{Bmatrix} \varepsilon^0_{xx} \\ \kappa_{xx} \end{Bmatrix} + \begin{bmatrix} A_{22} & B_{22} \\ B_{22} & D_{22} \end{bmatrix} \begin{Bmatrix} \varepsilon^0_{yy} \\ \kappa_{yy} \end{Bmatrix} - \begin{Bmatrix} N_{Tyy} \\ M_{Tyy} \end{Bmatrix}. \tag{3.21}$$

Since the problem described is a one-dimensional beam, the force and moment resultants are zero ($N_{yy} = N_{xy} = 0; M_{yy} = M_{xy} = 0$) in the *y* and *xy* axis.

Eq. (3.21) is redefined into a 1D beam as follows:

$$\begin{Bmatrix} \varepsilon^0_{yy} \\ \kappa_{yy} \end{Bmatrix} = \begin{bmatrix} A_{22} & B_{22} \\ B_{22} & D_{22} \end{bmatrix}^{-1} \left(\begin{Bmatrix} N_{Tyy} \\ M_{Tyy} \end{Bmatrix} - \begin{bmatrix} A_{12} & B_{12} \\ B_{12} & D_{12} \end{bmatrix} \begin{Bmatrix} \varepsilon^0_{xx} \\ \kappa_{xx} \end{Bmatrix} \right). \tag{3.22}$$

After simplification and rearranging Eq. (3.20), N_{xx} and M_{xx} are written in the form:

$$\begin{Bmatrix} N_{xx} \\ M_{xx} \end{Bmatrix}_{(i)} = \begin{bmatrix} A^e_{11} & B^e_{11} \\ B^e_{11} & D^e_{11} \end{bmatrix} \begin{Bmatrix} \varepsilon^0_{xx} \\ \kappa_{xx} \end{Bmatrix}_{(i)} - \begin{Bmatrix} N^e_{Txx} \\ M^e_{Txx} \end{Bmatrix}_{(i)}, \tag{3.23}$$

where $A^e_{11}, B^e_{11}, D^e_{11}$ are the effective stiffness coefficients of the FG stiff layer, which is given as:

$$D^*_{(i)} = \begin{bmatrix} A^e_{11} & B^e_{11} \\ B^e_{11} & D^e_{11} \end{bmatrix} = \begin{bmatrix} A_{11} & B_{11} \\ B_{11} & D_{11} \end{bmatrix} - \begin{bmatrix} A_{12} & B_{12} \\ B_{12} & D_{12} \end{bmatrix} \left(\begin{bmatrix} A_{22} & B_{22} \\ B_{22} & D_{22} \end{bmatrix}^{-1} \begin{bmatrix} A_{21} & B_{21} \\ B_{21} & D_{21} \end{bmatrix} \right), \tag{3.24}$$

N^e_{txx} and M^e_{txx} are effective thermal stress and moment resultants:

$$D^*_{T(i)} = \begin{bmatrix} N^e_{txx} \\ M^e_{txx} \end{bmatrix} = \begin{bmatrix} A_{12} & B_{12} \\ B_{12} & D_{12} \end{bmatrix} - \left(\begin{bmatrix} A_{22} & B_{22} \\ B_{22} & D_{22} \end{bmatrix}^{-1} \begin{Bmatrix} N_{Tyy} \\ M_{Tyy} \end{Bmatrix} \right) - \begin{Bmatrix} N_{txx} \\ M_{txx} \end{Bmatrix}. \tag{3.25}$$

D^* and $D_T{}^*$ are effective stiffness coefficient matrices for mechanical and thermal stresses.

The shear strain and stress for the viscoelastic core are given as follows:

$$\gamma_v = \frac{1}{h_v}\left[u_1 - u_2 + \frac{\partial w}{\partial x}H\right]; \tau_v = \frac{G_v}{h_v}\left[u_1 - u_2 + \frac{\partial w}{\partial x}H\right]; G_v = G^s(1 + i\eta_v), \tag{3.26}$$

H is the distance between the neutral plane of the upper and lower stiff layers. The shear stiffness coefficient of the core is given by,

$$D_v^* = \int_{h_v} G_v dz . \tag{3.27}$$

The total potential energy in a thermal environment is given by,

$$U_{pt} = U_{strain} - U_{thrm} + U_{ext}, \tag{3.28}$$

where U_{strain} and U_{thrm} are total strain energy due to mechanical and thermal effects, respectively, and U_{ext} is energy due to external mechanical load:

$$U_{strain} = \frac{1}{2}b\int_0^L \begin{Bmatrix} \varepsilon_{1xx} \\ \gamma_v \\ \varepsilon_{2xx} \end{Bmatrix}^T \begin{bmatrix} D_1^* & 0 & 0 \\ 0 & D_v^* & 0 \\ 0 & 0 & D_2^* \end{bmatrix} \begin{Bmatrix} \varepsilon_{1xx} \\ \gamma_v \\ \varepsilon_{2xx} \end{Bmatrix} dx, \tag{3.29}$$

$$U_{thrm} = b\int_0^L \begin{Bmatrix} \varepsilon_{1xx} \\ \gamma_v \\ \varepsilon_{2xx} \end{Bmatrix}^T \begin{bmatrix} D_{T1}^* \\ D_{Tv}^* \\ D_{T2}^* \end{bmatrix} dx, \tag{3.30}$$

$$\begin{Bmatrix} \varepsilon_{1xx} \\ \gamma_v \\ \varepsilon_{2xx} \end{Bmatrix} = \begin{Bmatrix} \dfrac{\partial u_1}{dx} \\ \dfrac{\partial^2 w}{dx^2} \\ \gamma_{xz} \\ \dfrac{\partial u_2}{dx} \\ \dfrac{\partial^2 w}{dx^2} \end{Bmatrix} = [B]\{q\}. \tag{3.31}$$

Eq. (3.29) and Eq. (3.30) are replaced with Eq. (3.31).

The potential energy shown in Eq. (3.28) is minimized to get the static equilibrium equation of the sandwich beam with initial stresses due to the thermal environment and mechanical load:

$$\left[K_R + iK_I\right]\{q\} = \{F_T\} + \{F_M\}, \tag{3.32a}$$

$$\{F_T\} + \{F_M\} = \{F\}, \tag{3.32b}$$

where stiffness matrix [*K*] involves real [K_R] parts and imaginary [K_I] parts because of the complex shear modulus of the viscoelastic layer. {F_T} and {F_M} are thermal and mechanical force vectors, respectively.

The loss factor and accompanying loss modulus are only valid for dynamic conditions; the imaginary stiffness matrix vanishes ([K_I]=0) for static conditions (Lakes 2009).

3.2.1 Geometric stiffness matrix

The initial stress resultants (N_x^0) due to temperature rise and nonlinear strains are involved in the nonlinear strain energy equation (U_{geo}) as given by,

$$U_{geo} = \frac{1}{2} b \int_0^L \left((N_x^0)_1 (N_x^0)_2\right) \begin{pmatrix} \left(\dfrac{\partial w}{\partial x}\right)_1^2 \\ \left(\dfrac{\partial w}{\partial x}\right)_2^2 \end{pmatrix} dx \ ; \ \begin{pmatrix} \left(\dfrac{\partial w}{\partial x}\right)_1^2 \\ \left(\dfrac{\partial w}{\partial x}\right)_2^2 \end{pmatrix} = [B_{geo}]\{q\}. \tag{3.33}$$

Solving and rearranging Eq. (3.33) leads to the following:

$$U_{geo} = \frac{1}{2}\{q\}^T [K_{geo}]\{q\}, \tag{3.34}$$

where [K_{geo}] is the geometric stiffness matrix given as,

$$[K_{geo}] = b\int_0^L \left\{B_{geo}\right\}^T [\sigma_0]\left\{B_{geo}\right\} dx. \tag{3.35}$$

3.2.2 Thermal buckling

Thermal buckling occurs when thermal stresses are induced in the sandwich beam. The classical stability equation for buckling is given by,

$$[[K_R] - \lambda [K_{geo}]]\varphi = 0, \tag{3.36}$$

where λ is the critical buckling parameter (CBP), φ is the eigenvector.

Critical buckling temperature (CBT) is given by,

$$T_b = \lambda \Delta T + T_{room}, \tag{3.37}$$

where T_b is critical buckling temperature (CBT), and T_{room} is room temperature.

3.2.3 Free and forced vibration

The kinetic energy (KE) is written as:

$$KE = \frac{1}{2} b \int_V \begin{Bmatrix} \{\dot{q}_1\} \\ \{\dot{q}_c\} \\ \{\dot{q}_2\} \end{Bmatrix}^T \begin{bmatrix} \rho_1 & 0 & 0 \\ 0 & \rho_c & 0 \\ 0 & 0 & \rho_2 \end{bmatrix} \begin{Bmatrix} \{\dot{q}_1\} \\ \{\dot{q}_c\} \\ \{\dot{q}_2\} \end{Bmatrix} dv \,. \tag{3.38}$$

Minimizing the total energy to arrive equilibrium equation of the sandwich beam in dynamic conditions as:

$$[[K_R + iK_I] - [K_{geo}]]\varphi - \omega^2 [M]\varphi = F \,, \tag{3.39}$$

Solving the equilibrium equation considering the dynamic force zero (F=0), the sandwich beam's natural frequency and loss factors can be obtained. The loss factor of the sandwich beam is given by,

$$\eta_{b(m)} = \frac{\varphi_{(m)}^T [K_I] \varphi_{(m)}}{\varphi_{(m)}^T ([K_R] - [K_{geo}]) \varphi_{(m)}} \,, \tag{3.40}$$

where $\varphi_{(m)}$ is the Eigenvector for the m^{th} mode number.

3.2.4 Functional gradation of FG Stiff layers

FG stiff layer is a blend of metal (MT) and ceramic (CM). The ceramic content is gradually graded with metal as per the rule of the mixture through the layer thickness. The effective material property P_{eff} at any point of the thickness of FG layer is given by the relation,

$$P_{eff} = (P_{CM} - P_{MT}) V_{CM}(z) + P_{MT} \,, \tag{3.41}$$

where P is the property of metal (MT) and ceramic (CM); V_{CM} is the volume fraction of ceramic which varies with power law distribution (p) as follows:

$$\left. \begin{aligned} V_{CM}{}^{(1)}(z) &= \left(\frac{z - h_2}{h_3 - h_2} \right)^p && \text{for} \quad z \in [h_3, h_4] \\ V_{CM}{}^{(c)}(z) &= 0 && \text{for} \quad z \in [h_2, h_3] \\ V_{CM}{}^{(2)}(z) &= \left(\frac{h_1 - z}{h_1 - h_0} \right)^p && \text{for} \quad z \in [h_1, h_2] \end{aligned} \right\} . \tag{3.42}$$

Figure 3.4 shows the ceramic volume fraction variation along the thickness of the FG stiff layer.

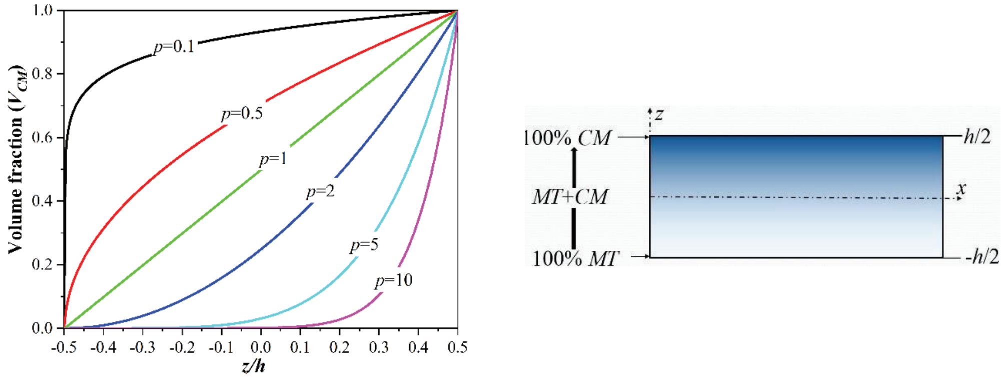

a) b)

Figure 3.4: Functional gradation along the thickness: a) Ceramic volume fraction along the thickness and b) metal and ceramic contents along the thickness of beam.

3.3 ANALYTICAL MODEL FOR FG SANDWICH BEAM

The analytical model is developed to validate the FE model. The equilibrium equations are derived considering only mechanical stresses (temperature independent). The assumptions, kinematics (Figure 3.3), and displacement equations (Eqs. 3.11-3.12) considered for the analytical model remain the same as that of the FE model. Based on the kinematics, the strain energy *(U_{strain})*, energy due to external force *(U_{ext})*, and kinetic energy *(KE)* of a sandwich beam are given by,

$$U_{strain} = \frac{1}{2}\int_0^l \int_A \left[\sigma_{1xx}\varepsilon_{1xx} + \sigma_{2xx}\varepsilon_{2xx} + \tau_{xz}\gamma_{xz}\right] dAdx, \tag{3.43}$$

$$U_{ext} = Fw, \tag{3.44}$$

$$KE = \frac{1}{2}\int_0^l \int_A \rho_1\left(\dot{u}_1^{\,2} + \dot{w}^2\right) + \rho_2\left(\dot{u}_2^{\,2} + \dot{w}^2\right) + \rho_v(\dot{w})^2\, dAdx, \tag{3.45}$$

where A is the cross-section area, l is the beam's length, and F is the transverse load acting on the sandwich beam, which remains constant for the static bending case and varies with time ($F(t)$) for the forced vibration case. The total energy of the sandwich beam is written as,

$$\prod = \int_0^l (KE - (U_{strain} + U_{ext}))dx, \tag{3.46}$$

The total energy can be written using the Lagrange density function (L)as,

$$\prod = \int_0^l L dx \,, \tag{3.47}$$

where $L = KE - (U_{strain} + U_{ext})$.

Substituting displacements and energies in Eq. (3.47), the Lagrange density function is derived in the form of displacements as follows:

$$L = \frac{1}{2}\left\{ \begin{gathered} \left[\begin{aligned} & I_{A1}\left[\left(\frac{\partial u_1}{\partial t}\right)^2 + \left(\frac{\partial w}{\partial t}\right)^2\right] + I_{A2}\left[\left(\frac{\partial u_2}{\partial t}\right)^2 + \left(\frac{\partial w}{\partial t}\right)^2\right] - 2I_{B1}\left(\frac{\partial u_1}{\partial t}\frac{\partial^2 w}{\partial t \partial x}\right) - 2I_{B2}\left(\frac{\partial u_2}{\partial t}\frac{\partial^2 w}{\partial t \partial x}\right) \\ & +(I_{D1} + I_{D2})\left(\frac{\partial^2 w}{\partial t \partial x}\right)^2 + I_v\left(\frac{\partial w}{\partial t}\right)^2 \end{aligned} \right] - \\ \left[\begin{aligned} & A_1\left(\frac{\partial u_1}{\partial x}\right)^2 + A_2\left(\frac{\partial u_3}{\partial x}\right)^2 - 2B_1\left(\frac{\partial u_1}{\partial x}\frac{\partial^2 w}{\partial x^2}\right) - 2B_2\left(\frac{\partial u_2}{\partial x}\frac{\partial^2 w}{\partial x^2}\right) + (D_1 + D_2)\left(\frac{\partial^2 w}{\partial x^2}\right)^2 \\ & + \frac{bG_v}{h_v}\left[u_1 - u_2 + w'H\right]^2 - F(t)w \end{aligned} \right] \end{gathered} \right. \tag{3.48}$$

where A_1, A_2, B_1, B_2, D_1, and D_2 are stiffness coefficients, I_{A1}, I_{A2}, I_{B1}, I_{B2}, I_{D1}, and I_{D2} are inertial coefficients of upper and lower stiff layers due to extension, coupling, and bending effects, respectively and I_v is the inertial coefficient for the core. These are given as follows:

$$(A_1, B_1, D_1) = \int_A E_1(z)\left[(1), (z - z_1), (z - z_1)^2\right] dA \,, \tag{3.49}$$

$$(A_2, B_2, D_2) = \int_A E_2(z)\left[(1), (z - z_2), (z - z_2)^2\right] dA \,, \tag{3.50}$$

$$(I_{A1}, I_{B1}, I_{D1}) = \int_A \rho_1(z)\left[(1), (z - z_1), (z - z_1)^2\right] dA \,, \tag{3.51}$$

$$(I_{A2}, I_{B2}, I_{D2}) = \int_A \rho_2(z)\left[(1), (z - z_2), (z - z_2)^2\right] dA \,, \tag{3.52}$$

$$I_V = \int_A \rho_v dA \,. \tag{3.53}$$

To obtain the governing differential equations, Euler-Lagrange equations are used, which are as follows:

$$\frac{\partial}{\partial x}\left(\frac{\partial L}{\partial u_1'}\right) + \frac{\partial}{\partial t}\left(\frac{\partial L}{\partial \dot{u}_1}\right) - \left(\frac{\partial L}{\partial u_1}\right) = 0 \,, \tag{3.54}$$

$$\frac{\partial}{\partial x}\left(\frac{\partial L}{\partial u_2'}\right)+\frac{\partial}{\partial t}\left(\frac{\partial L}{\partial \dot{u}_2}\right)-\left(\frac{\partial L}{\partial u_2}\right)=0\,, \tag{3.55}$$

$$\frac{\partial^2}{\partial x^2}\left(\frac{\partial L}{\partial w''}\right)+\frac{\partial^2}{\partial t^2}\left(\frac{\partial L}{\partial \ddot{w}}\right)-\frac{\partial}{\partial x}\left(\frac{\partial L}{\partial w'}\right)-\frac{\partial}{\partial t}\left(\frac{\partial L}{\partial \dot{w}}\right)+\frac{\partial^2}{\partial x\partial t}\left(\frac{\partial L}{\partial \dot{w}'}\right)+\frac{\partial L}{\partial w}=0\,, \tag{3.56}$$

where $\left(\cdot=\frac{\partial}{\partial t}\right)$ and $\left('=\frac{\partial}{\partial x}\right)$.

Substituting Eq. (3.48) in Eqs. (3.54-3.56) leads to equations of motion in the equilibrium condition of the sandwich beam as follows:

$$-A_1u_1''+B_1w'''+\frac{bG_v}{h_v}\left[u_1-u_2+w'H\right]+I_{A1}\ddot{u}_1-I_{B1}\ddot{w}'=0\,, \tag{3.57}$$

$$-A_2u_2''+B_2w'''-\frac{bG_v}{h_v}\left[u_1-u_2+w'H\right]+I_{A2}\ddot{u}_2-I_{B2}\ddot{w}'=0\,, \tag{3.58}$$

$$\begin{bmatrix}(D_1+D_3)w''''-B_1u_1'''-B_2u_2'''-\frac{bG_v}{h_v}\left[u_1-u_2+w'H\right]'H\\ +(I_{A1}+I_{A2}+I_v)\ddot{w}+I_{B1}\ddot{u}_1'+I_{B2}\ddot{u}_2'-(I_{D1}+I_{D2})\ddot{w}''\end{bmatrix}=F(t)\cdot \tag{3.59}$$

The above equilibrium equations are solved analytically by assuming trigonometric displacement fields.

3.3.1 Analytical solution for simply supported sandwich beam

Navier's solution method is followed to develop an analytical model for simply supported conditions. The boundary conditions for the simply supported beam at x=0, l is as follows:

$$u_1'(0)=u_1'(l)=0 \tag{3.60}$$

$$u_2'(0)=u_2'(l)=0 \tag{3.61}$$

$$w(0)=w(l)=0 \tag{3.62}$$

Trigonometric displacement fields which satisfy the boundary conditions are as follows:

$$u_1=U_{1m}\cos(\alpha x)e^{i\omega t} \tag{3.63}$$

$$u_2=U_{2m}\cos(\alpha x)e^{i\omega t} \tag{3.64}$$

$$w=W_m\sin(\alpha x)e^{i\omega t} \tag{3.65}$$

where $\alpha = \frac{m\pi}{l}$, *m* is the mode number and *ω* is the frequency of vibration. Substituting Eqs. (3.63-3.65) into Eqs. (3.57-3.59), equilibrium equation of the sandwich beam in the dynamic condition is obtained as follows:

$$\left(\begin{bmatrix} K_{11} & K_{12} & K_{13} \\ K_{21} & K_{22} & K_{23} \\ K_{31} & K_{32} & K_{33} \end{bmatrix} - \omega^2 \begin{bmatrix} M_{11} & M_{12} & M_{13} \\ M_{21} & M_{22} & M_{23} \\ M_{31} & M_{32} & M_{33} \end{bmatrix}\right) \begin{Bmatrix} U_{1m} \\ U_{2m} \\ W_m \end{Bmatrix} = \begin{Bmatrix} 0 \\ 0 \\ F(t) \end{Bmatrix}, \tag{3.66}$$

where $K_{11} = A_1\alpha^2 + \frac{b}{h_v}G_v$, $K_{12} = K_{21} = \left(-\frac{b}{h_v}G_v\right)$, $K_{13} = K_{31} = \left(-B_1\alpha^3 + \frac{bH\alpha}{h_v}G_v\right)$,

$K_{22} = A_2\alpha^2 + \frac{b}{h_v}G_v$, $K_{23} = K_{32} = \left(-B_1\alpha^3 - \frac{bH\alpha}{h_v}G_v\right)$,

$K_{33} = \left(\left(D_1 + D_2\right)\alpha^4 + \frac{bH^2\alpha^2}{h_v}G_v\right)$,

$M_{11} = I_{A1}$, $M_{12} = M_{21} = 0$, $M_{13} = M_{31} = -I_{B1}\alpha$, $M_{22} = I_{A2}$, $M_{23} = M_{23} = -I_{B2}\alpha$,

$M_{33} = -\left(\left(I_{A1} + I_v + I_{A2}\right) + (I_{D1} + I_{D2})\alpha^2\right)$.

Eq. (3.66) is written in a simplified form as follows,

$$([K_R + iK_I]_{ij} - \omega^2[M_{ij}])\{\varphi\} = \{F\}, \tag{3.67}$$

where K_{ij}, M_{ij}, *F,* and *φ* are stiffness, mass, force matrices, and Eigenvector, respectively.

Force (*F*) is considered zero for free vibration, and natural frequencies for different modes are obtained by solving Eq. (3.67). Since complex shear modulus is considered for viscoelastic core, the obtained natural frequencies are complex in nature with real and imaginary parts,

$$\omega_n = \omega^*_n(1 + i\eta_b). \tag{3.68}$$

where η_b is the loss factor of the sandwich beam

Once natural frequencies are obtained, the loss of mechanical energy in the form of loss factor is given by Arikoglu and Ozkol (2010),

$$\text{Loss Factor } (\eta_b) = \frac{imag(\omega_n^{\,2})}{real(\omega_n^{\,2})}. \tag{3.69}$$

Neglecting kinetic energy (KE) vanishes inertia terms in the Lagrange density function (L). Also, the imaginary stiffness matrix is zero ([KI]ij=0) in static conditions. This leads to the static equilibrium equation ([Mij]=0) as follows:

$$[K_{ij}]\{\varphi\} = \{F\}\,. \tag{3.70}$$

The force (*F*) can be represented in Fourier form as,

$$F = \sum_{j=1}^{m} F_j \sin\frac{m\pi x}{l}\,, \tag{3.71}$$

where F_j is the force coefficient that varies with the type of load. For point load and harmonic load, *Fj* is F_0 and $F_0\sin(\omega t)$ respectively.

3.4 Validation study for sandwich beam models

3.4.1 Example-1: Sandwich beam with isotropic stiff layer and viscoelastic core

In order to validate the FE and analytical models, an example from Arikoglu and Ozkol (2010) is considered. The thermal stresses are considered zero for the problem. The example consists of two sandwich beams with isotropic stiff layers and a viscoelastic core. The properties and dimension details of the beams are given in Table 3.1. The natural frequencies and the loss factors for different modes are listed in Tables 3.2 and 3.3. respectively. The tables show that the results of both FE and analytical models agree well with referred literature.

Table 3.1: Material properties and dimensions of example 1.

Layers	Properties	Problem 1	Problem 2
Stiff layers	Young's Modulus (GPa)	$E_1=E_2=207$	$E_1=E_2=207$
	Density (kg/m^3)	$\rho_1=\rho_2=7800$	$\rho_1=\rho_2=7800$
	Thickness(mm)	$h_{f1}=0.5$ $h_{f2}=5$	$h_{f1}=0.5$ $h_{f2}=5$
Viscoelastic Layer	Shear Modulus (MPa)	$G_v=0.2615$	$G_v=4$
	Density (kg/m^3)	$\rho_v=2000$	$\rho_v=2000$
	Thickness(mm)	$h_v=2.5$	$h_v=2.5$
	Loss Factor	$\eta_v=0.38$	$\eta_v=0.38$
Whole Beam	Length(mm)	$l=300$	$l=242.5$

Table 3.2: Natural frequencies of example 1 (rad/sec).

		Mode numbers			
Problem		**1**	**2**	**3**	**4**
1	FE model	740.415	2947.82	6624.05	11765.029
	Analytical model	740.2	2947.15	6623.95	11765.7
	Arikoglu et al. 2010)	740.489	2947.775	6623.477	11763.052
	Mead et al. (1970)	740.564	2949	6629.680	11782.60
	Lall et al. (1988)	740.56	2948.290	6629.660	11782.60
	Kung et al.(1998)	741	2949	6630	11783
	Tang et al. (2008)	740.564	2949	6629.680	11782.61
	Gao et al. (2005)	740.6	2949	6629.7	11783
	Yang et al. (2005)	741	2952	6647	-
2	FE model	1187.671	4570.05	10193.805	18052.497
	Analytical model	1187.1	4570.92	10192.98	18052.63
	Arikoglu et al. (2010)	1187.942	4570.224	10192.643	18047.992
	Mead et al. (1970)	1187.960	4573.080	10207.220	18093.90
	Lall et al. (1988)	1187.930	4573.050	10207.190	18093.870
	Tang et al. (2008)	1187.980	4573.140	10207.350	18094.130

Table 3.3: System loss factor values (%) of example 1.

Problem		**Mode 1**	**Mode 2**	**Mode 3**	**Mode 4**
1	FE model	0.44900	0.11505	0.050783	0.028645
	Analytical model	0.44900	0.11480	0.051640	0.028800
	Arikoglu et al. (2010)	0.44180	0.11477	0.051232	0.028859
	Mead et al. (1970)	0.44825	0.11484	0.051306	0.028932
	Lall et al. (1988)	0.45000	0.11000	0.051000	0.029000
	Kung et al.(1998)	0.45000	0.11000	0.051300	0.028900
	Tang et al. (2008)	0.44790	0.11470	0.051209	0.028850
	Gao et al. (2005)	0.45000	0.11000	0.051000	-
	Yang et al. (2005)	0.44819	0.11478	0.051243	0.028870
2	FE model	3.4249	1.0681	0.49622	0.28347
	Analytical model	3.4660	1.0600	0.49800	0.28152
	Arikoglu et al. (2010)	3.4257	1.0679	0.49577	0.28317
	Mead et al. (1970)	3.4271	1.0691	0.49693	0.28431
	Lall et al. (1988)	3.4250	1.0677	0.49577	0.28324
	Tang et al. (2008)	3.4261	1.0682	0.49597	0.28336

3.4.2 Example-2: Sandwich beam with FG stiff layer and viscoelastic core

An FG sandwich beam with a viscoelastic core with pinned-roller (P-R) support is considered as a validation problem. The properties and dimensions of the problem are given in Table 3.4. The natural frequency and loss factors of both FE and analytical models are well in agreement, as shown in Table 3.5.

Table 3.4: Properties of example 2.

Layer	**Material**	**Young's modulus (GPa)**	**Shear modulus (MPa)**	**Density (kg/m^3)**	**Poisons ratio**
FGM	Aluminium	69	-	2698	0.3
	Al_2O_3	348.5	-	3800	0.3
Core	Viscoelastic core	-	0.2615	2000	-
Dimensions (mm)	L=500, b=25, h_{f1}=h_{f2}=5,h_v=1				

Table 3.5: Natural frequency and loss factors of example 2.

Power law index (p)		**Mode number**					
		1		**2**		**3**	
		NF	**LF**	**NF**	**LF**	**NF**	**LF**
1	FE model	68.01	3.17	263.28	0.871	588.49	0.394
	Analytical model	68.18	3.08	264.21	0.836	590.94	0.377
5	FE model	60.75	4.79	230.80	0.14	513.79	0.643
	Analytical model	60.65	4.65	230.93	0.132	514.62	0.605
10	FE model	58.71	4.68	223.31	1.37	497.21	0.632
	Analytical model	58.67	4.62	223.39	1.33	497.80	0.607

3.5 Porosity models and viscoelastic boundary conditions

Various porosity patterns (Hadji and Avcar 2021), such as H, V, O, and X for FG stiff layers and viscoelastic boundary conditions (VBCs), are incorporated into the FE formulation.

3.5.1 Porosity patterns

Porosity is a common defect in manufacturing processes such as casting, powder metallurgy, and coating. The porosity may exist in FG structures due to the difference in melting temperature of the metal and ceramic constituents. Some of the possible types of porosities are shown in Figure 3.5. In H-type, porosity dispersion is equal at every point across the thickness. In O-type, porosity is maximum at the neutral axis and minimum at the top and bottom ends. In X-type, porosity is maximum at either end of the FG layer and minimum at the center. In V-type, porosity is maximum in the ceramic-rich region and minimum in the metal-rich region. The variation of effective material properties, such as elastic modulus and density in various porosity types, are given in Eq. (3.72) to Eq. (3.75).

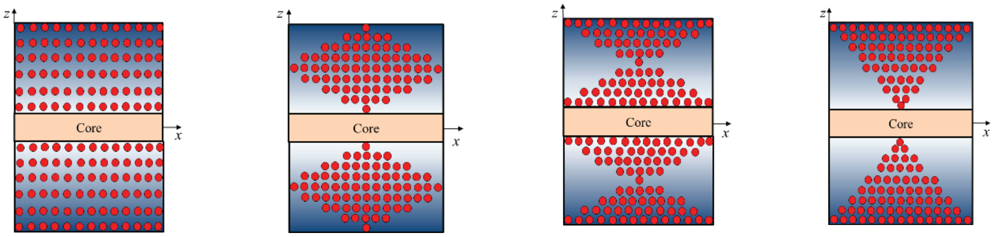

H-Type O-Type X-Type V-Type

Figure 3.5: Porosity distribution models.

- **Homogeneous (H-Type) porous stiff layers**

$$\left.\begin{aligned} P^{(1)}{}_{eff}(z) &= (P_{CM}-P_{MT})V^{(1)}{}_{CM}(z)+P_{MT}-\frac{\beta}{2}\left(P_{CM}+P_{MT}\right) \qquad (h_2 \le z \le h_3) \\ P^{(2)}{}_{eff}(z) &= (P_{CM}-P_{MT})V^{(2)}{}_{CM}(z)+P_{MT}-\frac{\beta}{2}\left(P_{CM}+P_{MT}\right) \qquad (h_0 \le z \le h_1) \end{aligned}\right\}. \tag{3.72}$$

- **O-Type porous stiff layers**

$$\left.\begin{aligned} P^{(1)}{}_{eff} &= (P_{CM}-P_{MT})V^{(1)}{}_{CM}(z)+P_{MT}-\frac{\beta}{2}\left(P_{CM}+P_{MT}\right)\left(1-\left|\frac{2z-\left(h_2+h_3\right)}{(h_3-h_2)}\right|\right) \qquad (h_2 \le z \le h_3) \\ P^{(2)}{}_{eff} &= (P_{CM}-P_{MT})V^{(2)}{}_{CM}(z)+P_{MT}-\frac{\beta}{2}\left(P_{CM}+P_{MT}\right)\left(1-\left|\frac{2z-\left(h_1+h_0\right)}{(h_0-h_1)}\right|\right) \qquad (h_0 \le z \le h_1) \end{aligned}\right\}. \tag{3.73}$$

- **X-Type porous stiff layers**

$$\left.\begin{aligned} P^{(1)}{}_{eff} &= (P_{CM}-P_{MT})V^{(1)}{}_{CM}(z)+P_{MT}-\frac{\beta}{2}\left(P_{CM}+P_{MT}\right)\left(\left|\frac{2z-\left(h_2+h_3\right)}{(h_3-h_2)}\right|\right) \qquad (h_2 \le z \le h_3) \\ P^{(2)}{}_{eff} &= (P_{CM}-P_{MT})V^{(2)}{}_{CM}(z)+P_{MT}-\frac{\beta}{2}\left(P_{CM}+P_{MT}\right)\left(\left|\frac{2z-\left(h_1+h_0\right)}{(h_0-h_1)}\right|\right) \qquad (h_0 \le z \le h_1) \end{aligned}\right\}. \tag{3.74}$$

- **V-Type porous stiff layers**

$$\left.\begin{aligned} P^{(1)}{}_{eff} &= (P_{CM}-P_{MT})V^{(1)}{}_{CM}(z)+P_{MT}-\frac{\beta}{2}\left(P_{CM}+P_{MT}\right)\left(\frac{z-h_2}{h_3-h_2}\right) \qquad (h_2 \le z \le h_3) \\ P^{(2)}{}_{eff} &= (P_{CM}-P_{MT})V^{(2)}{}_{CM}(z)+P_{MT}-\frac{\beta}{2}\left(P_{CM}+P_{MT}\right)\left(\frac{z-h_1}{h_0-h_1}\right) \qquad (h_0 \le z \le h_1) \end{aligned}\right\} \tag{3.75}$$

3.5.2 FE formulation for viscoelastic boundary conditions for beam

Viscoelastic supports or boundaries consist of four complex stiffness terms (Singh et al. 2015) at the beam's first and last node, as shown in Figure 3.6, to constrain four degrees of freedom at each node.

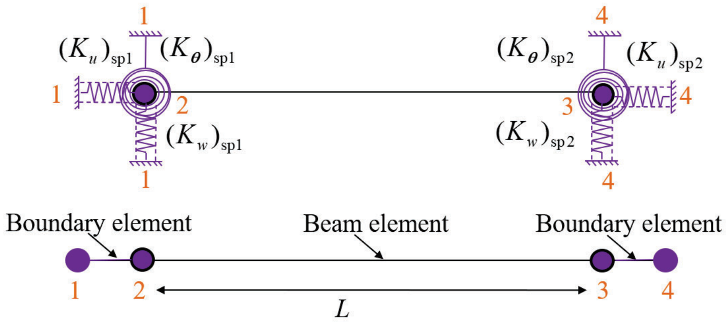

Figure 3.6: Two-noded beam element with viscoelastic boundary condition.

In FE modeling, supports at the boundaries are considered separate two-noded elements. During the assembly of elemental beam stiffness matrices of the beam, a support stiffness matrix is added to the first and last element of the beam. The support stiffness matrix is complex in nature, having real and imaginary parts added to the real and imaginary parts of the beam stiffness, respectively. The elemental support stiffness matrix is given by,

$$[K_{\mathrm{sp}1,2}]=\begin{bmatrix} K_u & 0 & 0 & 0 & -K_u & 0 & 0 & 0 \\ 0 & K_u & 0 & 0 & 0 & -K_u & 0 & 0 \\ 0 & 0 & K_w & 0 & 0 & 0 & -K_w & 0 \\ 0 & 0 & 0 & K_\theta & 0 & 0 & 0 & -K_\theta \\ -K_u & 0 & 0 & 0 & K_u & 0 & 0 & 0 \\ 0 & -K_u & 0 & 0 & 0 & K_u & 0 & 0 \\ 0 & 0 & -K_w & 0 & 0 & 0 & K_w & 0 \\ 0 & 0 & 0 & -K_\theta & 0 & 0 & 0 & K_\theta \end{bmatrix}. \tag{3.76}$$

where K_u, K_w, and K_θ are complex support stiffness coefficients, k_u, k_w and k_θ are storage stiffness values for longitudinal, transverse, and rotation, respectively. η_{sp} is the loss factor of viscoelastic support, as shown in Eq. (3.77).

$$\left.\begin{aligned} K_u &= k_u(1+i\eta_{sp}) \\ K_w &= k_w(1+i\eta_{sp}) \\ K_\theta &= k_\theta(1+i\eta_{sp}) \end{aligned}\right\}. \tag{3.77}$$

In the present study, arbitrary stiffness and loss factors are considered so that the study can be relatable to a sandwich beam supported by various viscoelastic materials with different properties. The variation of boundary stiffness values to achieve some of the common boundary conditions are as follows:

$$\left.\begin{aligned} &\text{At Support 1}: K_{sp1}=k_u=k_w=k_\theta\neq 0 \\ &\text{At Support 2}: K_{sp2}=k_u=k_w=k_\theta=0 \end{aligned}\right\}\ \text{Clamped Free (C-F)}$$

$$\left.\begin{aligned} &\text{At Support 1}: K_{sp1}=k_u=k_w=k_\theta\neq 0 \\ &\text{At Support 2}: K_{sp2}=k_u=k_w=k_\theta\neq 0 \end{aligned}\right\}\ \text{Clamped-Clamped (C-C)}$$

$$\left.\begin{aligned} &\text{At Support 1}: K_{sp1}=k_u=k_w=k_\theta\neq 0 \\ &\text{At Support 2}: K_{sp2}=k_u=k_w\neq 0\ \&\ k_\theta=0 \end{aligned}\right\}\ \text{Clamped-Pinned (C-P)}$$

$$\left.\begin{array}{l}\text{At Support 1}: K_{sp1}=k_u = k_w \neq 0\,\&\,k_\theta=0\\ \text{At Support 2}: K_{sp2}=k_u = k_w \neq 0\,\&\,k_\theta=0\end{array}\right\}\text{Pinned-Pinned (P-P)}$$

$$\left.\begin{array}{l}\text{At Support 1}: k_\theta = 0; k_u = k_w \neq 0\,\&\,K_{sp1}=k_u = k_w\\ \text{At Support 2}: k_u=k_\theta = 0;\ k_w \neq 0\,\&\,K_{sp2}=k_w\end{array}\right\}\text{Pinned-Roller (P-R)}$$

3.5.3 Validation and convergence study of viscoelastic boundary conditions

The validation and convergence study is done considering two cases. In case 1 (free vibration), the stiffness matrix and mass matrix accuracy is examined. Case 2 analyzes the geometric nonlinear matrix and temperature effects on sandwich beams.

3.4.1.1 Case-1: Free vibration of sandwich beam

As the exact problem statement is not documented in previous works of literature, the model is simplified to an isotropic sandwich beam (Arikoglu and Ozkol 2010) with a viscoelastic core by considering the power law index (*p*), porosity volume fraction (β), viscoelastic boundary loss factor (η_{sp}) and rise in temperature (ΔT) as zero. Table 3.6 shows the material properties of the problem. Figure 3.7 and Figure 3.8 depict the natural frequency (NF) and loss factor (LF) for varying support stiffness values (SSVs) for case 1, Table 3.7. and 3.8. show the converged natural frequency and loss factor for case 1. The results are good and in agreement with referred works of literature.

Table 3.6: Material properties and dimensions of case 1.

Layers	Properties	Case 1
Stiff layers	Young's Modulus (GPa)	E_1=E_2=207
	Density (kg/m^3)	ρ_1= ρ_2=7800
	Thickness(mm)	h_{f1}=0.5, h_{f2}=5
Viscoelastic Layer	Shear Modulus (MPa)	G_v=0.2615
	Density (kg/m^3)	ρ_v=2000
	Thickness(mm)	h_v=2.5
	Loss Factor	η_v=0.38
Whole Beam	Length(mm)	*l*=300

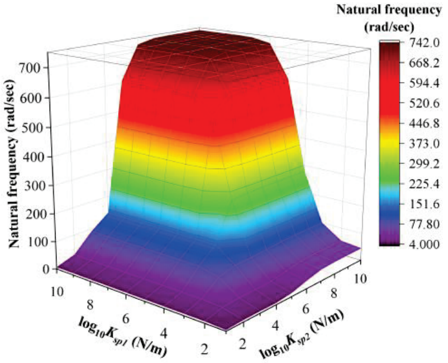

Figure 3.7: The natural frequency of case 1 (P-R).

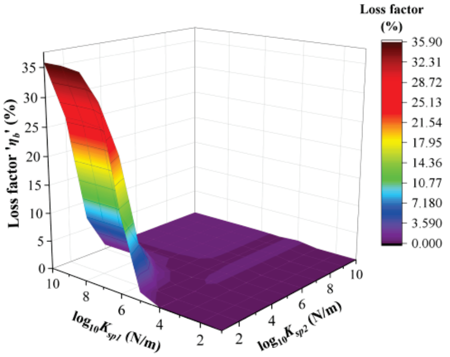

Figure 3.8: The loss factor of case 1 (P-R).

Table 3.7: Natural frequency of case 1 (rad/sec).

		Mode numbers			
Problem		**1**	**2**	**3**	**4**
	FE model	740.415	2947.82	6624.05	11765.029
1	Analytical model	740.2	2947.15	6623.95	11765.7
	Arikoglu et al. (2010)	740.489	2947.775	6623.477	11763.052
	Mead et al. (1970)	740.564	2949	6629.680	11782.60
	Lall et al. (1988)	740.56	2948.290	6629.660	11782.60
	Kung et al.(1998)	741	2949	6630	11783
	Tang et al. (2008)	740.564	2949	6629.680	11782.61
	Gao et al. (2005)	740.6	2949	6629.7	11783
	Yang et al. (2005)	741	2952	6647	-

Table 3.8: System loss factor values (%) of case 1.

Problem		**Mode 1**	**Mode 2**	**Mode 3**	**Mode 4**
	FE model	0.44900	0.11505	0.050783	0.028645
1	Analytical model	0.44900	0.11480	0.051640	0.028800
	Arikoglu et al. (2010)	0.44180	0.11477	0.051232	0.028859
	Mead et al. (1970)	0.44825	0.11484	0.051306	0.028932
	Lall et al. (1988)	0.45000	0.11000	0.051000	0.029000
	Kung et al.(1998)	0.45000	0.11000	0.051300	0.028900
	Tang et al. (2008)	0.44790	0.11470	0.051209	0.028850
	Gao et al. (2005)	0.45000	0.11000	0.051000	-
	Yang et al. (2005)	0.44819	0.11478	0.051243	0.028870

3.4.1.2 *Case-2: Thermal buckling of sandwich beam*

The clamped-clamped (C-C) sandwich beam with isotropic stiff layers and viscoelastic core is considered for the study (Bhangale and Ganesan 2006). The power law index (p), porosity volume fraction (β), and viscoelastic boundary loss factor (η_{sp}) are assumed as zero to validate with literature problem. The material properties of the problem are given in Table. 3.9.

Table 3.9: Material properties and dimension of case 2 (Bhangale and Ganesan 2006).

Material	**Young's modulus (GPa)**	**Shear modulus (GPa)**	**Density (kg/m^3)**	**Poisons ratio**	**Loss factor (η_v)**	**Coefficient of thermal expansion x10^{-6}/^{0}C**
Viscoelastic Core	-	9.8	2600	0.49	0.1	-
Steel	206	-	7850	0.3	-	14
Dimensions	L=500mm, b=50mm, h_{f1}=h_{f2}= h_v=3mm					

Figures 3.9 and 3.10 show the critical buckling parameter (CBP) and critical buckling temperature (CBT) (T_{room}=30^{0}C), respectively, for varying support stiffness values. Table 3.10. gives converged CBT which is good and in agreement with referred literature.

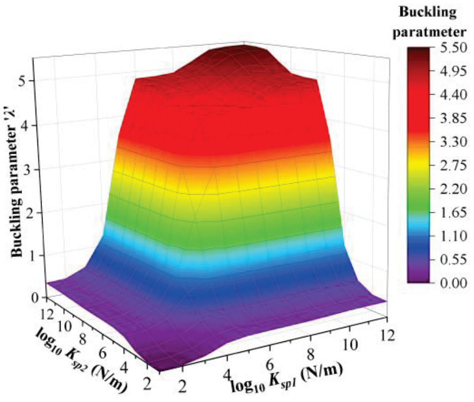

Figure 3.9: CBP of the case 2.

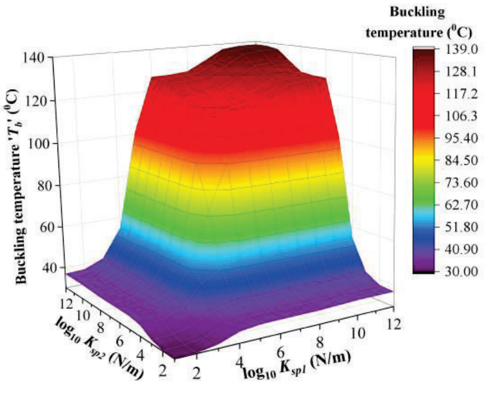

Figure 3.10: CBT of the case 2.

Table 3.10: Convergence of CBT of the sandwich beam.

	Critical buckling temperature (^{0}C)			
Number of elements	**10 elements**	**20 elements**	**30 elements**	**40 elements**
Present	142.00	139.336	138.85	138.85
Bhangale and Ganesan (2006)	142.55	139.16	138.55	-

3.6 ANALYTICAL MODEL FOR FG SANDWICH PLATE

Consider a three-layered sandwich plate with two stiff and a viscoelastic core of length l and breadth $b,$ as shown in Figure 3.11. The thickness of the upper stiff layer, core, and lower stiff layer is $h_{f1},$ $h_{f2},$ and $h_v,$ respectively.

The overall thickness of the sandwich plate is H_T. The neutral axis of the upper and lower stiff layers is at the distance z_1 and $z_2,$ respectively, from the core's center. H is the distance between the neutral axis of stiff layers. E_1 and E_2 are Young's modulus of upper and lower stiff layers, respectively. $h_1,$ $h_2,$ $h_3,$ and h_4 are measured from the center of the core. Complex shear modulus G_v is considered for the viscoelastic core. For FG stiff layer Young's modulus and density vary with z coordinate (thickness).

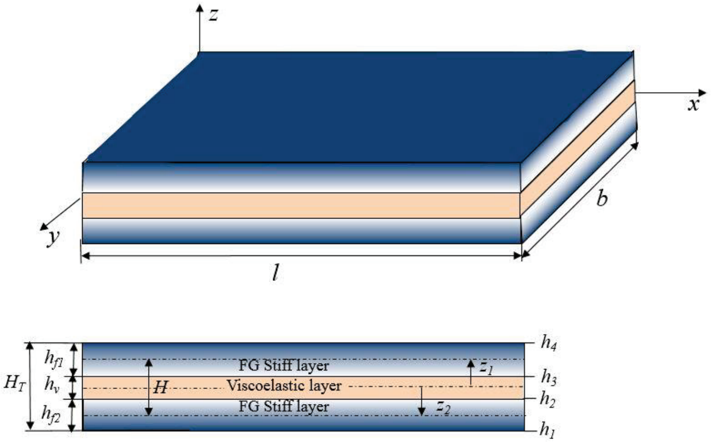

z
x
b
y
l
h_{f1}
H_T
h_v
h_{f2}
FG Stiff layer
H
Viscoelastic layer
FG Stiff layer
z_1
z_2
h_4
h_3
h_2
h_1

Figure 3.11: FG Sandwich plate.

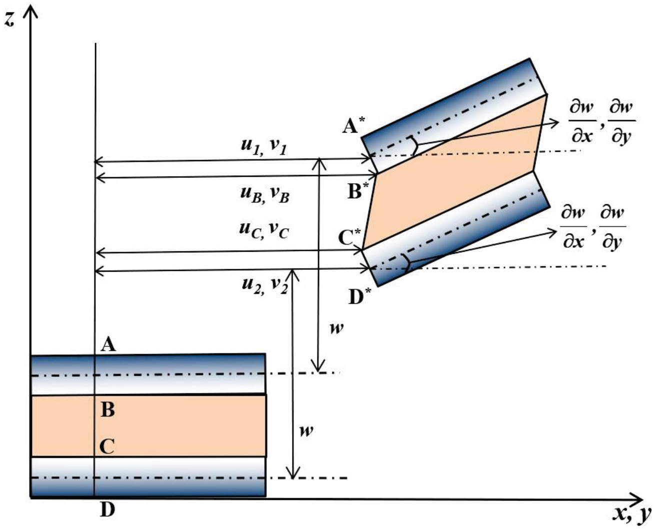

z
u_1, v_1
A*
$\frac{\partial w}{\partial x}, \frac{\partial w}{\partial y}$
u_B, v_B
B*
u_C, v_C
C*
$\frac{\partial w}{\partial x}, \frac{\partial w}{\partial y}$
u_2, v_2
D*
w
A
B
C
w
D
x, y

Figure 3.12: Kinematics of sandwich plate subjected to transverse load.

The kinematics of the sandwich plate is derived based on the same assumptions as that of the sandwich beam. Figure 3.12 shows the kinematics of the sandwich plate.
The axial and transverse displacements are given as follows:

$$u=\begin{cases} u_1-(z-z_1)\dfrac{\partial w}{\partial x} & (h_3\le z\le h_4) \\ u_2-(z-z_2)\dfrac{\partial w}{\partial x} & (h_1\le z\le h_2) \end{cases}, \tag{3.78}$$

$$v=\begin{cases} v_1-(z-z_1)\dfrac{\partial w}{\partial y} & (h_3\le z\le h_4) \\ v_2-(z-z_2)\dfrac{\partial w}{\partial y} & (h_1\le z\le h_2) \end{cases}, \tag{3.79}$$

$$w_1=w_2=w, \tag{3.80}$$

where u_1, u_2, v_1, and v_2 are the axial displacement at the neutral axis along the length and breadth of stiff layers (upper and lower). z_1 and z_2 are the distance of the neutral axis of stiff layers from the center of the core, and w is transverse deflection.

3.6.1 Static and dynamic equilibrium equations of sandwich plate

The strains associated with axial displacements are given by,

$$\begin{Bmatrix}\varepsilon_{xx}\\ \varepsilon_{yy}\\ \gamma_{xy}\end{Bmatrix}_{(i)}=\begin{Bmatrix}\varepsilon_{0xx}\\ \varepsilon_{0yy}\\ \gamma_{0xy}\end{Bmatrix}_{(i)}-(z-z_i)\begin{Bmatrix}\kappa_{xx}\\ \kappa_{yy}\\ \kappa_{xy}\end{Bmatrix}_{(i)}, \tag{3.81}$$

$$\begin{Bmatrix}\varepsilon_{0xx}\\ \varepsilon_{0yy}\\ \gamma_{0xy}\end{Bmatrix}_{(i)}=\begin{Bmatrix}\dfrac{\partial u_i}{\partial x}\\ \dfrac{\partial v_i}{\partial x}\\ \dfrac{\partial u_i}{\partial y}+\dfrac{\partial v_i}{\partial x}\end{Bmatrix},\begin{Bmatrix}\kappa_{xx}\\ \kappa_{yy}\\ \kappa_{xy}\end{Bmatrix}_{(i)}=\begin{Bmatrix}\dfrac{\partial^2 w}{\partial x^2}\\ \dfrac{\partial^2 w}{\partial y^2}\\ 2\dfrac{\partial^2 w}{\partial x\partial y}\end{Bmatrix}, \tag{3.82}$$

where i=1 and 2

From constitutive relations for stress and strains of the plate are given as follows:

$$\begin{Bmatrix}\sigma_{xx}\\ \sigma_{yy}\\ \tau_{xy}\end{Bmatrix}_{(i)}=\begin{bmatrix}C_{11} & C_{12} & 0\\ C_{12} & C_{22} & 0\\ 0 & 0 & C_{66}\end{bmatrix}\begin{Bmatrix}\varepsilon_{xx}\\ \varepsilon_{yy}\\ \gamma_{xy}\end{Bmatrix}_{(i)}, \tag{3.83}$$

where, $C_{11} = C_{22} = \dfrac{E(z)}{1-(\nu^2)}, C_{12} = \nu C_{11}, C_{66} = \dfrac{E(z)}{2(1+\nu)}$.

Strain energy (U_{strain}), kinematic energy (*KE*), and energy due to external work done (U_{ext}) by the force *F* are written as:

$$U_{strain} = \frac{1}{2}\int_V \left[\sigma_{xx}\varepsilon_{xx} + \sigma_{yy}\varepsilon_{yy} + \tau_{xy}\gamma_{xy} + \tau_{xz}\gamma_{xz} + \tau_{yz}\gamma_{yz}\right]_{(i)} dV\,, \tag{3.84}$$

Where; $\tau_{xz} = \dfrac{G_v}{h_v}\left[u_1 - u_2 + \dfrac{\partial w}{\partial x}H\right]$; $\tau_{yz} = \dfrac{G_v}{h_v}\left[v_1 - v_2 + \dfrac{\partial w}{\partial y}H\right]$.

$$KE = \frac{1}{2}\int_V \rho\left(\dot{u}^2 + \dot{v}^2 + \dot{w}^2\right)_{(i)} dV\,, \tag{3.85}$$

$$U_{ext} = Fw\,. \tag{3.86}$$

The total energy of a sandwich plate is defined as:

$$\prod = \int_0^l \int_0^b L dx dy\,. \tag{3.87}$$

The Lagrange density function for the system in vibration is given as,

$$L = KE - (U_{strain} - U_{ext})\,. \tag{3.88}$$

Substituting displacements and energies in Eq. (3.88), *L* can be rewritten as:

$$L = \frac{1}{2}\left\{\begin{array}{l}
\left[\sum_{i=1}^{2}\left(\begin{array}{l} I_A^{(i)}\left[\left(\dfrac{\partial u_i}{\partial t}\right)^2 + \left(\dfrac{\partial v_i}{\partial t}\right)^2 + \left(\dfrac{\partial w}{\partial t}\right)^2\right] - 2I_B^{(i)}\left(\dfrac{\partial u_i}{\partial t}\dfrac{\partial^2 w}{\partial t\partial x} + \dfrac{\partial v_i}{\partial t}\dfrac{\partial^2 w}{\partial t\partial y}\right) + \\ I_D^{(i)}\left(\left(\dfrac{\partial^2 w}{\partial t\partial x}\right)^2 + \left(\dfrac{\partial^2 w}{\partial t\partial y}\right)^2\right) \end{array}\right) + I_v\left(\dfrac{\partial w}{\partial t}\right)^2\right] - \\
\left[\begin{array}{l} \sum_{i=1}^{2}\left(\begin{array}{l} A_{11}^{(i)}\left(\dfrac{\partial u_i}{\partial x}\right)^2 + A_{22}^{(i)}\left(\dfrac{\partial v_i}{\partial y}\right)^2 - 2(B_{11}^{(i)} + B_{12}^{(i)})\left(\dfrac{\partial u_i}{\partial x}\dfrac{\partial^2 w}{\partial x^2}\right) - 2(B_{22}^{(i)} + B_{12}^{(i)})\left(\dfrac{\partial v_i}{\partial y}\dfrac{\partial^2 w}{\partial y^2}\right) + \\ D_{11}^{(i)}\left(\dfrac{\partial^2 w}{\partial x^2}\right)^2 + D_{22}^{(i)}\left(\dfrac{\partial^2 w}{\partial y^2}\right)^2 + 2A_{12}^{(i)}\left(\dfrac{\partial u_i}{\partial x}\dfrac{\partial v_i}{\partial y}\right) + 2D_{12}^{(i)}\left(\dfrac{\partial^2 w}{\partial x^2}\dfrac{\partial^2 w}{\partial y^2}\right) + \\ A_{66}^{(i)}\left[\left(\dfrac{\partial u_i}{\partial x}\right)^2 + \left(\dfrac{\partial v_i}{\partial y}\right)^2 + 2\dfrac{\partial u_i}{\partial x}\dfrac{\partial v_i}{\partial y}\right] - 4B_{66}^{(i)}\left[\dfrac{\partial u_i}{\partial x}\dfrac{\partial^2 w}{\partial x\partial y} + \dfrac{\partial v_i}{\partial y}\dfrac{\partial^2 w}{\partial x\partial y}\right] + D_{66}^{(i)}\left(\dfrac{\partial^4 w}{\partial x^2\partial y^2}\right)^2 \end{array}\right) + \\ \dfrac{G_v}{h_v}\left[u_1 - u_3 + \dfrac{\partial w}{\partial x}H\right]^2 + \dfrac{G_v}{h_v}\left[v_1 - v_3 + \dfrac{\partial w}{\partial y}H\right]^2 - Fw \end{array}\right]
\end{array}\right. \tag{3.89}$$

where *A, B,* and *D* are stiffness coefficients, and I_A, I_B, and I_D are inertial coefficients of graded stiff layers:

$$(A_{jk}^{(1)},B_{jk}^{(1)},D_{jk}^{(1)})=\int_{h_3}^{h_4}\left[1,(z-z_1),(z-z_1)^2\right]C_{jk}^{(1)}dz\,, \tag{3.90}$$

$$A_{jk}^{(2)},B_{jk}^{(2)},D_{jk}^{(2)})=\int_{h_1}^{h_2}\left[1,(z-z_2),(z-z_2)^2\right]C_{jk}^{(2)}dz\,, \tag{3.91}$$

$$(I_A^{(1)},I_B^{(1)},I_D^{(1)})=\int_{h_3}^{h_4}\left[1,(z-z_1),(z-z_1)^2\right]\rho^{(1)}dz\,, \tag{3.92}$$

$$(I_A^{(2)},I_B^{(2)},I_D^{(2)})=\int_{h_1}^{h_2}\left[1,(z-z_2),(z-z_2)^2\right]\rho^{(2)}dz\,, \tag{3.93}$$

where, *j= 1, 2,* 6; *k=1, 2.*

The energy equation has five functions (u_1, u_2, v_1, v_2, and w) and three variables (x, y, and t). Governing equations of motion for each function are derived using the Euler-Lagrange equation.

If there is a single unknown functional f dependent on three variables, X_1, X_2, and X_3, and if the functional depends on second-order derivatives of f such that:

$$I[f]=\int_{\Omega}L(X_1,X_2,X_3,f,f_1,f_{11},f_{12},f_{13}......,f_m,f_{mm},f_{mn})d\Omega\,, \tag{3.94}$$

$$f_m=\frac{\partial f}{\partial X_m}\,,\ f_{mn}=\frac{\partial^2 f}{\partial X_m\partial X_n}\,, \tag{3.95}$$

$$\frac{\partial L}{\partial f}-\frac{\partial}{\partial X_m}\left(\frac{\partial L}{\partial f_m}\right)+\frac{\partial^2}{\partial X_m\partial X_m}\left(\frac{\partial L}{\partial f_{mm}}\right)+\frac{\partial^2}{\partial X_m\partial X_n}\left(\frac{\partial L}{\partial f_{mn}}\right)=0\,. \tag{3.96}$$

m=1, 2 & 3 and n=1, 2 & 3

By substituting Eq. (3.89) in Eq. (3.96), partial differential equations of motion are derived:

$$\begin{gathered}A_{11}^{(1)}\frac{\partial^2u_1}{\partial x^2}-B_{11}^{(1)}\frac{\partial^3w}{\partial x^3}+A_{12}^{(1)}\frac{\partial^2v_1}{\partial x\partial y}-\left(B_{12}^{(1)}+2B_{66}^{(1)}\right)\frac{\partial^3w}{\partial x\partial y^2}+A_{66}^{(1)}\left(\frac{\partial^2u_1}{\partial y^2}+\frac{\partial^2v_1}{\partial x\partial y}\right)\\-\frac{G_v}{h_v}\left(u_1-u_2+H\frac{\partial w}{\partial x}\right)-I_A^{(1)}\left(\frac{\partial^2u_1}{\partial t^2}\right)+I_B^{(1)}\frac{\partial^3w}{\partial x\partial t^2}=0\end{gathered}\,, \tag{3.97}$$

$$\begin{array}{l} A_{11}^{(2)}\dfrac{\partial^2 u_2}{\partial x^2} - B_{11}^{(2)}\dfrac{\partial^3 w}{\partial x^3} + A_{12}^{(2)}\dfrac{\partial^2 v_2}{\partial x\partial y} - \left(B_{12}^{(2)} + 2B_{66}^{(2)}\right)\dfrac{\partial^3 w}{\partial x\partial y^2} + A_{66}^{(2)}\left(\dfrac{\partial^2 u_2}{\partial y^2} + \dfrac{\partial^2 v_2}{\partial x\partial y}\right) \\ + \dfrac{G_v}{h_v}\left(u_1 - u_2 + H\dfrac{\partial w}{\partial x}\right) - I_A^{(2)}\left(\dfrac{\partial^2 u_2}{\partial t^2}\right) + I_B^{(2)}\dfrac{\partial^3 w}{\partial x\partial t^2} = 0 \end{array} , \quad (3.98)$$

$$\begin{array}{l} A_{22}^{(1)}\dfrac{\partial^2 v_1}{\partial y^2} - B_{22}^{(1)}\dfrac{\partial^3 w}{\partial y^3} + A_{12}^{(1)}\dfrac{\partial^2 u_1}{\partial x\partial y} - \left(B_{12}^{(1)} + 2B_{66}^{(1)}\right)\dfrac{\partial^3 w}{\partial x^2\partial y} + A_{66}^{(1)}\left(\dfrac{\partial^2 v_1}{\partial x^2} + \dfrac{\partial^2 u_1}{\partial x\partial y}\right) \\ - \dfrac{G_v}{h_v}\left(v_1 - v_2 + H\dfrac{\partial w}{\partial y}\right) - I_A^{(1)}\left(\dfrac{\partial^2 v_1}{\partial t^2}\right) + I_B^{(1)}\dfrac{\partial^3 w}{\partial y\partial t^2} = 0 \end{array} , \quad (3.99)$$

$$\begin{array}{l} A_{22}^{(2)}\dfrac{\partial^2 v_2}{\partial y^2} - B_{22}^{(2)}\dfrac{\partial^3 w}{\partial y^3} + A_{12}^{(2)}\dfrac{\partial^2 u_2}{\partial x\partial y} - \left(B_{12}^{(2)} + 2B_{66}^{(2)}\right)\dfrac{\partial^3 w}{\partial x^2\partial y} + A_{66}^{(2)}\left(\dfrac{\partial^2 v_2}{\partial x^2} + \dfrac{\partial^2 u_2}{\partial x\partial y}\right) \\ + \dfrac{G_v}{h_v}\left(v_1 - v_2 + H\dfrac{\partial w}{\partial y}\right) - I_A^{(2)}\left(\dfrac{\partial^2 v_2}{\partial t^2}\right) + I_B^{(2)}\dfrac{\partial^3 w}{\partial y\partial t^2} = 0 \end{array} , \quad (3.100)$$

$$\begin{array}{l} \displaystyle\sum_{i=1}^{2}\left(\begin{array}{l} -D_{11}^{(i)}\dfrac{\partial^4 w}{\partial x^4} + B_{11}^{(i)}\dfrac{\partial^3 u_i}{\partial x^3} + \left(B_{12}^{(i)} + 2B_{66}^{(i)}\right)\left(\dfrac{\partial^3 u_i}{\partial x\partial y^2} + \dfrac{\partial^3 v_i}{\partial x^2\partial y}\right) - 2\left(D_{12}^{(i)} + 2D_{66}^{(i)}\right)\dfrac{\partial^4 w}{\partial x^2\partial y^2} \\ -D_{22}^{(i)}\dfrac{\partial^4 w}{\partial y^4} + B_{22}^{(i)}\dfrac{\partial^3 v_i}{\partial y^3} + I_D^{(i)}\left(\dfrac{\partial^4 w}{\partial x^2\partial t^2} + \dfrac{\partial^4 w}{\partial y^2\partial t^2}\right) - I_A^{(i)}\dfrac{\partial^2 w}{\partial t^2} - I_B^{(i)}\left(\dfrac{\partial^3 u_i}{\partial x\partial t^2} + \dfrac{\partial^3 v_i}{\partial y\partial t^2}\right) \end{array}\right) - I_v\dfrac{\partial^2 w}{\partial t^2} \\ + \dfrac{G_v H}{h_v}\left(\dfrac{\partial u_1}{\partial x} + \dfrac{\partial v_1}{\partial x} - \dfrac{\partial u_2}{\partial x} - \dfrac{\partial v_2}{\partial x} + H\dfrac{\partial^2 w}{\partial x^2} + H\dfrac{\partial^2 w}{\partial y^2}\right) - F = 0 \end{array}$$

.

(3.101)

3.6.2 Analytical solution for the sandwich plate with simple support

Navier's approach solves the derived governing equations for all side simply supported (SSSS) conditions. The trigonometric displacement fields are considered as follows:

$u_1 = U_{1mn}\cos(\alpha x)\sin(\beta y)e^{i\omega t}$; $u_2 = U_{2mn}\cos(\alpha x)\sin(\beta y)e^{i\omega t}$,

$v_1 = V_{1mn}\sin(\alpha x)\cos(\beta y)e^{i\omega t}$; $v_2 = V_{2mn}\sin(\alpha x)\cos(\beta y)e^{i\omega t}$,

$w = W_{mn}\sin(\alpha x)\sin(\beta y)e^{i\omega t}$, (3.102)

where $i = \sqrt{-1}$, $\alpha = \dfrac{m\pi}{l}$, $\beta = \dfrac{n\pi}{b}$ and ω is the natural frequency.

where *m* and *n* are mode numbers of the sandwich plate in dynamic conditions Substituting Eq. (3.102) in Eqs. (3.97-3.101), the solution is obtained in the form of the matrix:

$$\left(\begin{bmatrix} k_{11} & k_{12} & k_{13} & k_{14} & k_{15} \\ k_{12} & k_{22} & k_{23} & k_{24} & k_{25} \\ k_{13} & k_{23} & k_{33} & k_{34} & k_{35} \\ k_{14} & k_{24} & k_{34} & k_{44} & k_{45} \\ k_{15} & k_{25} & k_{35} & k_{45} & k_{55} \end{bmatrix} - \omega^2 \begin{bmatrix} m_{11} & m_{12} & m_{13} & m_{14} & m_{15} \\ m_{12} & m_{22} & m_{23} & m_{24} & m_{25} \\ m_{13} & m_{23} & m_{33} & m_{34} & m_{35} \\ m_{14} & m_{24} & m_{34} & m_{44} & m_{45} \\ m_{15} & m_{25} & m_{35} & m_{45} & m_{55} \end{bmatrix}\right) \begin{Bmatrix} U_{1mn} \\ U_{2mn} \\ V_{1mn} \\ V_{2mn} \\ W_{mn} \end{Bmatrix} = \begin{Bmatrix} 0 \\ 0 \\ 0 \\ 0 \\ F_{mn} \end{Bmatrix}, \tag{3.103}$$

where,

$$k_{11} = A_{11}^{(1)}\alpha^2 + A_{66}^{(1)}\beta^2 + \left(\frac{G_v}{h_v}\right); \quad k_{12} = k_{34} = -\left(\frac{G_v}{h_v}\right); \quad k_{13} = (A_{12}^{(1)} + A_{66}^{(1)})\alpha\beta; \quad k_{14} = 0;$$

$$k_{15} = -B_{11}^{(1)}\alpha^3 - \left(B_{12}^{(1)} + 2B_{66}^{(1)}\right)\alpha\beta^2 + \left(\frac{G_v}{h_v}\right)\alpha H; \quad k_{22} = A_{11}^{(2)}\alpha^2 + A_{66}^{(2)}\beta^2 + \left(\frac{G_v}{h_v}\right); \quad k_{23} = 0;$$

$$k_{24} = (A_{12}^{(2)} + A_{66}^{(2)})\alpha\beta; \quad k_{25} = -B_{11}^{(2)}\alpha^3 - \left(B_{12}^{(2)} + 2B_{66}^{(2)}\right)\alpha\beta^2 - \left(\frac{G_v}{h_v}\right)\alpha H;$$

$$k_{33} = A_{22}^{(1)}\beta^2 + A_{66}^{(1)}\alpha^2 + \left(\frac{G_v}{h_v}\right); \quad k_{35} = -B_{22}^{(1)}\beta^3 - \left(B_{12}^{(1)} + 2B_{66}^{(1)}\right)\alpha^2\beta + \left(\frac{G_v}{h_v}\right)\beta H;$$

$$k_{44} = A_{22}^{(2)}\beta^2 + A_{66}^{(2)}\alpha^2 + \left(\frac{G_v}{h_v}\right); \quad k_{45} = -B_{22}^{(2)}\beta^3 - \left(B_{12}^{(2)} + 2B_{66}^{(2)}\right)\alpha^2\beta - \left(\frac{G_v}{h_v}\right)\beta H;$$

$$k_{55} = \sum_{i=1}^{2}\left(D_{11}^{(i)}\alpha^4 + 2\left(D_{12}^{(i)} + 2D_{66}^{(i)}\right)\alpha^2\beta^2 + D_{22}^{(i)}\beta^4\right) + \left(\frac{G_v}{h_v}\right)\alpha^2 H^2 + \left(\frac{G_v}{h_v}\right)^2 \beta H^2. \tag{3.104}$$

$$m_{11} = I_A^{(1)}; \quad m_{12} = m_{13} = m_{14} = 0; \; m_{15} = -I_B^{(1)}\alpha; \quad m_{22} = I_A^{(2)};$$

$$m_{23} = m_{24} = 0; \; m_{25} = -I_B^{(2)}\beta; \quad m_{33} = I_A^{(1)}; \; m_{34} = 0; \; m_{35} = -I_B^{(1)}\beta;$$

$$m_{44} = I_A^{(2)}; \; m_{45} = -I_B^{(2)}\beta; \; m_{55} = \left(I_A^{(1)} + I_A^{(2)} + I_v\right) + \left(I_D^{(1)} + I_D^{(2)}\right)\left(\alpha^2 + \beta^2\right). \tag{3.105}$$

Eq. (3.103) is written in a simplified form as follows,

$$([K_R + iK_I]_{ij} - \omega^2[M_{ij}])\{\varphi\} = \{F\}, \tag{3.106}$$

where, $\omega_n = \omega^*{}_n(1 + i\eta_p)$, (3.107)

η_p is the loss factor of the sandwich plate.

The loss factor of the sandwich plate is given by,

$$\text{Loss Factor } (\eta_p) = \frac{imag(\omega_n{}^2)}{real(\omega_n{}^2)}. \tag{3.108}$$

Neglecting kinetic energy (*KE*) vanishes inertia terms in the Lagrange density function (*L*). Also, the imaginary stiffness matrix is zero ($[K_I]_{ij}$=0) in static conditions. This leads to the static equilibrium equation ($[M_{ij}]$=0) as follows:

$$[K_{ij}]\{\varphi\}=\{F\}\,. \tag{3.109}$$

The force (*F*) can be represented in Fourier form as,

$$F=\sum_{j=1}^{m}\sum_{k=1}^{n}F_{jk}\sin\frac{m\pi x}{l}\sin\frac{n\pi y}{b}\,. \tag{3.110}$$

where F_{jk} is the force coefficient that varies with the type of load.

For UDL and harmonic load,

$$F_{jk}=\frac{4}{lb}\int_0^l\int_0^b F_0\sin\frac{m\pi x}{l}\sin\frac{n\pi y}{b}\,dxdy\ \ ,F_0\sin(\omega t)\,. \tag{3.111}$$

3.6.3 Validation of analytical sandwich plate model

The proposed model is validated for different combinations of sandwich plates by considering various examples from available works of literature.

3.6.3.1 Example-1: FG stiff layers with homogeneous flexible core

In this example, a square simply supported sandwich plate is considered with Al-Al_2O_3 FG upper and lower stiff layers in which Al_2O_3 volume fraction (V_{CM}) varies as per the power law index (*p*=1). The core is made of aluminium. The properties of each component of the sandwich plate are given in Table 3.11. The rule of mixture governs the properties along the thickness of FG stiff layers. Three different stiff layer and core thickness ratios are considered (1-2-1, 1-1-1, and 2-1-2). The non-dimensional natural frequencies ($\bar{\omega}$) of example 1 for various modes are tabulated in comparison with previous works of literature in Table 3.12. Non-dimensional natural frequency ($\bar{\omega}$) is defined as:

$$\bar{\omega}=\frac{\omega l^2}{h}\sqrt{\frac{\rho_0}{E_0}}\text{, where }\rho_0=1kg/m^3\text{ and }E_0=1GPa \tag{3.112}$$

Table 3.11: Properties of sandwich plate materials of example 1.

Material	**Young's modulus (GPa)**	**Density (kg/m^3)**	**Poisons ratio**
Aluminium (Al)	70	2707	0.3
Aluminium oxide (Al_2O_3)	380	3800	0.3

Table 3.12: Non-dimensional natural frequency of example 1.

Source	***l/h*=10**			***l/h*=100**		
	1-1-1	**1-2-1**	**2-1-2**	**1-1-1**	**1-2-1**	**2-1-2**
Present model	1.675	1.568	1.71	1.744	1.644	1.791
Moita et al. (2018)	1.661	1.587	1.699	1.747	1.644	1.785
Liu et al. (2015)	1.656	1.562	1.674	1.746	1.644	1.790
Li et al. (2008)	1.631	1.558	1.674	1.754	1.675	1.792

Table 3.12 shows that an increase in core thickness reduces the natural frequency, whereas an increase in stiff layer thickness enhances the frequency. It means the structure's stiffness is inversely proportional to the softcore thickness and directly proportional to the stiff layer thickness.

3.6.3.2 Example-2: Isotropic stiff layers with viscoelastic core

In this example, isotropic stiff layers are considered with the viscoelastic core. Table 3.13 gives the material properties and dimensions of example 2. The natural frequency and loss factors, for example 2, are presented in Tables 3.14 and 3.15, respectively.

After discussing two examples, it is seen that the results obtained from the present solution method agree well with the available works of literature. The developed sandwich beam and plate formulations are used to study the static and dynamic behavior of FG sandwich structures with the viscoelastic core.

Table 3.13: Dimensions and material properties of example 2.

Material	**Density (kg/m^3)**	**Young's modulus (GPa)**	**Shear modulus (MPa)**	**Poisons ratio**	**Loss factor**
Stiff layers	2740	68.9	-	0.3	-
Viscoelastic core	999	-	0.896	0.49	0.5
Dimensions	l =348mm; b=304.8mm; h_{stiff}=0.762mm; h_{core}=0.254mm				

Table 3.14: Natural frequency (Hz) of example 2 in different modes of vibration.

Source	1,1	2,1	1,2	2,2	1,3
Present model	60.506	115.81	131.072	179.19	196.167
Wang et al. (2000)	60.300	115.40	130.600	178.70	195.700
Johnson et al. (1982)	57.400	113.20	129.300	179.30	196.000
Huang et al. (2014)	57.270	112.12	127.240	-	-

Table 3.15: Loss factor of example 2 in different modes of vibration.

Source	1,1	2,1	1,2	2,2	1,3
Present model	0.190	0.203	0.199	0.181	0.174
Wang et al. (2000)	0.190	0.203	0.199	0.181	0.174
Johnson et al. (1982)	0.176	0.188	0.188	0.153	0.153
Huang et al. (2014)	0.178	0.192	0.195	-`	-

3.7 SUMMARY

In this chapter, a detailed formulation of the static and dynamic behavior of FG sandwich beams and plates with a viscoelastic interlayer is presented. In the first section, the FE model is developed to study the static bending, buckling, free, and forced vibration of FG sandwich beams with a viscoelastic core in a thermal environment. The developed FE model is validated with an analytical model, shown in the second section. Once the model is examined for accuracy, various porosity patterns for FG stiff layers and viscoelastic boundary conditions (VBCs) are incorporated into the FE model. The validation and convergence study of VBCs is carried out with available literature. In the last section, an analytical sandwich plate model is developed for static bending and free vibration of the FG sandwich plate with a viscoelastic core. The model is validated with various literature. The results show that the developed sandwich plate model is accurate enough to give appropriate results.

CHAPTER 4

RESULTS AND DISCUSSION

4.1 INTRODUCTION

In this chapter, an FG sandwich beam with a viscoelastic interlayer is considered in a thermal environment for static bending, buckling, and vibration studies. Different types of porosity models (H, O, V, X) are incorporated into the study. The FG sandwich beam is presumed to have viscoelastic boundary conditions (VBCs) with varying support stiffness. First static bending and free vibration studies are carried out at room temperature. This section also discusses the effect of several parameters, such as support stiffness, loss factor, porosity dispersion, and power-law variation, on the sandwich beam's bending and vibration. Further, thermal buckling and free vibration studies are carried out for various working temperatures. The temperature effect on critical buckling temperature (CBT), natural frequency (NF), and loss factor (LF) of the FG porous sandwich beam is also discussed.

4.2 STATIC BENDING AND FREE VIBRATION OF FG SANDWICH BEAM (ROOM TEMPERATURE)

For the study, Ti-6Al-4V/ZrO_2 FG sandwich beam is considered with the DYAD606 core. Young's modulus (E) and coefficients of thermal expansion (α) of FG stiff layers are temperature dependent; density remains constant in all temperatures. The temperature coefficients and densities of FG constituents are given in Table 4.1. Figures 4.1 and 4.2 show the temperature-dependent shear modulus and loss factor of DYAD606. Figures 4.3 and 4.4 show variations of Young’s modulus and density of FG stiff layers along the thickness of the sandwich beam for different porosity dispersion models and power-law index.

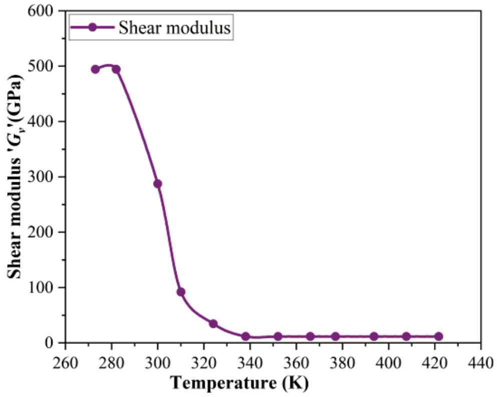

Figure 4.1: Temperature-dependent shear modulus of DYAD 606 core.

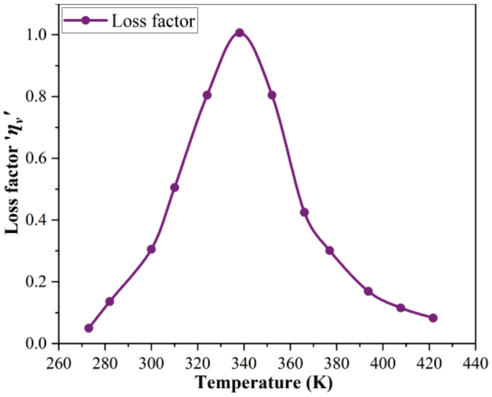

Figure 4.2: Temperature-dependent loss factor of DYAD 606 core.

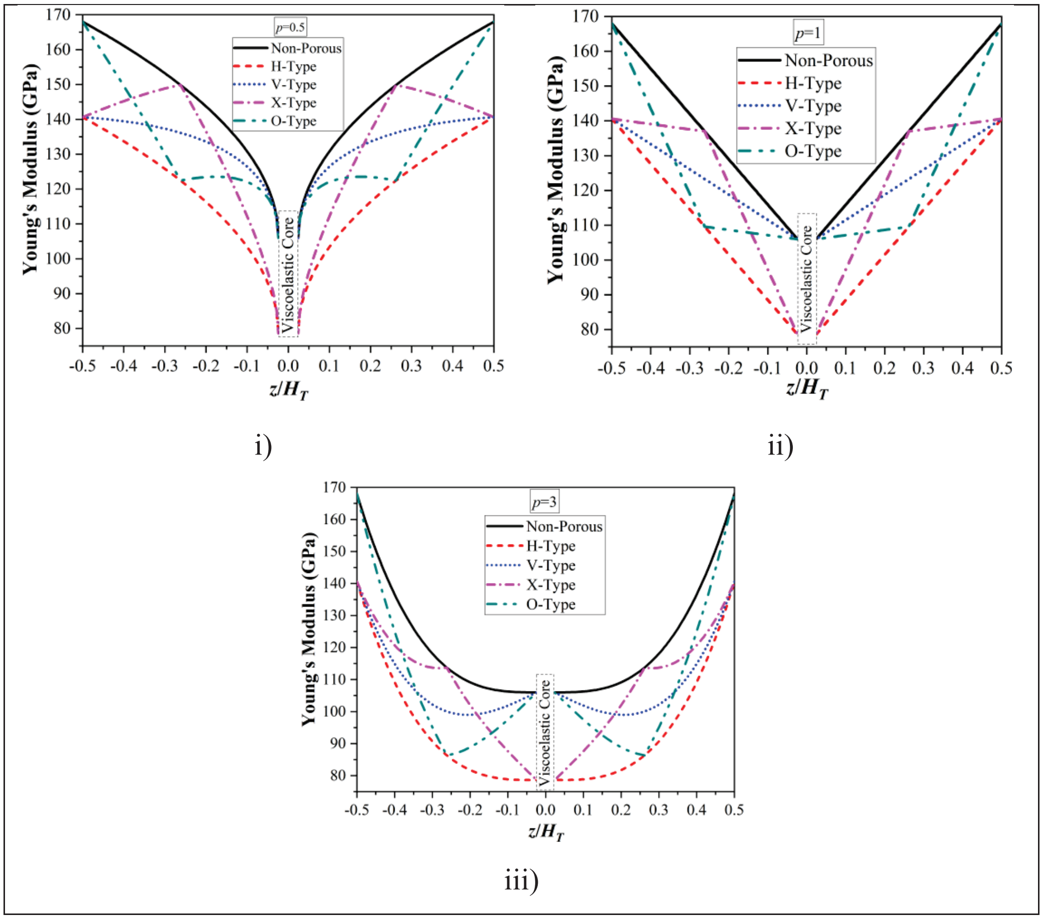

i)

ii)

iii)

Figure 4.3: Young's modulus of Ti-6Al-4V/ZrO_2 FG stiff layers with various porosity patterns at β=0.2: i) p=0.5, ii) p=1 and iii) p=3)

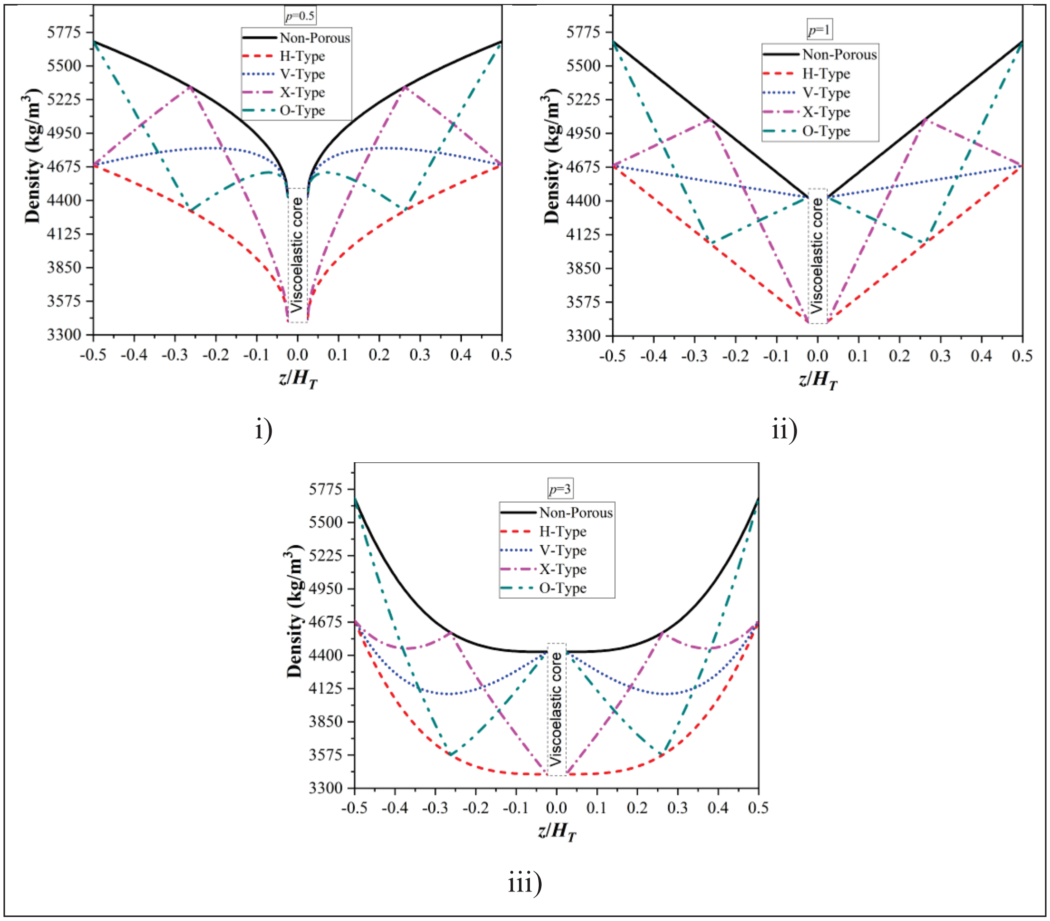

i)

ii)

iii)

Figure 4.4: Density of Ti-6Al-4V/ZrO$_2$ FG stiff with various porosity patterns at β=0.2: i) p=0.5, ii) p=1 and iii) p=3)

Calculation of Young's modulus of ZrO$_2$ at T=300K

$$P(T)=P_0(P_{-1}T^{-1}+1+P_1T+P_2T^2+P_3T^3)$$

$$E_{ZrO_2}(300K)=244.27X10^9(1-1.37X10^{-3}(300)+1.214X10^{-6}(300)^2-3.68X10^{-10}\left(300\right)^3)$$

$$E_{\mathrm{ZrO_2}}(300K)=168.063GPa$$

Similarly, properties such as Young's modulus and coefficient of thermal expansion for each constituent at a temperature of 300K are calculated, and the properties are listed in Table 4.1.

Table 4.1 Temperature coefficients for FG constituents (Reddy and Chin 1998).

Material	**Properties**	P_0	P_{-1}	P_1	P_2	P_3	$P(T=300K)$
ZrO_2	E(Pa)	$244.27 X 10^9$	0	$-1.37 X 10^{-3}$	$1.214 X 10^{-6}$	$-3.68 X 10^{-10}$	168.063
	α(1/K)	$12.766 X 10^{-6}$	0	$-1.49 X 10^{-3}$	$1.006 X 10^{-5}$	$-6.77 X 10^{-11}$	$18.59 X 10^{-6}$
	ρ(kg/m^3)	-	-	-	-	-	5700
Ti-6Al-4V	E(Pa)	$122.56 X 10^9$	0	$-4.58 X 10^{-4}$	0	0	105.698
	α(1/K)	$7.578 X 10^{-6}$	0	$-6.63 X 10^{-4}$	$-3.147 X 10^{-6}$	0	$6.941 X 10^{-6}$
	ρ(kg/m^3)	-	-	-	-	-	4429
Si_3N_4	E(Pa)	$348.43 X 10^9$	0	$-3.07 X 10^{-4}$	$2.160 X 10^{-7}$	$-8.946 X 10^{-11}$	322.2715
	α(1/K)	$5.8723 X 10^{-6}$	0	$9.095 X 10^{-4}$	0	0	$7.4746 X 10^{-6}$
	ρ(kg/m^3)	-	-	-	-	-	2370
SUS304	E(Pa)	$201.04 X 10^9$	0	$3.079 X 10^{-4}$	$-6.534 X 10^{-7}$	0	207.7877
	α(1/K)	$12.330 X 10^{-6}$	0	$8.086 X 10^{-4}$	0	0	$15.321 X 10^{-6}$
	ρ(kg/m^3)	-	-	-	-	-	8166

Dimensions (mm) : L=500mm, b=20mm, $h_{f1}=h_{f2}=10$, $h_v=1$

4.2.1 Static bending studies

A static deflection study is carried out for the FG sandwich beam with a viscoelastic interlayer. The power law is considered unity (p=1) for the first case. The variation of Young's modulus and density for power law index p=1 are shown in Figures 4.3 (ii) and 4.4 (ii). The beam is assumed as non-porous (β=0), and a constant point load of 10N is applied at the free end of the C-F beam and at the center of the C-C, P-R beam. Since the complex shear modulus phenomenon is seen only in dynamic conditions, the loss factor will not come into the frame for both viscoelastic support and core (η_{sp}=η_v=0) for static studies.

Accordingly, the maximum transverse deflection (w_{max}) is plotted in Figure 4.5 for different support conditions. The transverse deflection diagrams for symmetric boundary conditions (C-C) can be drawn using 2D and 3D graphs, but for unsymmetric boundary conditions (P-R), only 3D graphs are suitable to show transverse deflections. It is observed that resistance to deformation is enhanced at either end by increasing the boundary stiffness of the beam. Therefore, transverse deflection reduces with an increase in boundary stiffness. The deflection reaches a constant value at higher support stiffness.

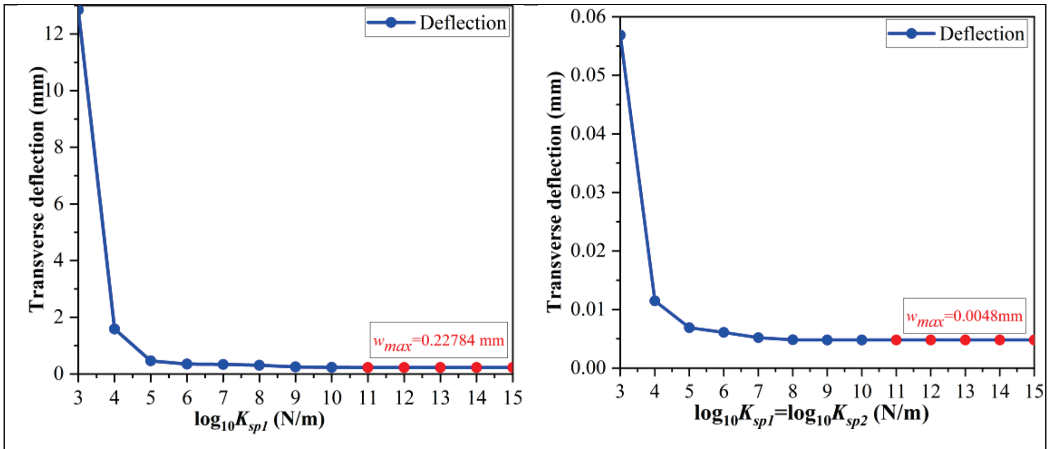

i) ii)

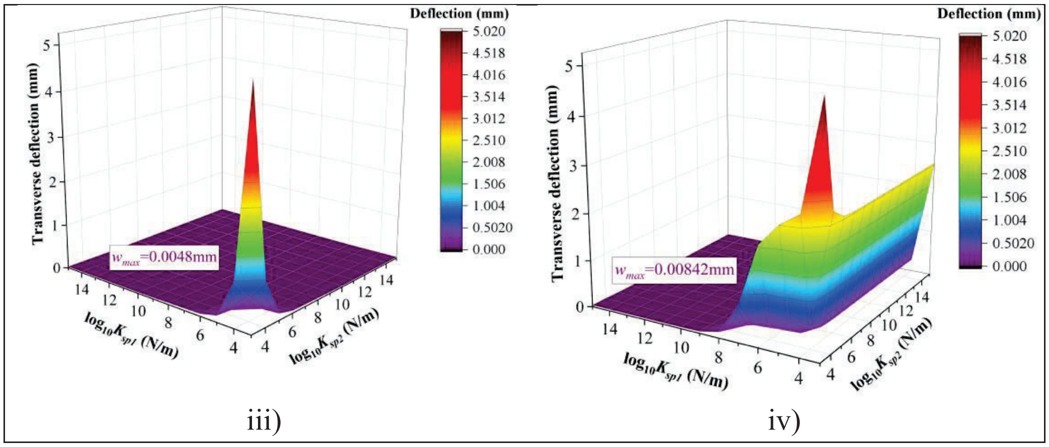

iii) iv)

Figure 4.5 Transverse deflection (w_{max}) of sandwich beam under varying support stiffness: i) C-F, ii) C-C (2D). iii) C-C (3D) iv) P-R (p=1, F=10N, β=0.0).

The deflection reaches a constant value at higher support stiffness. Based on the deflection results, the critical support stiffness values (SSVs) to achieve conventional boundary conditions are tabulated in Table 4.2. Once the conventional boundary conditions are known, further study is carried out for C-F, C-C, and P-R conditions.

Table 4.2: Support stiffness values (SSVs) for various boundary conditions of Ti-6Al-4V/ZrO$_2$ FG sandwich beam

	K_{sp1} (N/m)	**K_{sp2} (N/m)**
Clamped-Free (C-F)	10^{11}	0
Clamped-Clamped (C-C)	10^{9}	10^{9}
Pinned-Roller (P-R)	10^{11}	10^{8}

Figure 4.6 shows the transverse deflections with varying point loads for various power law indices. The higher power law indicates higher metal content in the FG stiff layers. Since Young's modulus of metal is less compared to ceramic, FG stiff layers with high metal content are less stiff compared to FG layers with more ceramic content. So, the FG sandwich beam deflection enhances with the power law index, and the C-F beam yields maximum deflection compared to C-C and P-R beams.

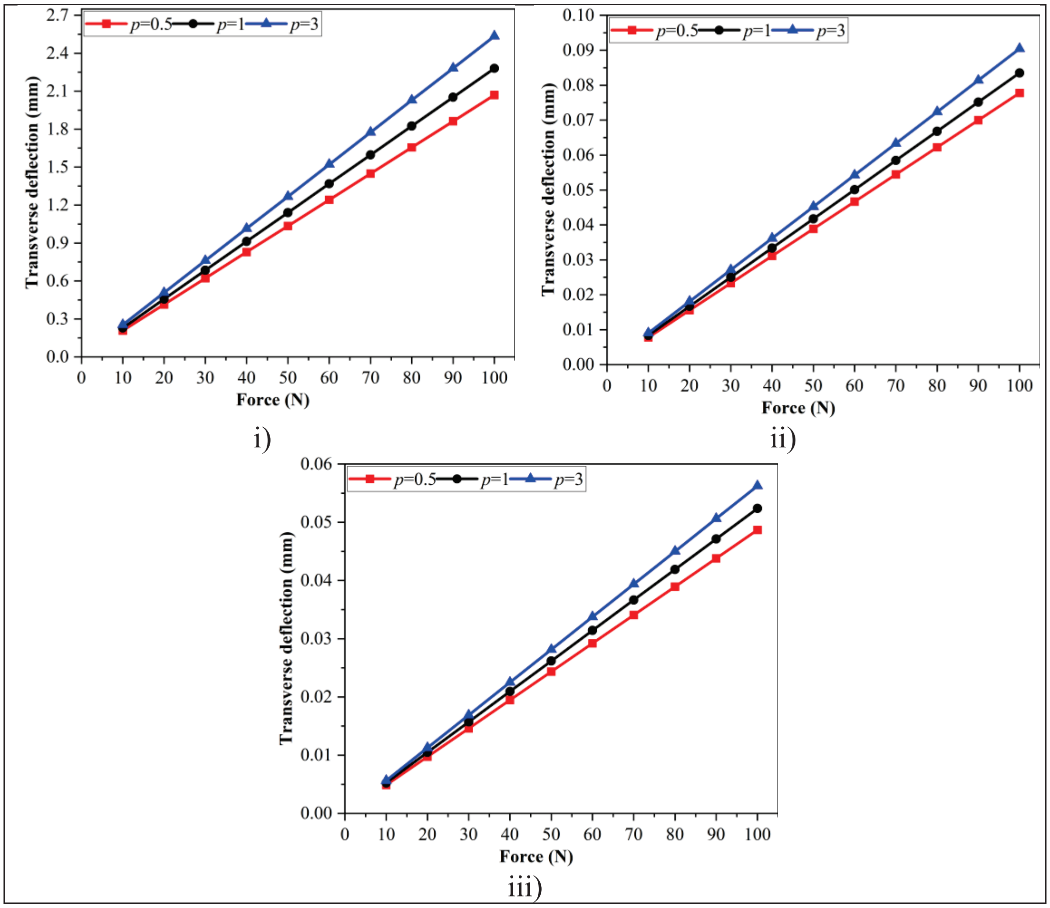

i) ii) iii)

Figure 4.6 Transverse deflection (w_{max}) of sandwich beam under varying point loads: i) C-F, ii) C-C. iii) P-R (β=0.0).

Further porosity dispersion models are incorporated, and transverse deflection is determined for various porosity volume fractions under C-C support. For a constant point load of 10N, V and H-type porosities give minimum and maximum transverse deflection, respectively, for a given porosity volume fraction. The transverse deflection of V-type porosity is 23.07% and 27.77% less than H-type porosity for power-law (p) 0.5 and 3, respectively.

From Figure 4.7, it is observed that when the porosity is more at the metal-rich part of the FG stiff layer, the stiffness of the beam is reduced considerably, which leads to higher deflection; when porosity is maximum at ceramic rich part, the reduction in beam stiffness is comparatively less which leads in lower deflection.

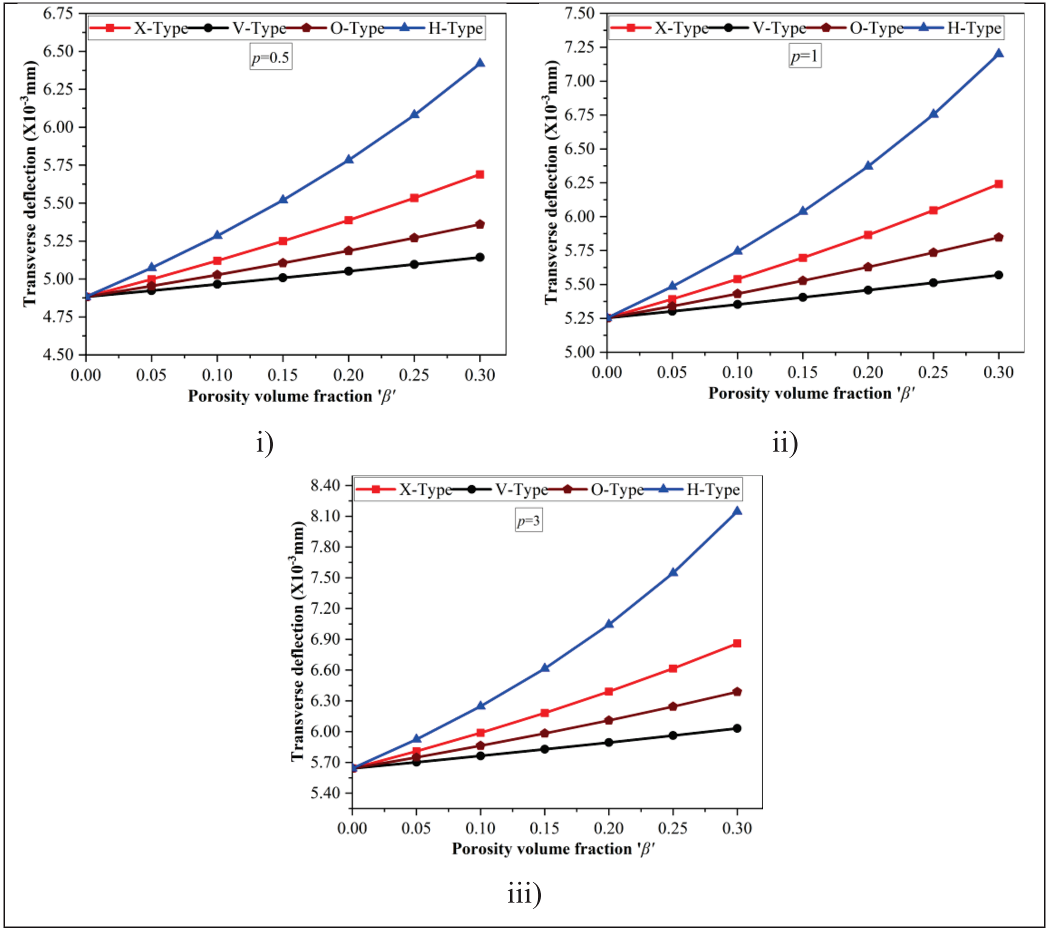

i)

ii)

iii)

Figure 4.7: Transverse deflection (w_{max}) of C-C sandwich beam for various porosity distribution models: i) p=0.5, ii) p=1. iii) p=3 (F=10N).

Figure 4.8 shows the transverse deflection of the FG porous sandwich beam along the length of the beam for conventional boundary conditions. As the constant point load of 10N is applied at the center of the C-C and P-R beam, the deflection is maximum at the center and reduces to zero at either end of the beam. The C-F sandwich beam deflection is zero at the clamped end and maximum at the free end where the load is applied. The C-F beam yields higher deflection than P-R and C-C beams as the C-F support is less stiff than the other two. The porosity patterns play an important role in deciding the stiffness of the sandwich beam. If the porosity is maximum away from the neutral axis of stiff layers, the stiffness reduces drastically, and transverse deflection will be maximum (H and X pattern). If the porosity is more at the neutral axis (O and V pattern), the reduction in stiffness is less.

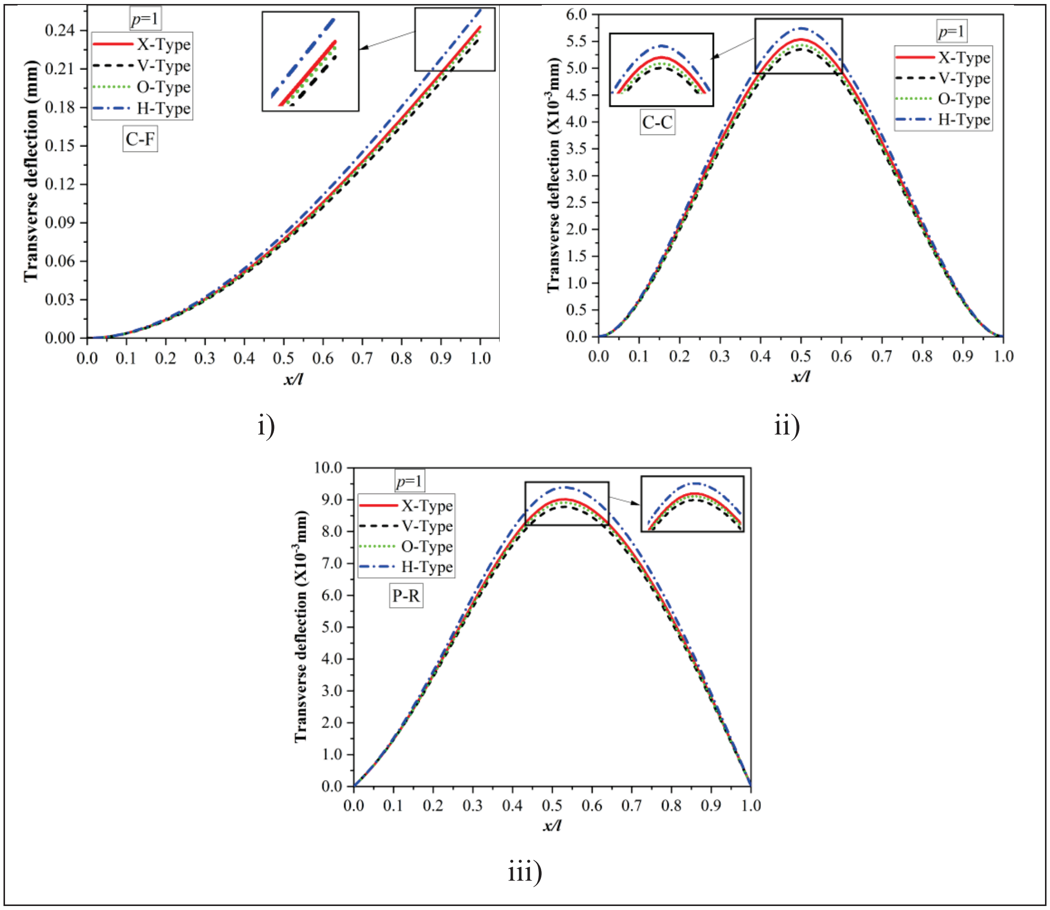

i) ii)

iii)

Figure 4.8: Transverse deflection of sandwich beam for varying *x/l* ratio: i) C-F, ii) C-C. iii) P-R (p=1, F=10N, β=0.2).

4.2.2 Vibration studies

Free vibration study is carried out for the FG sandwich beam with a viscoelastic interlayer. In the first case, non-porous FG stiff layers are considered (β=0) with power-law variation p=1. The core is considered viscoelastic (η_v=0.388), and the supports are treated as elastic (η_{sp}=0). Figures 4.9 and 4.10 indicate the natural frequency (NF) and loss factor (LF) of the C-F sandwich beam, respectively. The natural frequency increases gradually with an increase in elastic support stiffness (ESS), and the frequency enhancement rate reduces when the ESS nears the beam stiffness (BSS). Once the ESS crosses the BSS, a rise in frequency can be seen, and the frequency line flattens when the beam achieves the conventional C-F boundary condition.

On the other hand, the beam loss factor nearly equals zero (≈0) until the ESS values reach a critical value (≤10^4 N/m), which means the shear strain or shear deformation in the core is negligible as the ESS fails to offer remarkable resistance at the ends. As the ESS increases beyond 10^4 N/m and nears beam stiffness, the strain energy stored in the viscoelastic core and associated loss factor of the beam reaches their maximum. Once the ESS crosses BSS, there will be a reduction in the strain energy stored and the associated loss factor. The loss factor remains unchanged once the C-F boundary is achieved.

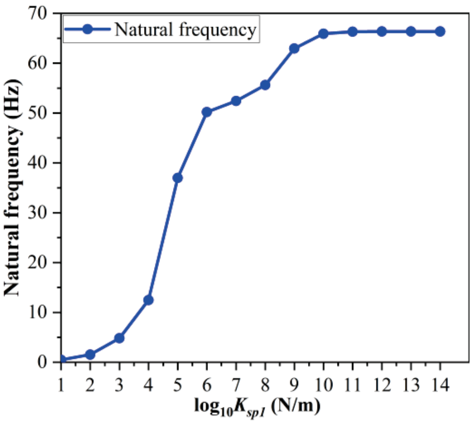

Figure 4.9 Natural frequency of sandwich beam under varying C-F support stiffness (p=1, β=0.0, η_{sp}=0.0).

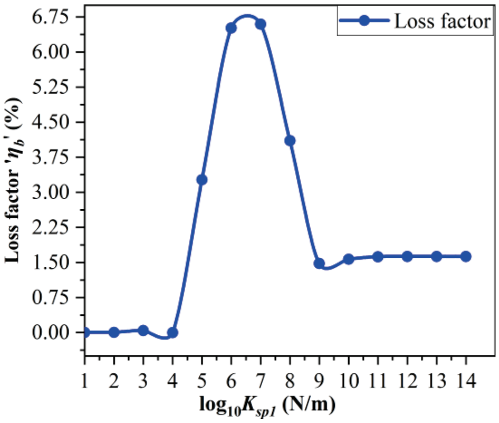

Figure 4.10 Loss factor of sandwich beam under varying C-F support stiffness (p=1, β=0.0, η_{sp}=0.0).

Figures 4.11 and 4.12 depict the natural frequency, and loss factor of C-C supports. The frequency, as well as the loss factor curve, remains flat (≈0) till the support offers some resistance to the load applied (≤10^4 N/m). Beyond the critical support value (>10^4 N/m), the natural frequency and loss factor increase and attain a constant value at higher ESS. The frequency and loss factor trends resemble the C-F beam when ESS is considerably high at one end and low at the other end of the C-C beam. Figures 4.13 and 4.14 indicate the P-R sandwich beam's natural frequency and loss factor. The natural frequency and loss factor curves follow similar trends in the P-R beam. The natural frequency and loss factor curves remain flat till the supports offer some resistance (≤10^4 N/m); after that, the values increase continuously till the P-R boundary is achieved and remain constant.

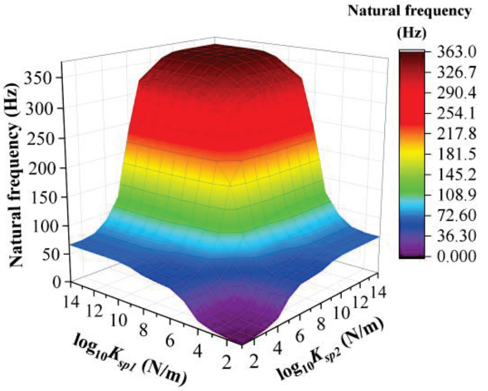

Figure 4.11: Natural frequency of sandwich beam under varying C-C support stiffness (p=1, β=0.0, η_{sp}=0.0).

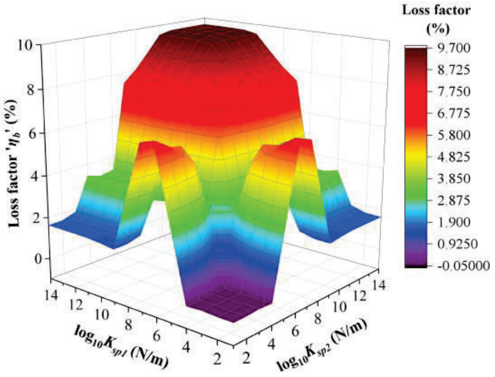

Figure 4.12: Loss factor of sandwich beam under varying C-C support stiffness (p=1, β=0.0, η_{sp}=0.0).

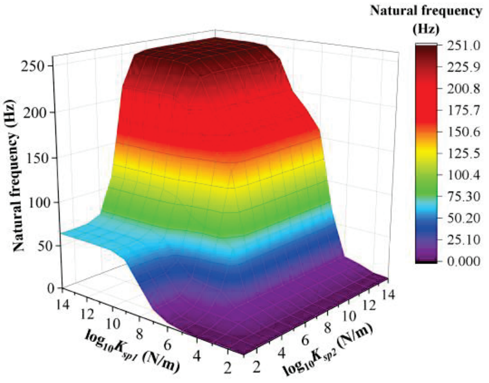

Figure 4.13: Natural frequency of sandwich beam under varying P-R support stiffness (p=1, β=0.0, η_{sp}=0.0).

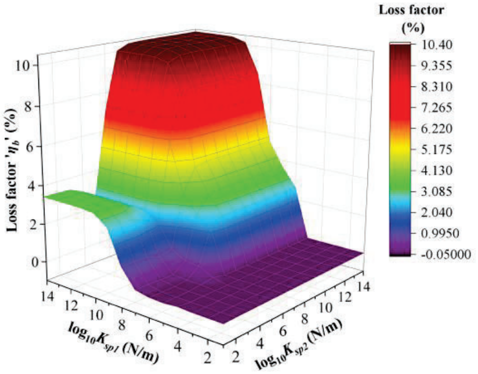

Figure 4.14: Loss factor of sandwich beam under varying P-R support stiffness (p=1, β=0.0, η_{sp}=0.0).

Figure 4.15 shows the mode shapes of the C-F, C-C, and P-R beams. Mode shapes are extracted for different stiffness values at both ends, where the frequency and loss factor curves exhibit drastic changes in their trends.

The mode shapes substantiate that there is hardly any shear deformation in the core until the supports offer some resistance to the applied forces. At 10^4 N/m, the supports offer some resistance but are not enough to hold the beam completely, because of which the negative deformation (mode shape) is observed. Once the critical value (10^4 N/m) is crossed, the shear deformation and strain energy associated with the viscoelastic core increase, enhancing the natural frequency and loss factor. In C-F mode shapes, shear in the core is high when the ESS nears the BSS, because of which the loss factor of the beam is high, as shown in Figure 4.10.

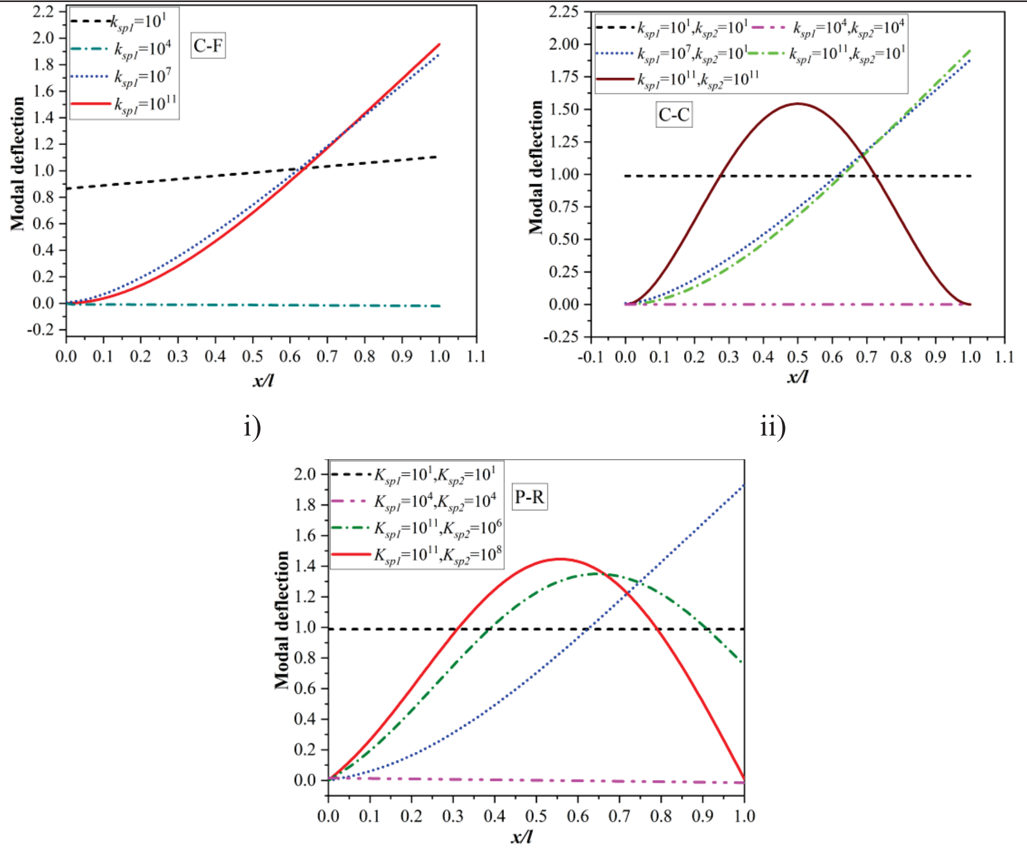

i) ii) iii)

Figure 4.15: Mode shapes of sandwich beam under varying support stiffness: i) C-F, ii) C-C. iii) P-R (p=1, β=0.0, η_{sp}=0.0).

The variation of beam loss factors for different viscoelastic support loss factors is shown in Figure 4.16. From the figure, it is noted that viscoelastic support contributes to the overall damping of the sandwich beam considerably when the support is more viscous (soft). The increase in viscoelastic support stiffness (VSS) makes the support more elastic (hard) than viscous. When the sandwich beam is on highly stiff supports, only the core contributes to the vibration damping of the beam. The maximum loss factor of the sandwich beam is noted at VSS 10^4 N/m, and the negative or positive signs depend on the beam's direction of deformation (mode shape).

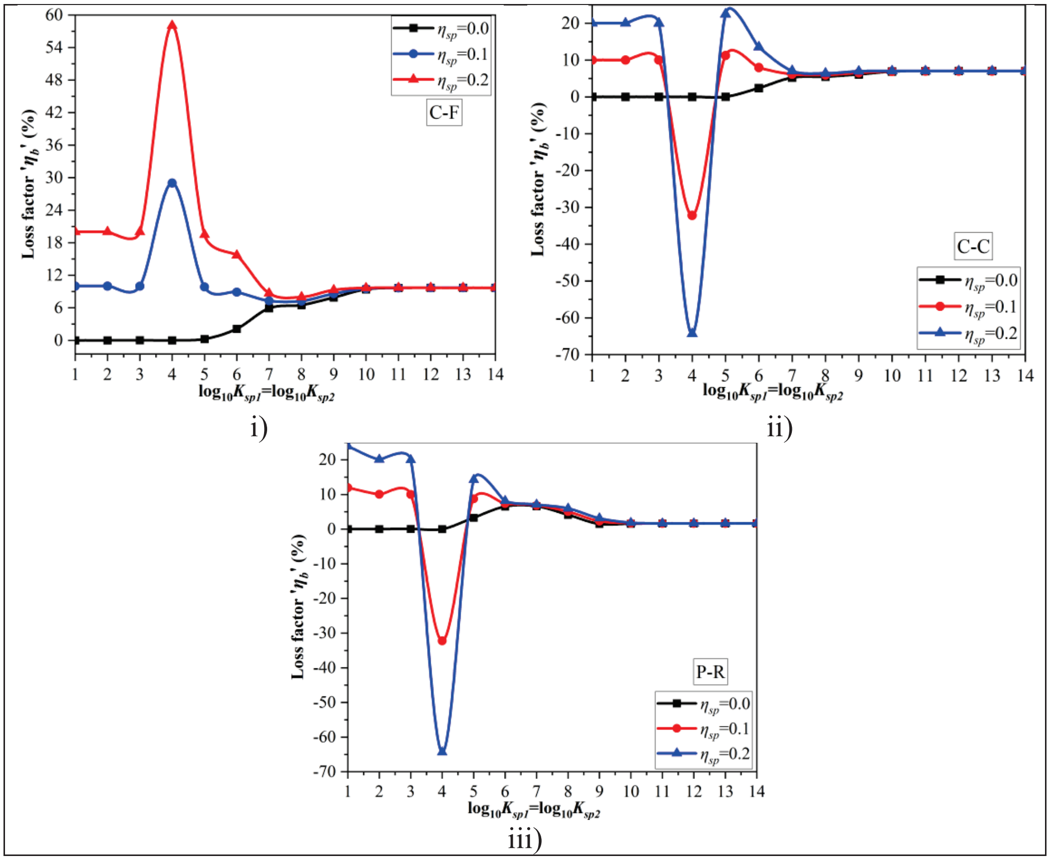

i)

ii)

iii)

Figure 4.16: Sandwich beam loss factor under varying viscoelastic support stiffness: i) C-F, ii) C-C. iii) P-R (*p*=1, *β*=0.0).

In the second case, various porosity dispersion models are incorporated into the study. The Natural frequency (NF) and loss factor (LF) are plotted for different power-law variations. Figure 4.17 depicts the natural frequency of sandwich beams for varying porosity volume fractions.

The C-C sandwich beam with V and X-type porosities portrays maximum and minimum natural frequency. The natural frequency of V-type porosity escalates from 5.177% to 6.63% at *β*=0.3 compared to X- type porosity when power law (*p*) is enhanced from 0.5 to 3. The natural frequency results show that if the porosity content is higher in the metal-rich-part, the reduction in beam stiffness is more compared to its mass, which leads to a reduction of natural frequency. As the porosity volume fraction increases, the mass reduction dominates the stiffness reduction up to a certain level, leading to natural frequency enhancement. A further increase in porosity reduces the natural frequency as discerned in H-type and X-type distribution.

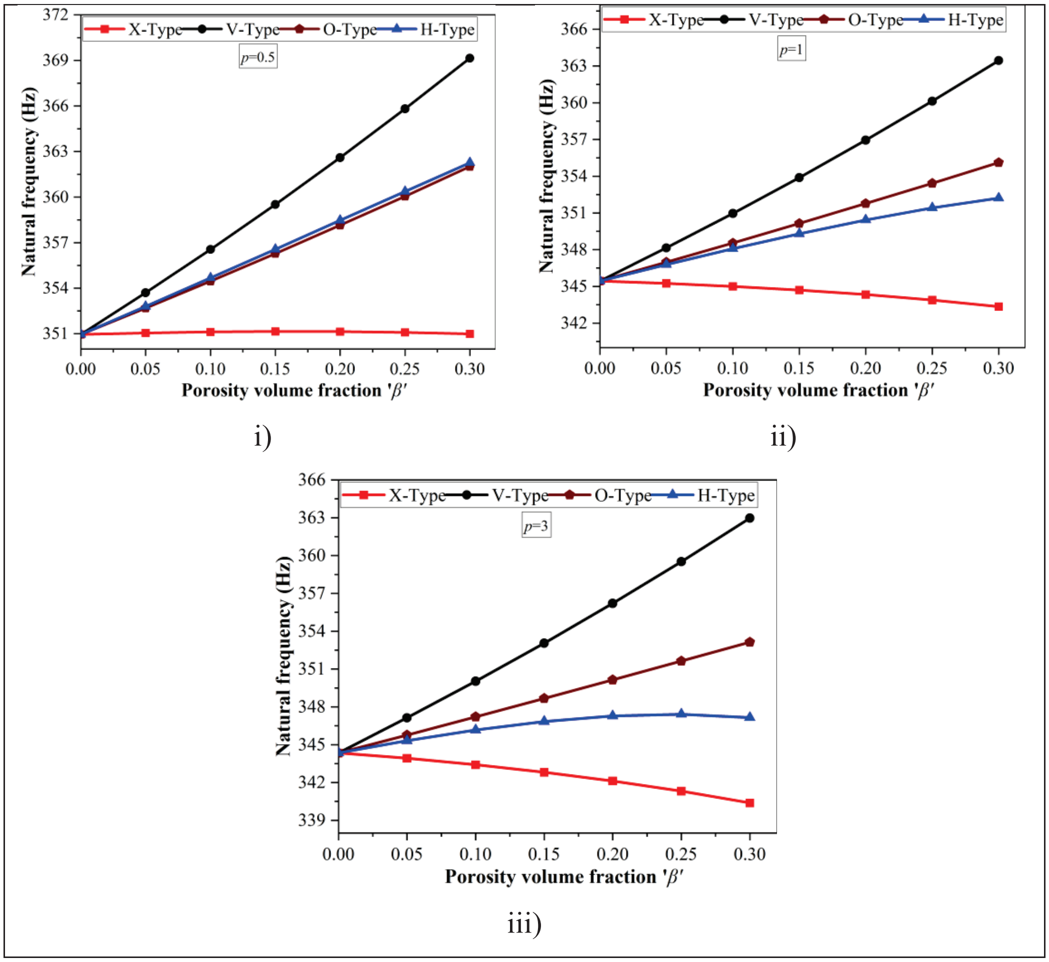

i)
ii)
iii)

Figure 4.17: Natural frequency of C-C sandwich beam for various porosity distribution models: i) p=0.5, ii) p=1. iii) p=3 (η_{sp}=0.1).

Figure 4.18 shows the sandwich beam loss factor for varying porosity volume fractions. The C-C sandwich beam with V and H-type porosities portrays maximum and minimum loss factors for a given porosity volume fraction. The loss factor of V-type porosity enhances from 12.42% to 17.54% at β=0.3 compared to H- type porosity when the power law (p) is increased from 0.5 to 3.

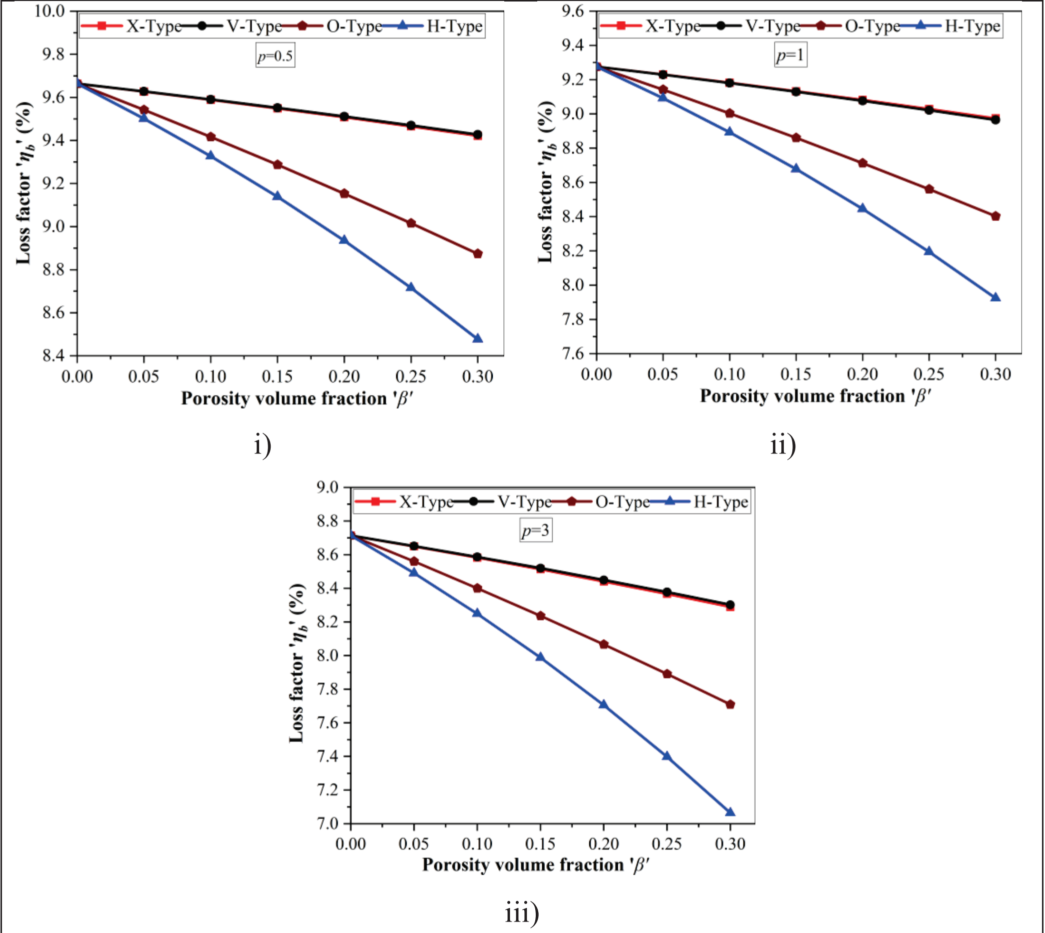

i)

ii)

iii)

Figure 4.18: Loss factor of C-C sandwich beam for various porosity distribution models: i) p=0.5, ii) p=1. iii) p=3 (η_{sp}=0.1).

Figure 4.19 shows the loss factor of the sandwich beam with varying viscoelastic support loss factors (η_{sp}). If the support is more viscous (high loss factor), it offers high damping to the structure. So overall loss factor of the sandwich beam increases with an increase in the support loss factor.

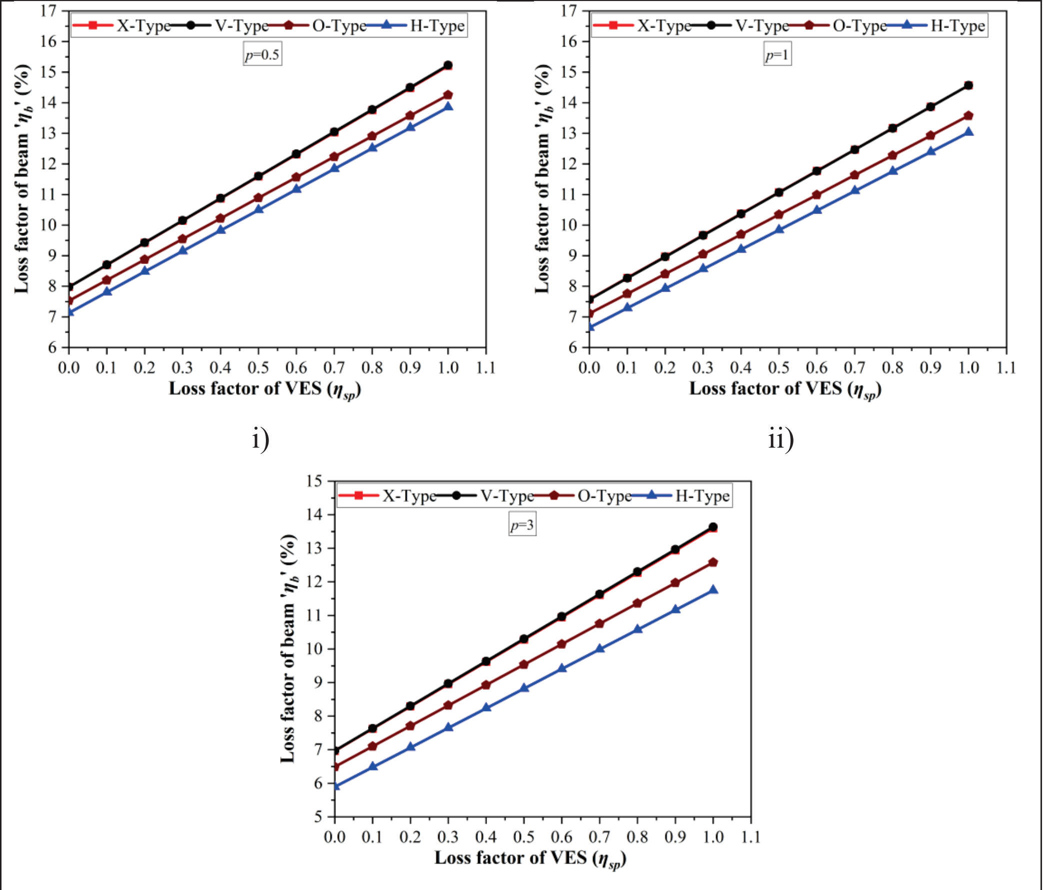

i)

ii)

iii)

Figure 4.19: Loss factor of C-C sandwich beam for various VES loss factors (η_{sp}): i) p=0.5, ii) p=1. iii) p=3 (β=0.3, η_v=0.388).

4.3 BUCKLING AND FREE VIBRATION OF FG SANDWICH BEAM IN UNDER THERMAL ENVIRONMENT

A SUS304/Si_3N_4 FG sandwich beam is considered for the study with a DYAD606 viscoelastic core. The temperature coefficients and densities of SUS304/Si_3N_4 FG constituents are given in Table 4.1.

4.3.1 Thermal buckling

In this section, the buckling of the sandwich beam in a thermal environment is studied. Critical buckling temperature and buckling mode shapes are extracted for various boundary conditions.

The effect of parameters such as temperature, porosity volume fraction, ceramic gradation, and boundary conditions (BCs) on critical buckling temperature (CBT) is discussed. The room temperature (T_{room}) is considered as 27^0C throughout the study. Buckling is a static phenomenon, so the support loss factor (η_{sp}) is zero (elastic support) for buckling. Figure 4.20 shows the CBT of the sandwich beam for various boundary conditions with varying support stiffness values (SSVs). The figure shows that as the SSVs increase, the beam's overall stiffness increases, leading to a rise in CBT. The CBT will remain unchanged after the SSVs hit a critical value, and the trend line will remain flat beyond that point. This phenomenon is referred to as ideal BCs or conventional BCs (C-C, C-P, P-P, and P-R). C-C shows the highest CBT, and P-R shows the lowest among the four BCs. Table 4.3. shows the critical support stiffness values to achieve conventional BCs.

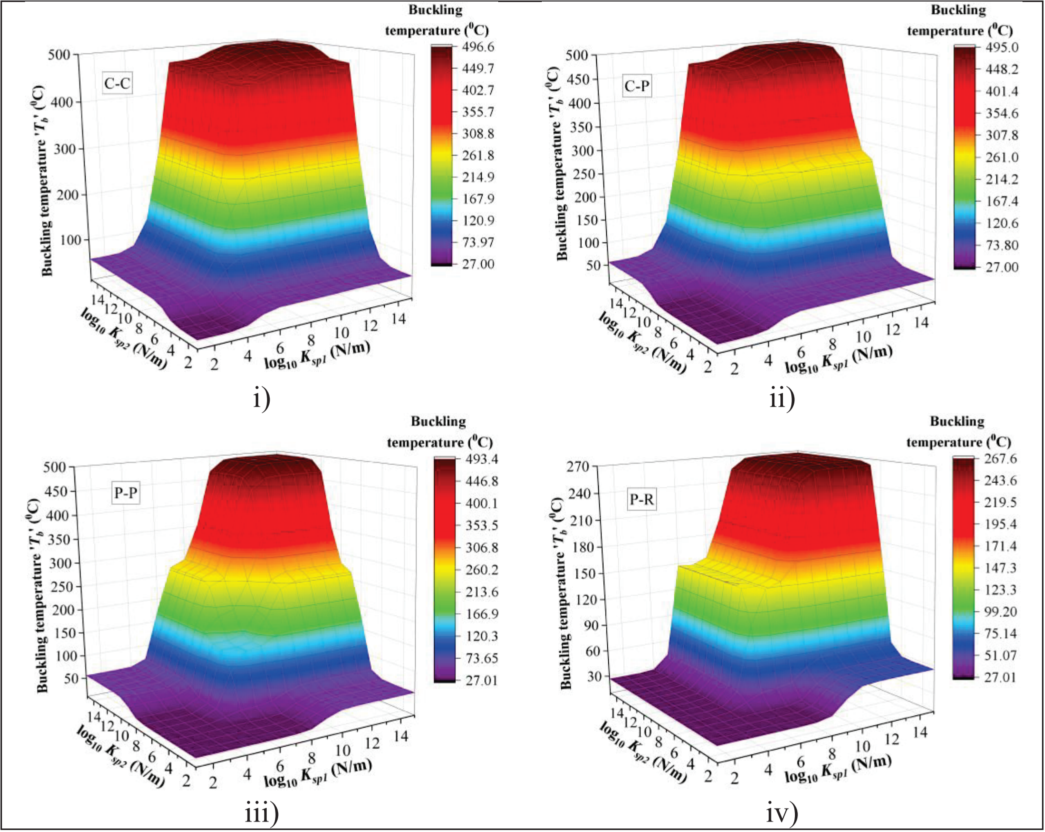

i) ii)

iii) iv)

Figure 4.20: CBT of sandwich beam: i) C-C, ii) C-P, iii) P-P, and iv) P-R (p=1, β =0.0, ΔT=50 ^{0}C and η_{sp}=0.0).

Table 4.3: Support stiffness values for various conditions (BCs) of SUS304/Si_3N_4 FG sandwich beam.

Boundary conditions	**K_{sp1} (N/m)**	**K_{sp2} (N/m)**
C-C	10^{12}	10^{12}
C-P	10^{14}	10^{14}
P-P	10^{13}	10^{13}
P-R	10^{12}	10^{8}

Figure 4.21 shows the buckling mode shapes for various BCs. From the figure, it is noticed that when the SSVs are significantly less (10^1 N/m to 10^5 N/m), the boundary fails to provide sufficient support to the beam, which means the thermal stresses are easing out without any resistance from the supports (nearly free-free condition), so buckling mode shape remains flat. Buckling peak can be observed when the SSVs are considerably high, and the peak attains maximum for a given temperature rise at a critical value. Once the beam attains conventional BCs, the peak remains unchanged.

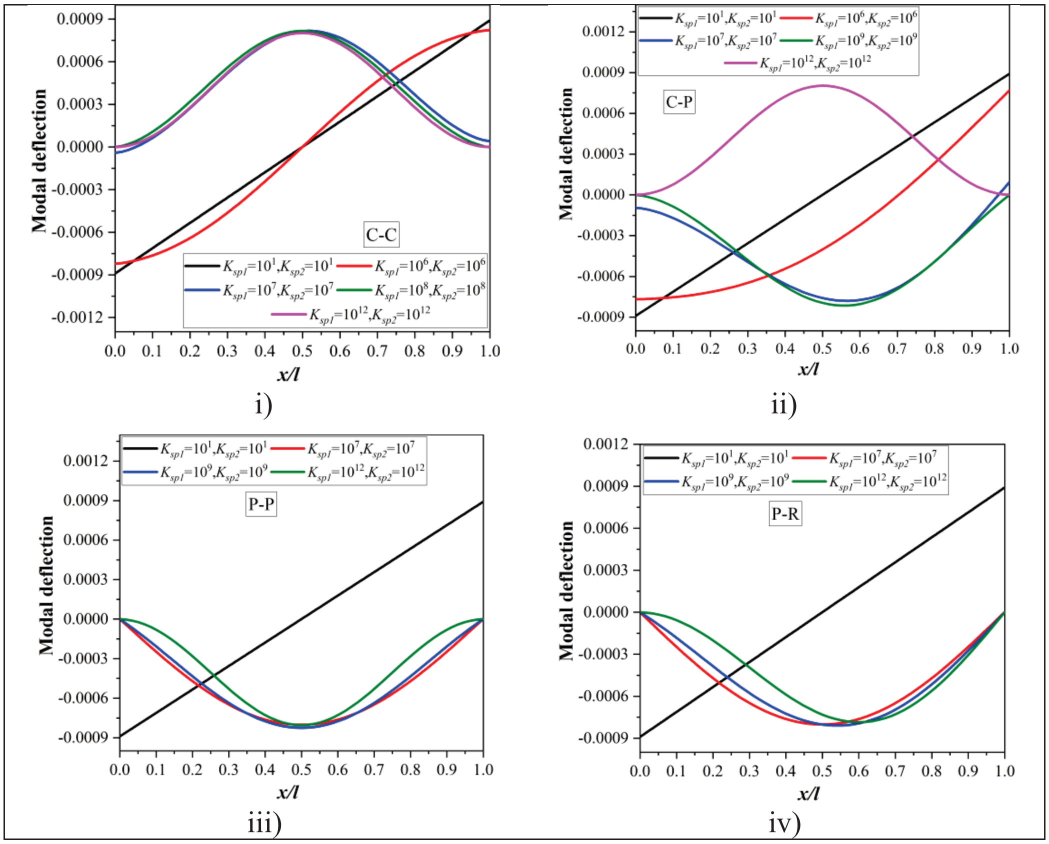

i) ii)

iii) iv)

Figure 4.21: Buckling mode shape of sandwich beam: i) C-C, ii) C-P, iii) P-P, and iv) P-R (p=1, β=0.0, ΔT=50 ^{0}C and η_{sp}=0.0).

The buckling takes a positive shape (Figure 4.21 i and ii) when the rotation degrees of freedom (DoF) are constrained at the boundaries (fixed), whereas buckling takes a negative shape (Figure 4.21 iii and iv) when the rotation DoF is not constrained (P-R). Further, the studies are carried out for the C-C sandwich beam.

Figure 4.22 shows the CBT of porous sandwich beams of various patterns at different temperatures. As the temperature increases, the thermal stresses increase, reducing the beam's stiffness and CBT. The presence of porosity reduces the effective coefficient of thermal expansion, and intern, reduces thermal stresses in the beam. Hence, the CBT increases with an increase in porosity volume fraction, as shown in Figure 4.23. A porous sandwich beam with H-pattern displays the highest CBT, and the V-pattern displays the lowest CBT among all four porosity patterns. Figure 4.24 shows the influence of the power law index on the CBT of the sandwich beam. The increase in *p*-value increases the metal content in FG stiff layers. Since the metal has a higher coefficient of thermal expansion, the thermal stresses induced will also be higher, reducing the sandwich beam's CBT.

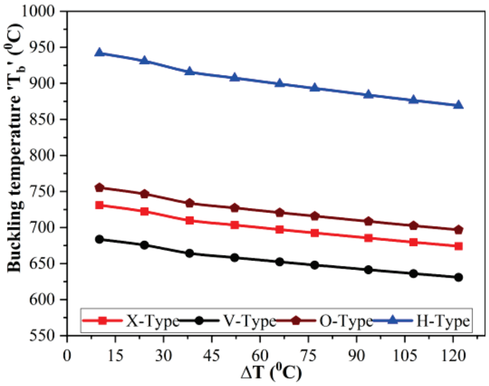

Figure 4.22: CBT of C-C sandwich beam at different temperature rise (p=1, β=0.3, and η_{sp}=0.0).

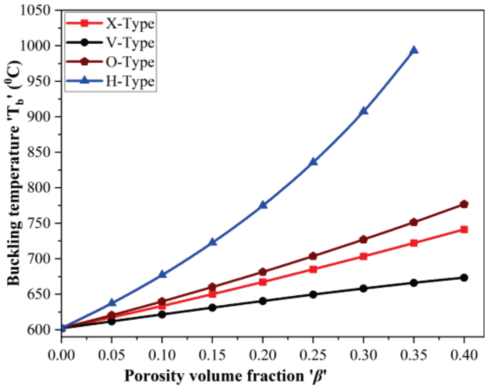

Figure 4.23: CBT of C-C sandwich beam at different porosity (p=1, ΔT=50 ^{0}C, and η_{sp}=0.0).

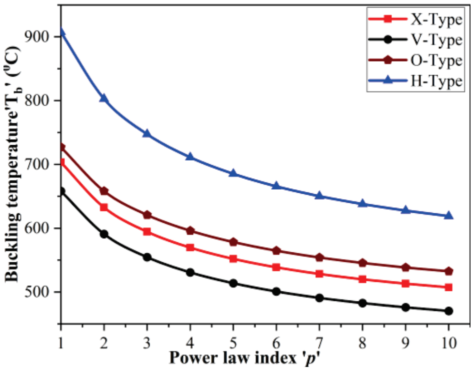

Figure 4.24: CBT of C-C sandwich beam at different power law index (β=0.3, ΔT=50 ^{0}C, and η_{sp}=0.0).

Table 4.4. shows the CBT of porous sandwich beams at various temperatures and BCs (C-C, C-P, P-P, and P-R). The C-C condition offers more stiffness to the beam compared to P-R, and the C-C condition exhibits maximum stiffness, which leads to higher CBT compared to the P-R beam among the four BCs.

Table 4.4: CBT for various boundary conditions (β=0.3, p=1, and η_{sp}=0.0).

		ΔT (^{0}C)			
BCs	**Porosity patterns**	**10**	**40**	**70**	**80**
C-F	NP	626.27	607.41	596.74	592.71
	X	730.96	709.77	697.12	692.38
	V	683.60	664.10	652.30	647.87
	O	755.31	733.71	720.63	715.72
	H	941.85	915.84	899.19	893.02
C-P	NP	624.79	602.77	592.20	588.22
	X	729.46	704.94	692.40	687.71
	V	682.42	660.39	648.68	644.28
	O	753.45	727.78	714.83	709.98
	H	939.84	909.19	892.69	886.58
P-P	NP	623.32	598.19	587.73	583.78
	X	727.97	700.18	687.74	683.09
	V	681.24	656.72	645.08	640.72
	O	751.60	721.93	709.11	704.30
	H	937.84	902.61	886.27	880.21
P-R	NP	332.92	323.19	317.75	315.69
	X	386.44	375.48	369.03	366.61
	V	362.34	352.50	346.48	344.21
	O	398.69	387.15	380.49	377.99
	H	494.03	480.03	471.53	468.40

4.3.2 Free vibration

In this section, the free vibration of the sandwich beam in a thermal environment is studied. The natural frequency (NF), loss factor (LF), and mode shapes of the sandwich beam in the first mode of vibration are plotted for various boundary conditions. A parametric study is conducted to know the effect of temperature, porosity volume fraction, power law distribution, and boundary conditions (BCs) on natural frequency and loss factors. Figures 4.25 and 4.26 show the natural frequency and loss factor of sandwich beams with various BCs, respectively. C-C sandwich beam yields maximum natural frequency and minimum loss factor among four BCs. When the support stiffness values (SSVs) of one support are higher and nearly the same as beam stiffness, whereas the SSVs of another support are lower than beam stiffness, the thermal stresses induced in the beam dominate the beam stiffness, because of which the negative loss factor can be observed in Figure 4.26.

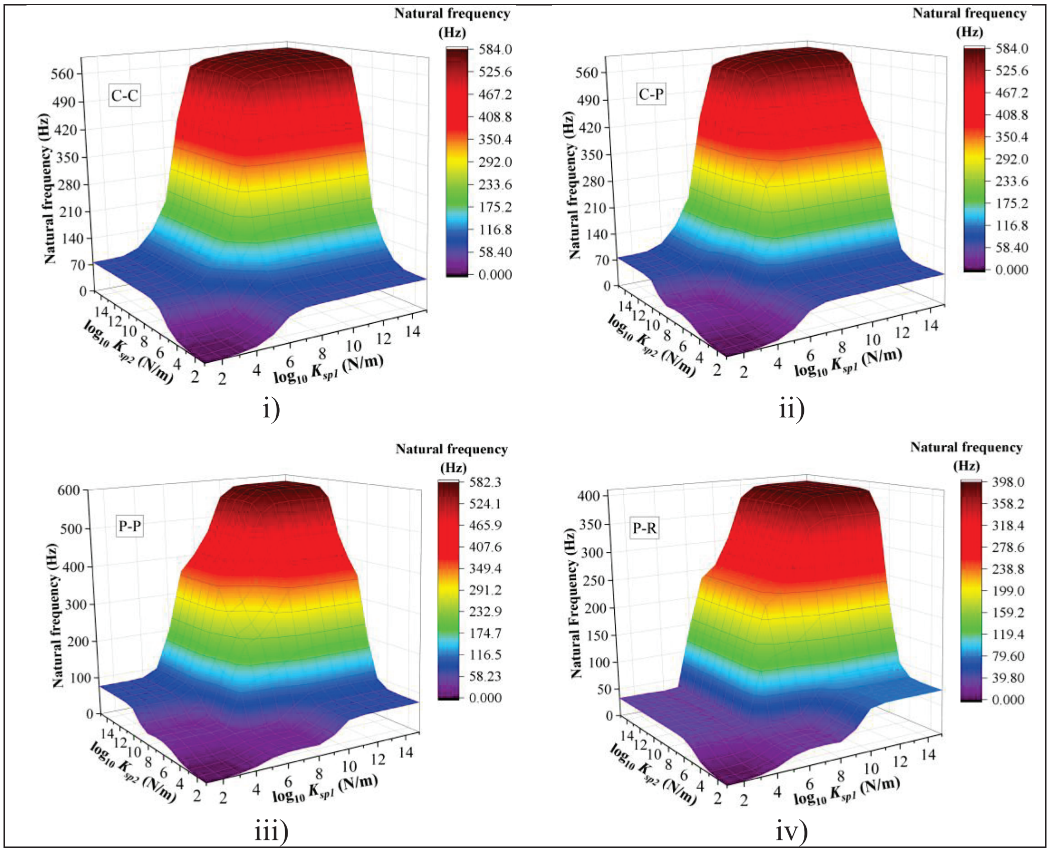

i) ii)

iii) iv)

Figure 4.25: Natural frequency of sandwich beam: i) C-C, ii) C-P, iii) P-P, and iv) P-R (p=1, β=0.0, ΔT=10 ^{0}C and η_{sp}=0.0).

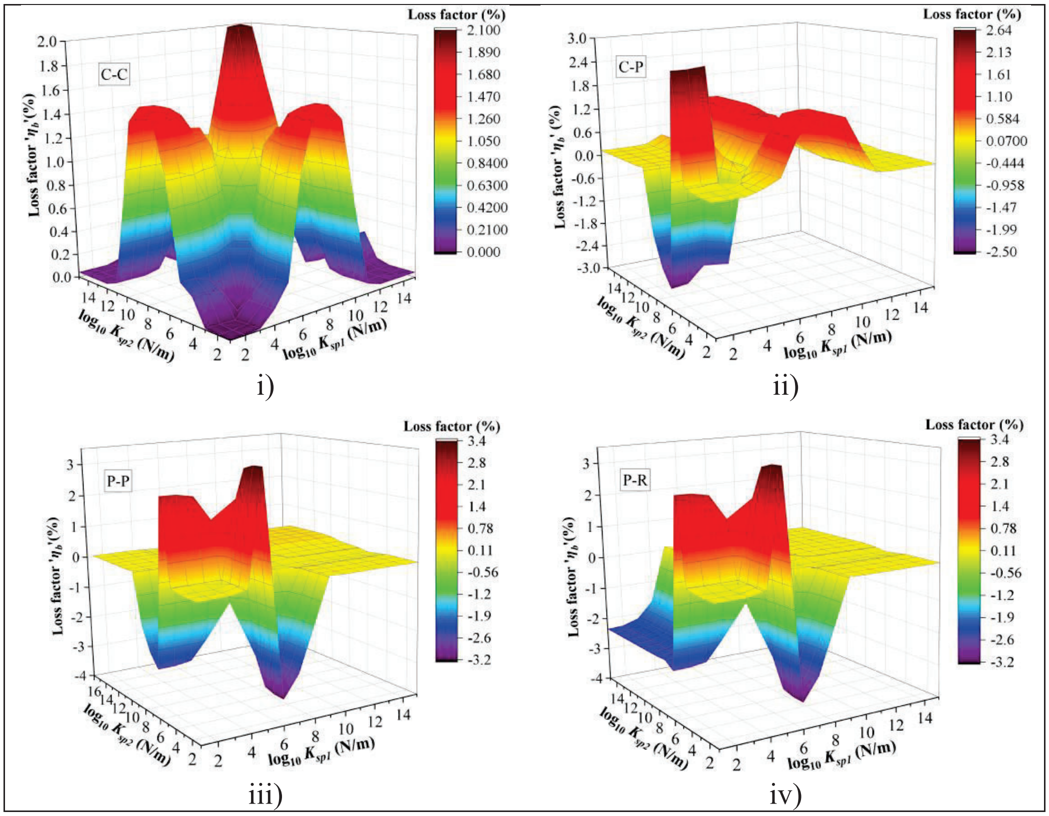

i) ii) iii) iv)

Figure 4.26: Loss factor of sandwich beam: i) C-C, ii) C-P, iii) P-P, and iv) P-R (p=1, β=0.0, ΔT=10 ^{0}C and η_{sp}=0.0).

Figure 4.27 shows the transverse mode shapes of sandwich beams for various BCs. The amplitude of mode shapes changes with SSVs. It is observed that as SSVs increase, the peak of the mode shape increases in the case of all BCs.

Figures 4.28 and 4.29 show the natural frequency and loss factor of FG sandwich beams with various porosity models at different temperatures. The temperature rise enhances the beam's thermal stresses, which reduces the beam's overall stiffness. This leads to a reduction in natural frequency. The loss factor of the beam follows a similar trend of the viscoelastic core loss factor, as depicted in Figure 4.2. The natural frequency and loss factor are almost equal to zero and infinity, respectively, as the temperature gets close to the buckling temperature. FG porous beams with H and V patterns exhibit maximum and minimum natural frequency, and X and H patterns show maximum and minimum loss factors among the porosity patterns. The presence of higher porosity reduces the thermal stresses induced in the beam, because of which the reduction in the frequency of the H-pattern slows down and gives better natural frequency at higher temperatures compared to the O-pattern.

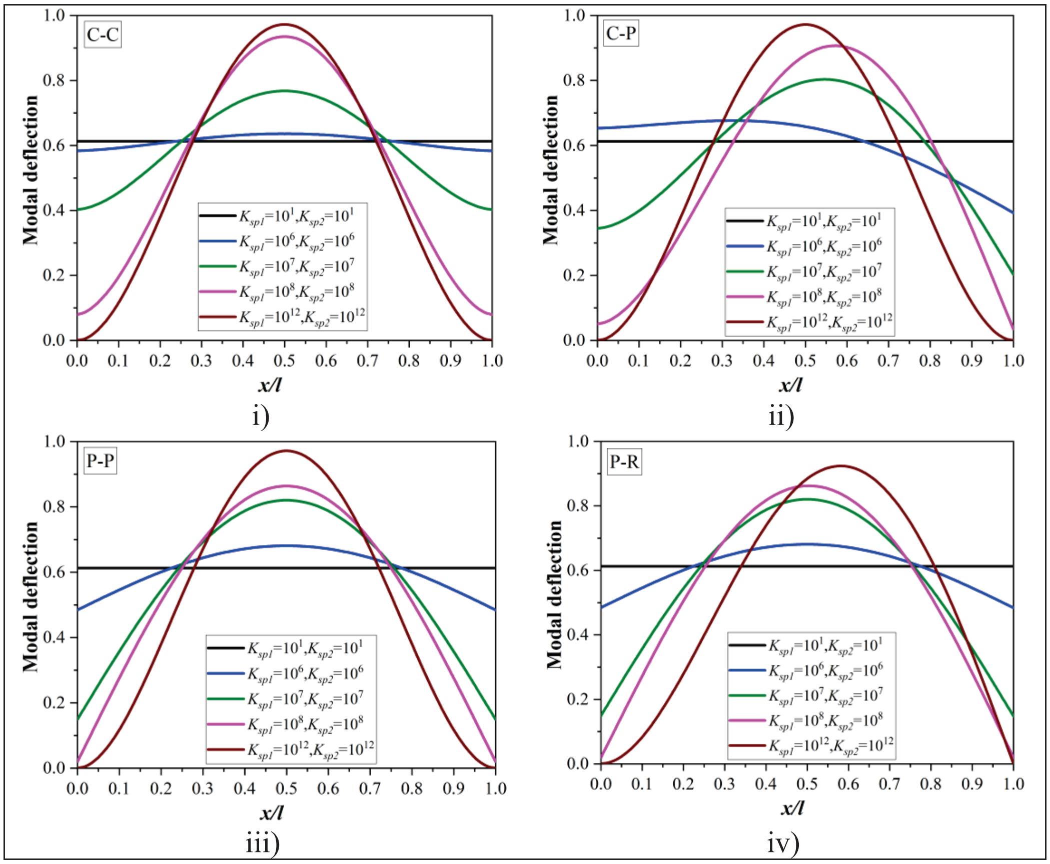

i)
ii)
iii)
iv)

Figure 4.27: Transverse mode shape of sandwich beam in vibration: i) C-C, ii) C-P, iii) P-P, and iv) P-R (p=1, β=0.0, ΔT=10 ^{0}C and η_{sp}=0.0).

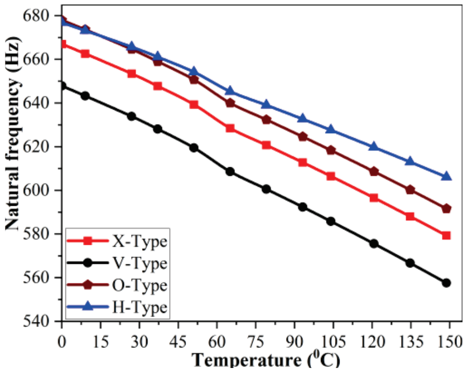

Figure 4.28: Natural frequency of C-C sandwich beam at different temperatures (p=1, β=0.3, and η_{sp}=0.2).

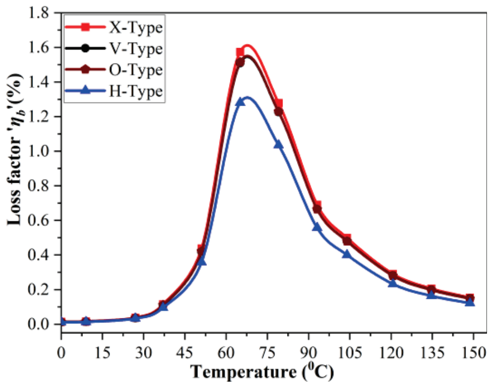

Figure 4.29: Loss factor of C-C sandwich beam at different temperatures (p=1, β=0.3, and η_{sp}=0.2).

Figures 4.30 and 4.31 show the natural frequency and loss factor for different porosity volume fractions. In H and O-pattern porosity, the mass reduction rate dominates the stiffness reduction rate. This improves natural frequency, whereas it is vice-versa in other patterns (V and X), which reduces the natural frequency for higher porosity volume fractions which is clearly observed in V-pattern. As the porosity volume fraction increases, energy dissipation of the sandwich beam decreases, which is indicated by the loss factor trend in Figure 4.31. The influence of the power law index on the natural frequency and loss factor of the porous sandwich beam is observed in Figures 4.32 and 4.33. The stiffness of FG layers and shear in the core reduces with an increase in the power-law index, which reduces the natural frequency and loss factor.

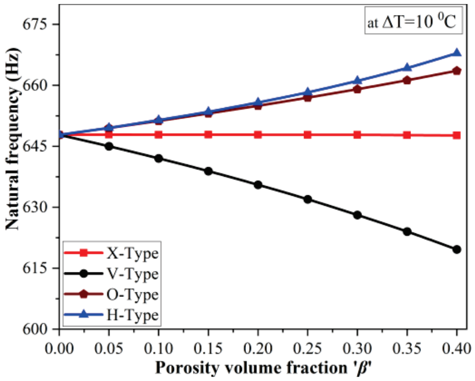

Figure 4.30: Natural frequency of C-C sandwich beam at different porosity (p=1, and η_{sp}=0.2).

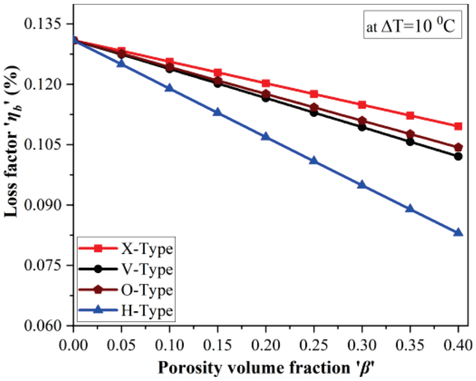

Figure 4.31: Loss factor of C-C sandwich beam at different porosity (p=1, and η_{sp}=0.2).

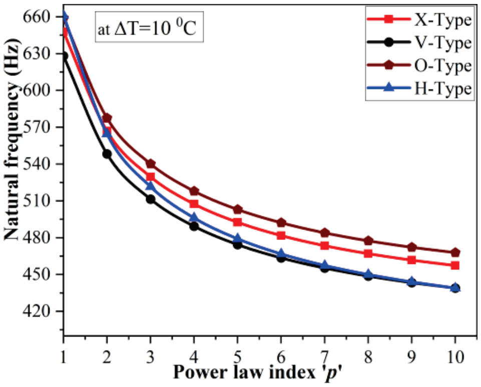

Figure 4.32: Natural frequency of C-C sandwich beam at different power law index (β=0.3 and η_{sp} =0.2).

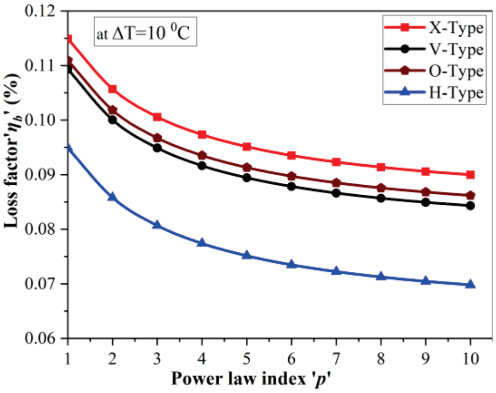

Figure 4.33: Loss factor of C-C sandwich beam at different power law index (β=0.3 and η_{sp} =0.2).

Figures 4.34 and 4.35 depict the natural frequency and loss factor behavior near the buckling temperature. The increase in temperature reduces the beam stiffness, which diminishes the natural frequency. The natural frequency approaches zero at CBT, whereas the loss factor increases with temperature and approaches infinity at CBT.

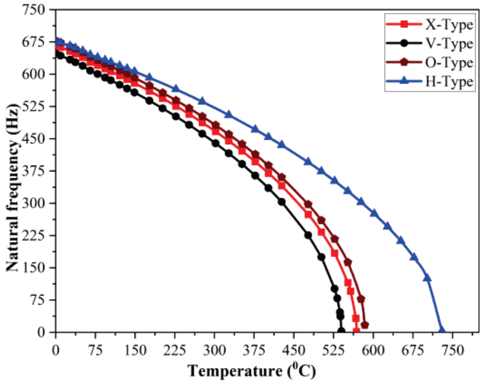

Figure 4.34: Natural frequency of C-C sandwich beam at CBT (p=1, β=0.3, and η_{sp}=0.2).

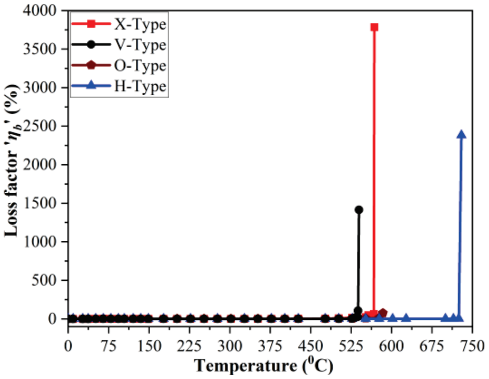

Figure 4.35: Loss factor of C-C sandwich beam at CBT (p=1, β=0.3, and η_{sp}=0.2).

Figure 4.36 shows the change in the loss factor of the porous sandwich beam with boundary loss factor (η_{sp}). The viscoelastic boundaries contribute to energy dissipation in vibrating structures, increasing the loss factor of the beam with the boundary loss factor. Table 4.5 displays the natural frequency and loss factor of porous sandwich beams for various BCs. C-C and P-R show the maximum and minimum natural frequency, respectively, and P-P and C-C beams show the highest and lowest loss factors among the four BCs.

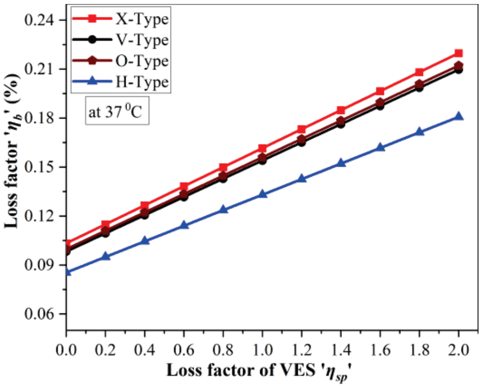

Figure 4.36: Loss factor of C-C sandwich beam with change in support damping (η_{sp}) (p=1, β=0.3).

Table 4.5: Natural frequency and loss factor for various boundary conditions at $\Delta T=10\ ^{0}C$ (β=0.3, p=1, and η_{sp}=0.2).

		BCs			
	Porosity patterns	**C-C**	**C-P**	**P-P**	**P-R**
Natural frequency (Hz)	NP	647.81	646.10	649.39	441.89
	X	647.79	646.33	644.87	442.56
	V	628.10	626.88	625.67	429.00
	O	659.03	657.26	655.49	450.13
	H	661.09	659.57	658.06	452.31
Loss factor (%)	NP	0.131	0.311	0.491	0.250
	X	0.115	0.273	0.432	0.220
	V	0.109	0.243	0.376	0.192
	O	0.11	0.296	0.481	0.244
	H	0.094	0.258	0.422	0.214

4.4 SUMMARY

In this chapter, the bending, buckling, and vibration of FG porous sandwich beams with viscoelastic boundary conditions (VBCs) in a thermal environment are discussed. Initially, bending and free vibration studies are done at room temperature. Transverse deflection, natural frequency, loss factors, and mode shapes are studied for various boundary conditions (C-F, P-R, and C-C) of the sandwich beams with varying support stiffness. Further porosity dispersion patterns (H, O V, and X) and VBCs are incorporated into the studies. The effect of various parameters such as power law index, porosity volume fraction, and viscoelastic support loss factor on transverse deflection, natural frequency, and loss factor of C-C FG porous sandwich beams are also discussed. In the next section, the temperature effect is incorporated into the studies; buckling and free vibration studies are carried out in a thermal environment. Finally, the effect of various parameters (porosity volume fraction, power law index, and VES loss factor) on critical buckling temperature (CBT), natural frequency, and loss factor is also investigated in a thermal environment.

CHAPTER 5

STUDIES ON DISC BRAKE PAD WITH Al-Al_2O_3 FG BACK PLATE AND BRAKE INSULATOR

5.1 INTRODUCTION

In recent years, many advancements have taken place in the automobile sector. As a result, the performance and comfort of new vehicles have improved compared to old vehicles. Disc brake squeal is one of the significant and challenging problems in automobiles which reduces both performance and comfort of the vehicle. The vibration induced by the friction between the wheel disc and brake pad generates the squeal. Brake insulators are being used to suppress the squeal. Different types of brake insulators are available in the market in which single-layer insulators, constrained-layer insulators, and multilayer-constrained insulators are primarily used in automobiles. A single-layer insulator combines a metal (steel) and a viscoelastic layer (Acrylic rubber or NBR rubber) (Glisovic and Miloradovic 2010). The back plate is a significant part of the disc brake system. In the actual case, the back plate is bound with friction material on one face and the brake insulator on the other. The whole assembly is treated as a brake pad.

In general, brake pads are rectangular in shape. The dimensions of brake pads vary with vehicles. This brake pad is held in a caliper by an anchor bracket. The maximum thickness of the brake insulator will be 1-1.2mm (Glisovic and Miloradovic 2010). Figure 5.1 shows the schematic diagram of the disc brake system and its mechanics. The brake pad attached to the brake insulator is held in a caliper by an anchor bracket. Generally, commercial softwares are being used to analyze the complete disc brake system in which various types of constraints are used along with boundary conditions to achieve the exact working environment of the disc brake system. When a vibration study of any individual part is to be done, the study can be carried out with any boundary condition (Patil et al. 2020).

The present study proposes $Al\text{-}Al_2O_3$ functionally graded (FG) back plate as a replacement for a steel back plate, which enhances the damping capacity of the overall disc brake pad by providing similar mechanical properties as that of a conventional steel back plate. The reason behind the proposal of FG back plate over steel back plate are listed as follows:

- $Al\text{-}Al_2O_3$ FG back plate improves the vibration-damping capability of the overall disc brake pad
- The ceramic-rich face of the $Al\text{-}Al_2O_3$ FG back plate resists the friction that occurs between the wheel disc and pad when the brake is applied.
- $Al\text{-}Al_2O_3$ FG back plate provides a high stiffness-to-mass ratio compared to steel.

The study is divided into two parts. In the first case, only the back plate with brake insulator is considered as a sandwich beam; a free and forced vibration study is carried out for a simply supported or pinned-roller case (P-R). In the second case, a complete brake pad (including friction material) is considered as a sandwich plate; free and forced vibration studies are carried out on the brake pad for a simply supported case (SSSS).

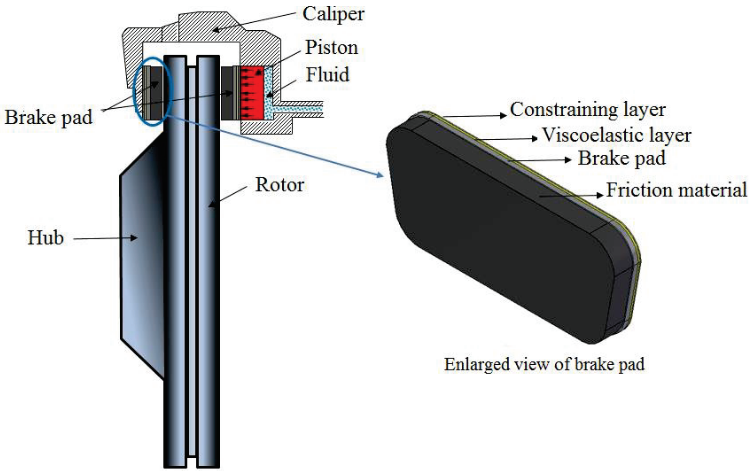
Caliper
Piston
Fluid
Brake pad
Constraining layer
Viscoelastic layer
Brake pad
Friction material
Rotor
Hub
Enlarged view of brake pad

Figure 5.1: Disc brake system.

5.2 CASE-1: VIBRATION OF STEEL AND AL-AL$_2$O$_3$ FG BACK PLATE WITH BRAKE INSULATOR

In this section, a three-layered sandwich beam is considered, which consists of a back plate with a brake insulator (viscoelastic material + steel constraining layer), as shown in Figure 5.2.

Accordingly, a comparison study is presented in terms of free and forced vibration characteristics of different material combinations for sandwich beams such as Steel-Acrylic-Steel, FGM-Acrylic-Steel, FGM-Acrylic-Aluminium, and Steel-Acrylic-Aluminium as shown in Figure 5.2. The material properties and dimensions of sandwich beams are given in Table 5.1. The Loss factor for Acrylic rubber is 0.38 at 30^{0}C (Wu et al. 2008).

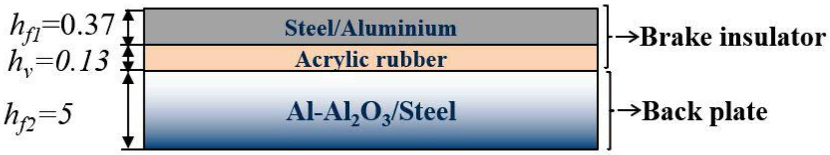

Figure 5.2: Back plate with brake insulator.

Table 5.1: Material properties and dimensions of sandwich beams.

Material	Density (kg/m^3)	Young's modulus (Pa)	Poisons ratio	Loss factor
Steel	7624	2.02X10^{11}	0.29	-
Acrylic	1100	1.25 X10^7	0.48	0.38
Aluminium (Al)	2698	0.69 X10^{11}	0.26	-
Aluminium oxide (Al$_2$O$_3$)	3750	3.4855 X10^{11}	0.33	-
Dimensions (mm) (McDaniel et al. 2005)	h_{f1}=0.37, h_v= 0.13, h_{f2}==5, l=400, b=50			

Al-Al$_2$O$_3$ metal-ceramic combination is such that one surface is metal-rich, and the other is partly ceramic-rich. Accordingly, Al$_2$O$_3$ varies from 0 to 40% more or less in a smooth gradation (Figure 1.1) such that one outer surface is Aluminium rich (100%) and the other is 40% Aluminium oxide (Al$_2$O$_3$), and the remaining is 60% Aluminium.

As the percentage gradation of Al_2O_3 with Aluminium base metal varies along the thickness, the properties like Young's modulus and density also vary. The natural frequency and loss factors are discussed for steel and Al-Al_2O_3 FG back plates with brake insulators. Further, a forced vibration study is also carried out for the back plate-brake insulator combinations under transverse point harmonic load in order to examine the maximum transverse deflection of back plates.

5.2.1 Free Vibration results

Free vibration study of back plate-brake insulator assembly akin to a sandwich beam is carried out with different material combinations. The natural frequencies of sandwich beams for the first three bending modes are given in Figure 5.3. The natural frequency of FGM-Acrylic-Steel is around 25.6%, 6.3%, and 25.3% higher than Steel-Acrylic-Steel, FGM-Acrylic-Aluminium, and Steel-Acrylic-Aluminium, respectively, as the rigidity and inertia coefficient ratio due to bending (D/I_D) is higher for FGM-Acrylic-Steel, as shown in Table 5.2. Figure 5.4 shows the loss factor of sandwich beams for bending modes. The loss factor of the FGM-Acrylic-Steel combination is around 80.21%, 303.1%, and 90.6% higher than Steel-Acrylic-Steel, FGM-Acrylic-Aluminium, and Steel-Acrylic-Aluminium, respectively. The sandwich beam loss factor depends on the core loss factor and strain energy stored in the core. The difference in axial displacement of upper and lower stiff layers at the core and stiff layer interface is more in FGM-Acrylic-Steel. Subsequently, the strain energy stored in the core is also more. The high-strain energy yields a high loss factor.

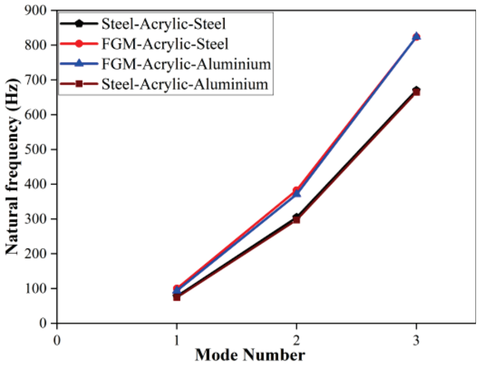

Figure 5.3: Natural frequency of sandwich beams.

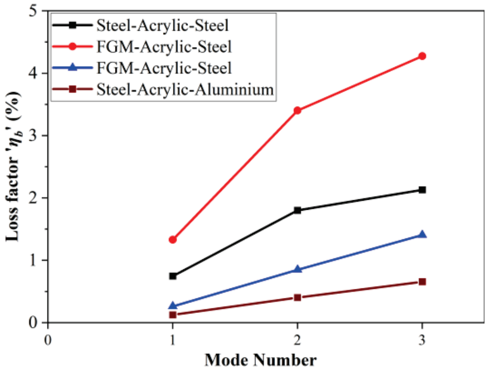

Figure 5.4: Loss factor of sandwich beams.

Table 5.2: Rigidity and inertia coefficients of sandwich beams for different material combinations.

Material Combination	**A**	**B**	**D**	**I_A**	**I_B**	**I_D**
Steel-Acrylic-Steel	$5.37 X 10^7$	0	104.588	2.047	0	$3.97 X 10^{-6}$
FGM-Acrylic-Steel	$3.5 X 10^7$	$1.4 X 10^4$	65.202	0.868	$5.03 X 10^{-5}$	$1.51 X 10^{-6}$
FGM- Acrylic-Aluminium	$3.253 X 10^7$	$1.4 X 10^4$	65.174	0.7769	$5.03 X 10^{-5}$	$1.51 X 10^{-6}$
Steel-Acrylic-Aluminium	$5.177 X 10^7$	0	104.1745	1.9559	0	$3.97 X 10^{-6}$

Figures 5.5 and 5.6 show the effect of beam length on the system's natural frequency and loss factor. The trend in Figure 5.6 implies that the loss factor is maximum for a particular beam length, and the deviation of beam length from that critical value reduces the loss factor. The figure affirms that finding the critical beam length is significant in sandwich beams to get high vibration damping. They are owing to the fact that an increase in beam length increases the mass and reduces the stiffness, the curves in Figure 5.5 exhibit continuous reduction of natural frequencies with an increase in beam length.

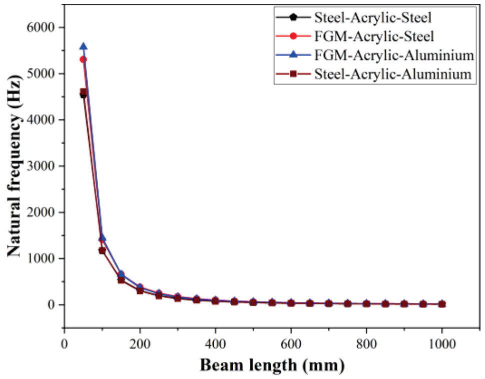

Figure 5.5:Variation in frequency with beam length.

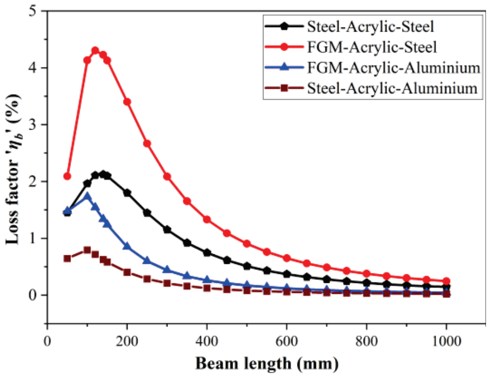

Figure 5.6: Variation in loss factor with beam length.

Figures 5.7 and 5.8 show the effect of core thickness on the natural frequency and loss factor of the beam in the second mode of vibration. A steady reduction in natural frequency shown in Figure 5.7 is due to a beam's stiffness reduction with an increase in core thickness, which leads to a reduction in natural frequency.

As previously reported loss factor of the sandwich beam is dependent on the core loss factor as well as the strain energy stored by the core. There will be an increase in the core loss factor and a decrease in strain energy stored by the core with the rise in core thickness. Up to a certain point, an increase in the core loss factor dominates the loss of strain energy in the core, leading to an increase in the beam loss factor, as shown in Figure 5.8. Once the beam loss factor reaches a global maximum, strain energy loss dominates the core loss factor, leading to a continuous decrease in the sandwich beam's loss factor.

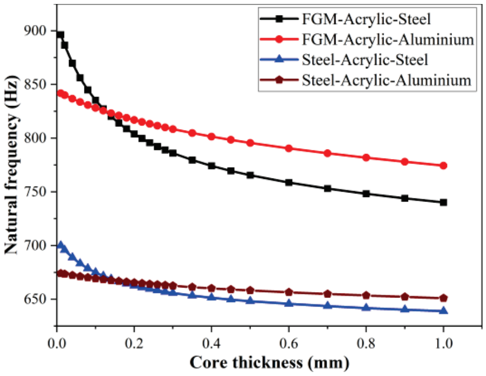

Figure 5.7: Variation in natural frequency with core thickness (l=400mm).

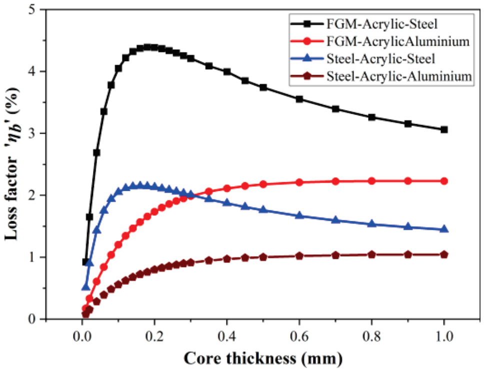

Figure 5.8: Variation in loss factor with core thickness (l =400mm).

After the free vibration, it is essential to study the behavior of back plate-brake insulator assembly under dynamic loading for different material combinations. For the present study, harmonic load of 1N is considered, which is applied at the frequency of 10rad/sec. In a sandwich beam under vibration, the shear stress and strain in the core vary sinusoidally with time '*t,'* but the strain response lags the stress by a certain phase angle. As a result, the shear modulus is treated as a complex number. Viscoelastic material's dynamic behavior is referred to as internal friction or mechanical damping. The displacement, strain, and stress will have two parts called real and imaginary due to the complex shear modulus of the core. The imaginary part of displacements, strains, and stresses always tries to resist the real part. So, the displacement, strain, and stress amplitude reduce with respect to time; in other words, damping occurs.

Initially, real and imaginary displacements, strains, and stresses are plotted separately for the backplate at its neutral axis to interpret the behavior of imaginary parts and their contribution to damping. Further, only real parts of displacements, strains, and stresses are plotted for backplate-brake insulator assembly (sandwich beam) along the thickness to analyze the behavior of the back plate and constraining layers in the presence of the core. Figures 5.9 and 5.10 exhibit the real and imaginary parts of transverse deflection with time, respectively. The real transverse deflection of Steel-Acrylic-Steel is less, meaning the particular combination gives better stiffness among the combinations. The imaginary transverse deflection of FGM-Acrylic-Steel is more, meaning the combination gives better damping results among all four combinations.

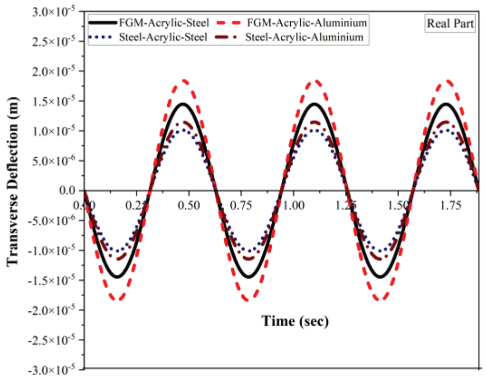

Figure 5.9: Real part of transverse deflection of sandwich beams (*x/l*=0.5).

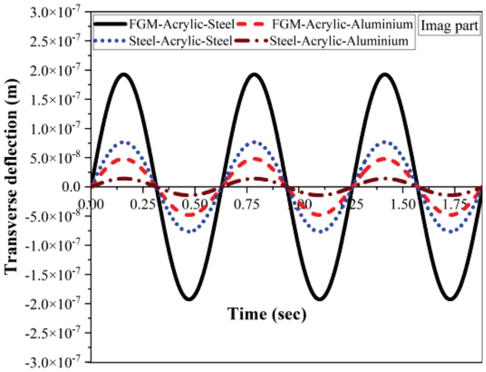

Figure 5.10: Imaginary part of transverse deflection of sandwich beams (*x/l*=0.5).

Figures 5.11-5.12 show real and imaginary axial displacements, Figures 5.13-5.14 show real and imaginary axial strains, and Figures 5.15-5.16 show real and imaginary axial stresses at the neutral axis of back plates. The real part of axial displacement, axial strain, and axial stress at the neutral axis of the FG back plate is marginally higher than steel, but the imaginary part of displacement, strain and stress of the FG back plate is significantly higher compared to steel. This indicates that up to 40% ceramic-rich FG back plate behaves similar to steel in terms of deformation, but the damping behavior of FG back plate is considerably improved compared to steel. So, the FG back plate improves the damping capacity of the disc brake pad compared to steel. The axial displacement and strain at the neutral axis vary with the constraining layer (steel/aluminium), even though the back plate remains the same (steel).

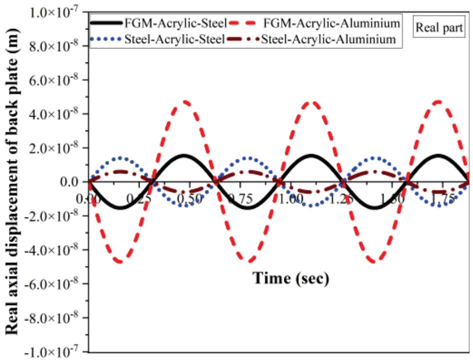

Figure 5.11: Real part of axial displacement of back plate at neutral axis of back plates (*x/l*=0.5).

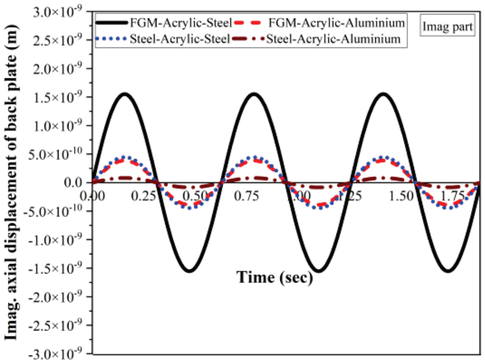

Figure 5.12: Imaginary part of axial displacement of back plate at neutral axis of back plates (*x/l*=0.5).

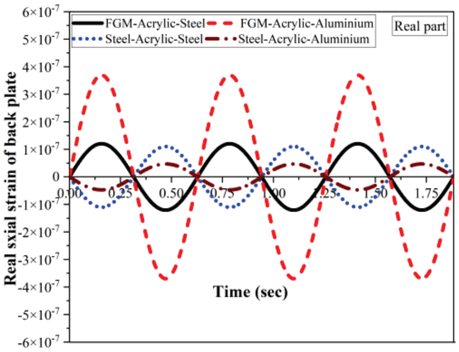

Figure 5.13: Real part of axial strain at neutral axis of back plates (*x/l*=0.5).

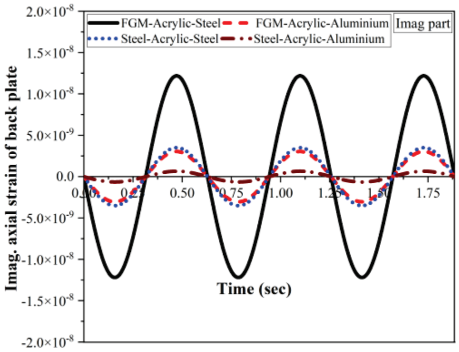

Figure 5.14: Imaginary part of axial strain at neutral axis of back plates (*x/l* =0.5).

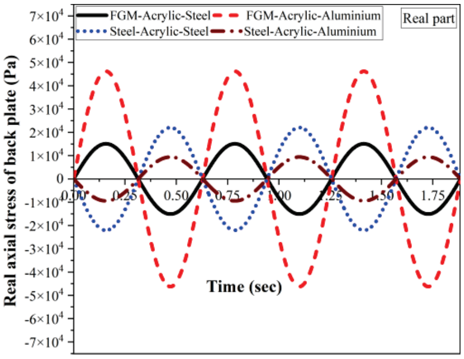

Figure 5.15: Real part of axial stress at neutral axis of back plates (*x/l* =0.5).

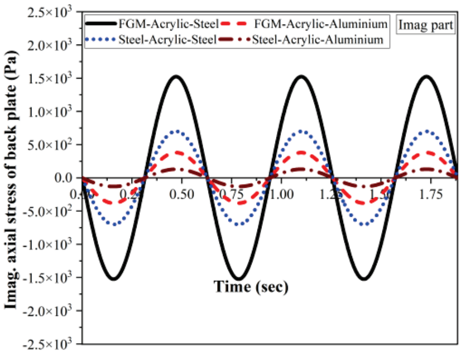

Figure 5.16: Imaginary part of axial stress at neutral axis of back plates (*x/l* =0.5).

Figure 5.17 shows that the axial displacement's real part varies linearly along the thickness. Figures 5.18 and 5.19 show the linear variation of the real part of axial strain and stress of the sandwich beams along the thickness of the beam, respectively. The reduction in axial displacement is observed in the constraining layer due to the higher shear deformation in the core. Figures 5.20 and 5.21 show the real part of shear strain and stress in the core along the length of the sandwich beam. Since the axial displacement and rotation at the supports are maximum, the shear stress and shear strain are maximum at the supports. In the middle of the beam, there will be zero rotation and zero axial displacements. So, the shear strain and stresses are zero. Figures 5.20 and 5.21 show that the FGM-Acrylic-Steel combination shows higher shear stress and strain, implying that the core's strain energy stored is maximum for that combination compared to the other three. The higher the stored strain energy higher will be the loss factor. In other words, damping is more for the FGM-Acrylic-Steel combination.

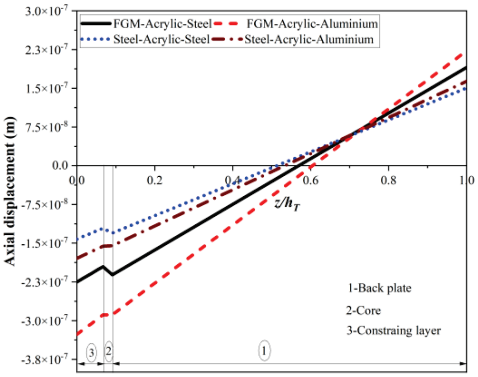

Figure 5.17: Axial displacement along the thickness direction *z* (*x/l* =0.25, *t*=0.157sec).

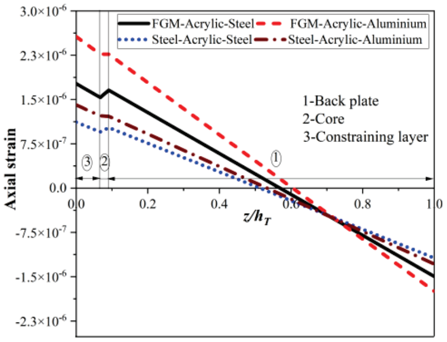

Figure 5.18: Axial strain along the thickness direction *z* (*x/l* =0.25, *t*=0.157sec).

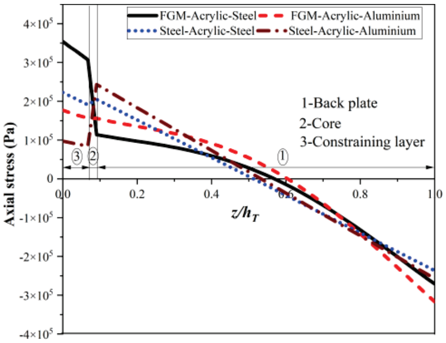

Figure 5.19: Axial stress along the thickness direction *z* (*x/l* =0.25, *t*=0.157sec).

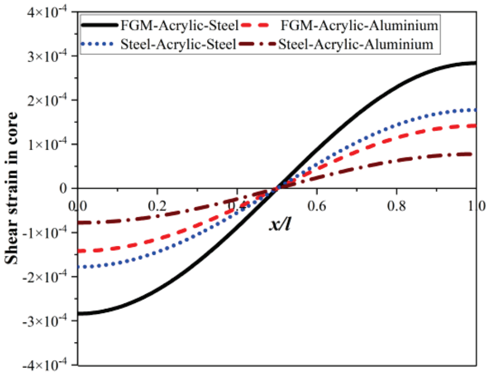

Figure 5.20: Shear strain in core along the length of beam (t=0.157sec).

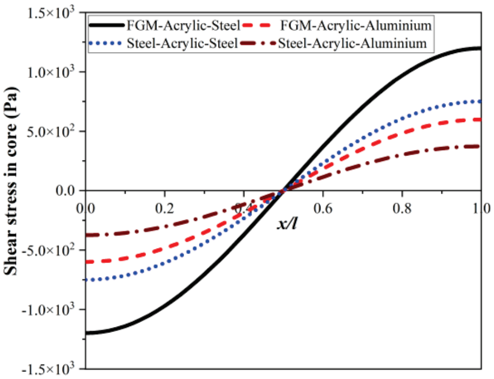

Figure 5.21: Shear stress in core along the length of beam (t=0.157sec).

5.3 CASE-2: VIBRATION OF COMPLETE BRAKE PAD (STEEL/AL-AL$_2$O$_3$ FG BACK PLATE AND FRICTION MATERIAL) WITH BRAKE INSULATOR

A comparison study presented in terms of the free and forced vibration characteristics of different material combinations for back plate-brake insulator sandwich beams in the previous section confirms the enhancement in damping capacity of disc brake pad by replacing steel back plate with Al-Al$_2$O$_3$ FGM. Still, the stiffness of Al-Al$_2$O$_3$ FGM with a maximum ceramic volume fraction of 40% is marginally less than steel.

To overcome the limitations of the previous analysis, in this section, the vibration study is carried out with some modifications as listed below:

- The study is elaborated to complete the brake pad (including friction material) instead of only the back plate, as shown in Figure 5.22.
- The sandwich plate model is adopted instead of the beam model to make the study more appropriate and convincing.
- The acrylic rubber is replaced with NBR rubber to show the significance of the brake insulator loss factor on the overall damping of the disc brake pad, which has similar shear modulus and density but a different loss factor.

- Uniformly distributive load (UDL) is considered instead of point load since, in actual conditions, the brake force is distributed to the whole surface of the brake pad

The properties of NBR rubber and frictional material with the dimension of the brake pad are shown in Table 5.3 (McDaniel et al. 2005).

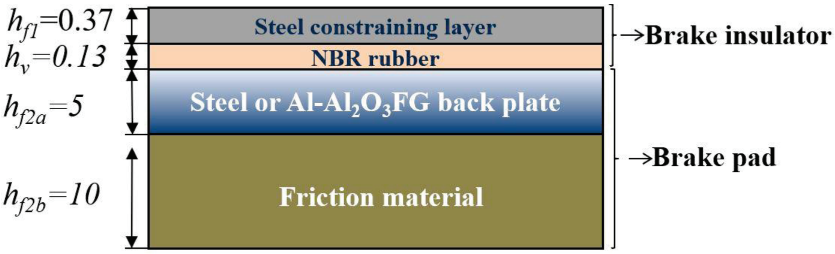

Figure 5.22: Brake pad with brake insulator.

Table 5.3: Material properties of brake insulator and friction materials.

Material	Young's Modulus (Pa)	Density (kg/m^3)	Loss factor	Poisons ratio
NBR (Liu et al. 2006)	1.51 X10^7	1100	0.126	0.48
Friction material (Nouby et al. 2011)	4 X10^9	2045	-	0.26
Dimensions (mm)	h_{f1}=0.37, h_v= 0.13, h_{f2a}==5, h_{f2b}=10, l=400, b=160			

5.3.1 Free vibration

In free vibration studies, natural frequency and loss factors are obtained for a brake pad with a steel (steel-NBR-steel) and FG back plate (FGM-NBR-steel), and a parametric study is carried out for sandwich plate combinations. Figure 5.23 shows the natural frequency, and Figure 5.24 shows the loss factor of brake pads. The ratio of stiffness to inertia coefficients (A_{ij}/I_A, D_{ij}/I_D) of FGM-NBR-steel is higher, as shown in Tables 5.4 and 5.5. Therefore, the natural frequencies of FGM-NBR-Steel are 21.21%, 20.75%, 19.52%, and 19.37% higher than Steel-NBR-Steel for the first four modes of vibrations. The shear deformation of the viscoelastic core influences the loss factor of the sandwich plate. The shear deformation is directly proportional to the difference in in-plane displacements (*xz* and *yz*) of upper and lower stiff layers at the interface (Khatua and Cheung 1973).

Since the difference in upper and lower stiff layer in-plane displacements are higher for FGM-NBR-Steel, the loss factors of that combination are 4.7%, 4.78%, 5.25%, and 4.66% higher than Steel-NBR-Steel for the first four modes of vibrations.

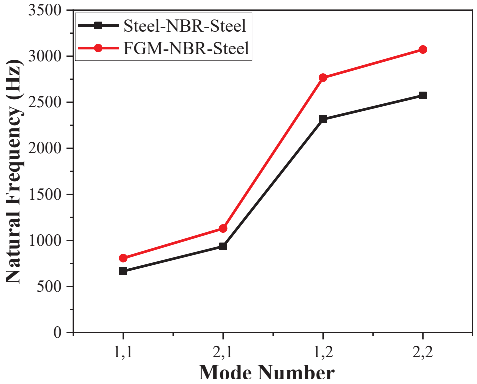

Figure 5.23: Natural frequency of brake pad assembly.

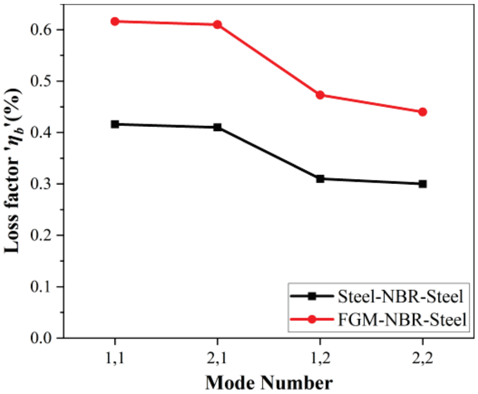

Figure 5.24: Loss factor of the brake pad assembly.

Table 5.4: Stiffness coefficients of brake pad with steel/FGM back plates.

Back plate material	$A_{11}^{(3)}$	$A_{12}^{(3)}$	$A_{66}^{(3)}$	$B_{11}^{(3)}$	$B_{12}^{(3)}$	$B_{66}^{(3)}$	$D_{11}^{(3)}$	$D_{12}^{(3)}$	$D_{66}^{(3)}$
Steel	1.15E9	3.48E8	4.03E8	-5.43E6	-1.62E6	-1.9E6	3.07E4	9242.1	1.07E4
FGM	1.28E9	3.86E8	4.47E8	-5.35E6	-1.6E6	-1.87E6	2.70E4	8139.7	9452.4

Table 5.5 Inertia coefficients of brake pad with steel/FGM back plates.

Back plate material	$I_A^{(3)}$	$I_B^{(3)}$	$I_D^{(3)}$
Steel	59.45	-0.143	1.35E-3
FGM	36.71	-0.028	7.16E-4

Figures 5.25 and 5.26 show the natural frequency and loss factor variation with change in the *b/l* ratio of sandwich plates (length is constant). The volume of the sandwich plate increases with breadth, increasing the plate's mass. So natural frequency reduces with an increase in breadth. The result trend in Figure 5.26 shows that the loss factor increases with an increase in breadth until the breadth reaches 0.4*l*; after that, the loss factor reduces continuously with an increase in breadth beyond 0.4*l*. This indicates that the shear deformation in the core is maximum if the breath is less than half its length.

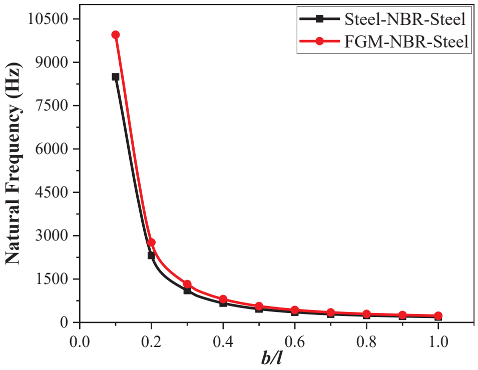

Figure 5.25: Effect of *b/l* ratio on natural frequency (*l* =400mm).

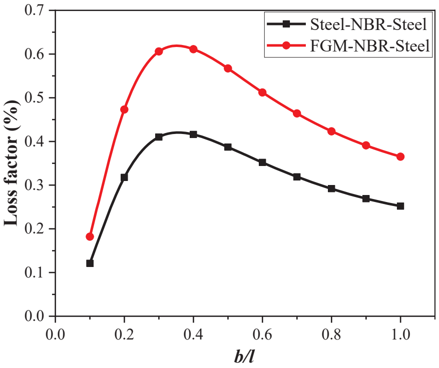

Figure 5.26: Effect of *b/l* ratio on loss factor (*l* =400mm).

Figures 5.27 and 5.28 show the effect of core thickness on the sandwich plate's natural frequency and loss factor. The higher the core thickness, the lower the sandwich plate's stiffness, reducing the natural frequency. An increase in core thickness increases the strain energy stored up to a certain value, resulting in a higher loss factor; if the thickness is increased beyond the critical value, compression of the core dominates the shear during transverse deflection. This leads to a reduction in the loss factor. Figures 5.29 and 5.30 show the effect of constraining layer thickness on the sandwich plate's natural frequency and loss factor, respectively. The natural frequency reduces with increasing constraining layer thickness due to increased inertia. In contrast, the inplane displacement reduces with increasing constraining layer thickness, which results in higher shear deformation in the core. The increase in shear deformation results in a high loss factor for the sandwich plates.

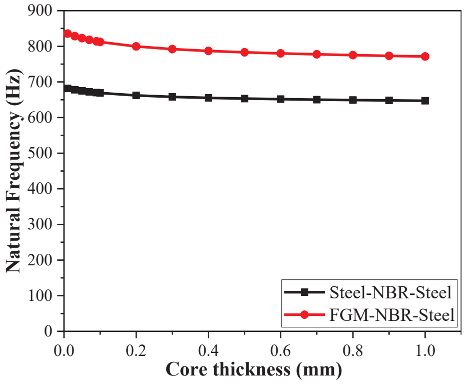

Figure 5.27: Influence of core thickness on natural frequency.

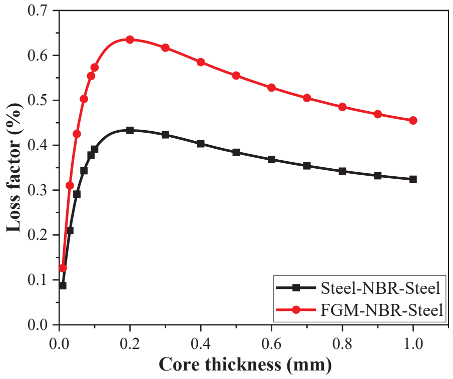

Figure 5.28: Influence of core thickness on loss factor.

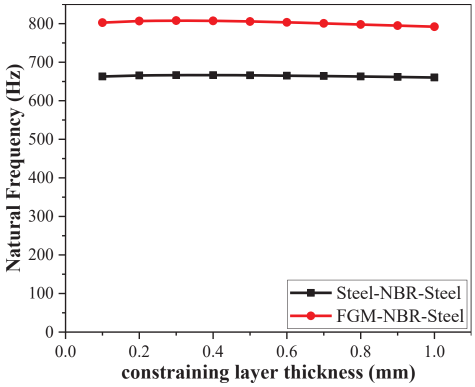

Figure 5.29: Influence of constraining layer thickness on the natural frequency.

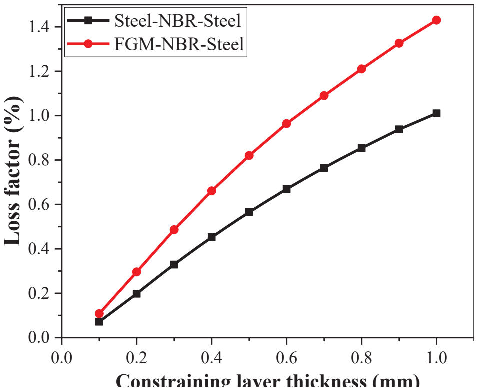

Figure 5.30: Influence of constraining layer thickness on loss factor.

Figures 5.31 and 5.32 show the sandwich plate's natural frequency and loss factor, respectively, with varying core loss factors. The core loss factor hardly affects the natural frequency of the sandwich plate, as seen in Figure 5.31. In contrast, the sandwich plate loss factor increases with the core loss factor, as shown in Figure 5.32. The variation of natural frequency and loss factor with power law index *p* is shown in Figures 5.33 and 5.34. Higher the *p*-value, the lower the Al_2O_3 content in FGM, leading to reduced stiffness. This results in a reduction of the natural frequency with an increase in *p*, whereas the less stiff FG layer shows higher in-plane displacement, which leads to an increase in the loss factor of the sandwich plate.

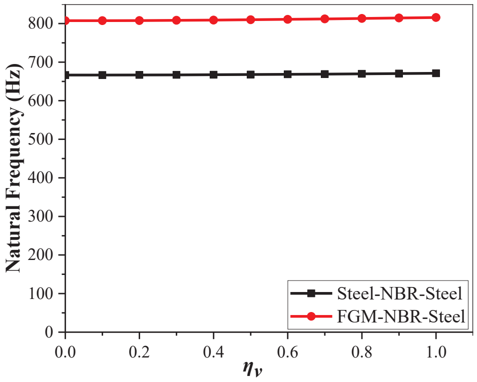

Figure 5.31: Influence of core loss factor on natural frequency.

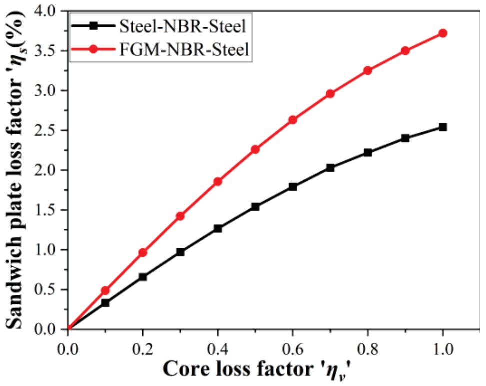

Figure 5.32: Influence of core loss factor on sandwich plate loss factor.

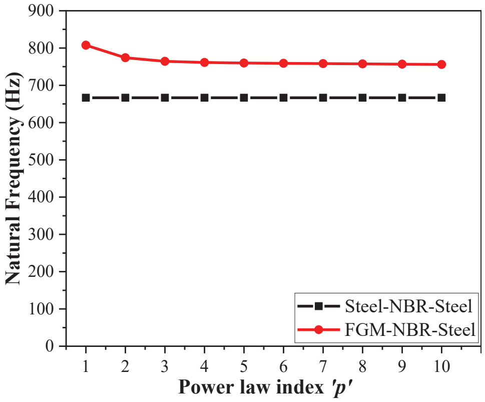

Figure 5.33: Influence of power law index on natural frequency.

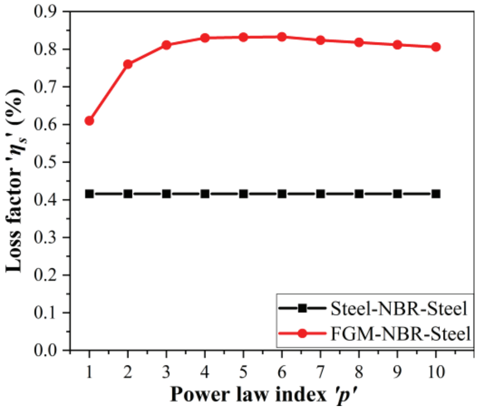

Figure 5.34: Influence of power law index on loss factor.

5.3.2 Transient response and steady state response

A transient study is carried out for simply supported sandwich plates to analyze the behavior of brake pads with a brake insulator under dynamic load. Initially, the plate is subjected to a uniformly distributed transverse load (UDL) of 10000N/m^2, which is applied as step load (Δt_{step}=0); the load is removed at Δt_{step}=1E-4 sec to set the plate into vibration. The Newmark method (Bathe K. 2016) is used to obtain the transient response. Since the viscoelastic core properties are complex in nature, the stiffness coefficients [*K*] are also complex with the real part [K_R] and imaginary part [K_I]. It is shown in the equation:

$$[K] = [K_R] + [K_I] \tag{5.1}$$

In the time domain, the imaginary stiffness coefficients are considered as damping coefficients (Moita et al. 2018) and are given as,

$$[C] = \frac{1}{\omega}[K_I] \tag{5.2}$$

The Eqn. 28 can be rewritten in the time domain as,

$$M\ddot{X} + C\dot{X} + KX = F \tag{5.3}$$

Where [*M*] is the mass matrix, [*C*] is the damping matrix, K_R is the stiffness matrix (consists of only real parts) and [*F*] is the force matrix, and [*X*] is the displacement matrix.

Figures 5.35 and 5.36 show the central transverse deflection of Steel-NBR-Steel and FGM-NBR-Steel, respectively, for damped and undamped conditions.

The shear deformation in the core for FGM-NBR-Steel is higher than Steel-NBR-Steel, which increases the dissipation of energy in the particular combination, resulting in high damping.

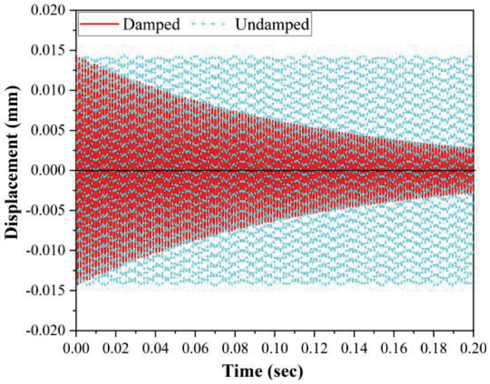

Figure 5.35: Damped and undamped transverse deflection of Steel-NBR-Steel at the center of plate (η_v=0.126).

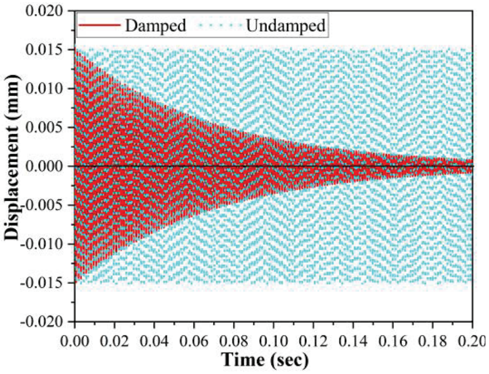

Figure 5.36: Damped and undamped transverse deflection of FGM-NBR-Steel at the center of plate (η_v=0.126).

Table 5.6 shows the depletion in the transverse deflection of brake pad with FG back plate is 89.61% higher compared to pad with steel back plate at 0.2 sec. The transverse deflection is reduced by 98.45% and 84.43% in FGM-NBR-Steel and Steel-NBR-Steel, respectively, in 0.2sec when compared with their respective initial displacements as shown in Table 5.7, also replicates the maximum damping in FGM-NBR-Steel.

Table 5.6: Damped transverse deflection of FGM-NBR-Steel and Steel-NBR-Steel at different points of time.

Time sec	**Displacement (mm)**		**Difference in (%)**
	FGM-NBR-Steel	**Steel-NBR-Steel**	
0	0.01564	0.01497	0.4
0.2	0.000242	0.00233	89.61

Table 5.7: Percentage damping of transverse deflection in FGM-NBR-Steel and Steel-NBR-Steel in 0.2 sec.

Material combination	**Displacement (mm)**		**Damping (%)**
	0 sec	**0.2 sec**	
FGM-NBR-Steel	0.01564	0.000242	98.45
Steel-NBR-Steel	0.01497	0.00233	84.43

Figure 5.37 shows the influence of the viscoelastic core on the dynamic behavior of the FGM-NBR-Steel back plate-brake insulator assembly. It is seen that as the core loss factor increases from 0.05 to 0.3 (η_v = 0.05, 0.1, 0.2, 0.3), the damping time decreases. A higher loss factor indicates a higher phase difference of stress compared to strain, which causes energy loss in the system.

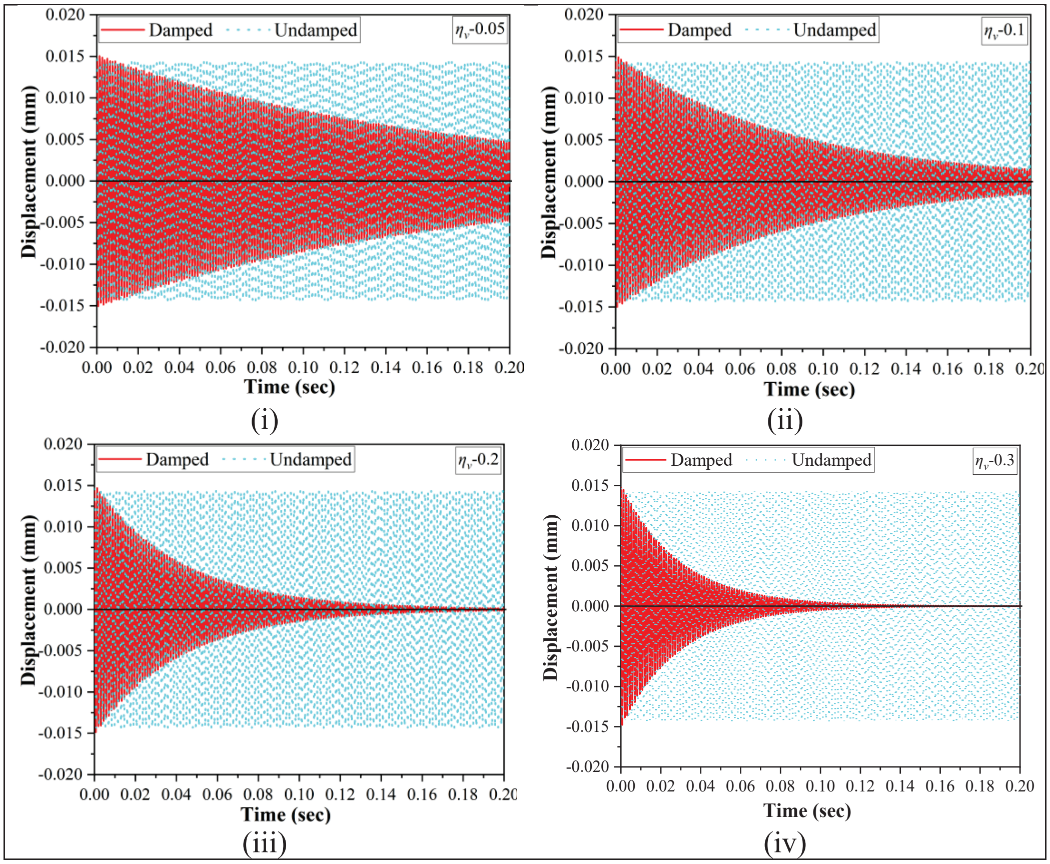

Figure 5.37: Influence of core loss factor on damping of central transverse deflection of FGM-NBR-Steel (η_v= 0.05, 0.1, 0.2, 0.3).

Further, the study is extended to forced vibration. A uniformly distributed sinusoidal load of 10000 N/m^2 is considered with a 10 Hz frequency ($F = 10000\sin(\omega t)$). Figure 5.38 shows the transverse deflection of brake pads with FG and steel back plates. The figure shows that the displacement of the FG back plate is only 0.4% higher than steel, which means both steel and FG back plates undergo similar deformation under brake loads.

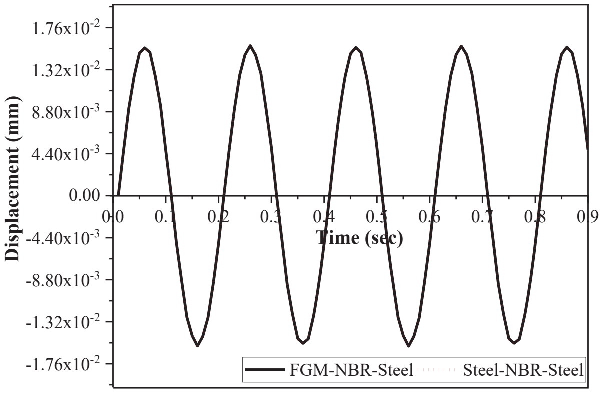

Figure 5.38: Transverse deflection of brake pad under UDL harmonic loading.

5.4 SUMMARY

In this chapter vibration behavior of a disc brake pad is discussed. Initially, only the back plate-brake insulator assembly is considered as sandwich beam, free and forced vibration studies are carried out. Four combinations of sandwich beam akin to the sandwich beam are considered; their natural frequency and loss factor is obtained. Further, forced vibration studies are also done on the sandwich beams under a sinusoidal load. Similarly, in the next section, a complete brake pad (including friction material) is considered as a sandwich plate; free and forced vibration studies are carried out. The free and forced vibration results in both studies confirm that the steel back plate can be replaced with Al-Al_2O_3 functionally graded material, enhancing the brake pad's damping capacity without compromising the back plate's stiffness.

CHAPTER 6

SUMMARY AND CONCLUSIONS

6.1 SUMMARY

The present work discusses FE and analytical formulations of functionally graded (FG) sandwich structures with viscoelastic interlayers. FE model is developed for bending, buckling, and free vibration of FG sandwich beams with viscoelastic boundary conditions in a thermal environment. The developed FE model is validated with the analytical model. The strain and kinetic energies of the stiff and core layers and work done by external forces are derived based on certain assumptions, as discussed in previous sections. Static and dynamic equilibrium equations of sandwich beams are derived using Euler-Lagrange equations. FE and Navier's solution methods are used to solve the equilibrium equations of sandwich beams.

Further porosity models and viscoelastic boundary conditions are incorporated into the study; bending, buckling, and vibration studies are carried out in a thermal environment using the FE model. Similarly, an analytical sandwich plate model is developed FG sandwich plate with a viscoelastic interlayer. Finally, sandwich beam and plate models are used to study the free and forced vibration of the disc brake pad. The results reveal that replacing back plate material from steel to Al-Al_2O_3 FGM with a ceramic variation of 0% to 100% along the thickness enhances the damping capacity of the disc brake pad and resists the transverse load (Stiff) as effectively as steel back plate.

6.2 CONCLUSIONS

The conclusions of bending, buckling and free vibration of FG sandwich beam and vibration studies on disc brake pad with Al-Al_2O_3 FG back plate with brake insulators are discussed as follows:

6.2.1 Studies on FG porous sandwich beam with viscoelastic boundary conditions in thermal environment

The complex shear modulus and complex stiffness are taken into account to model the viscoelastic core and supports (boundaries), respectively. The FG stiff layers are assumed to have various porosity patterns (H, O, V and X), which influence the material properties such as modulus of elasticity and density. Some of the critical observations from the static bending and free vibration study of FG sandwich beams at room temperature are listed as follows:

- The viscoelastic supports (VES) with variable stiffness act as conventional constraints (C-F, C-C, and S-S) as the viscoelastic support stiffness (VSS) reaches a critical value. The deflection, natural frequency, and loss factors of the sandwich beam remain constant beyond the critical values.
- VES contributes to the overall damping of the sandwich beam along with the viscoelastic core, and the effect of support damping is predominant when the VSS is less (soft support). In contrast, the core damping dominates with increased VSS (Hard support).
- The stiffness of the sandwich beam reduces considerably when the porosity percentage is higher in the metal-rich region of the FG stiff layer, which results in the reduction of natural frequency.
- For a constant point load of 10N, The C-C sandwich beam with V and H-type porosities gives maximum and minimum transverse deflection. The transverse deflection of V-type porosity is 23.07% and 27.77% less than H-type porosity for power-law (*p*) 0.5 and 3, respectively, at β=0.3.
- The C-C sandwich beam with V and X-type porosities portrays maximum and minimum natural frequency. V-type porosity natural frequency escalates from 5.177% to 6.63% at β=0.3 when power law (*p*) is enhanced from 0.5 to 3 compared to X- type porosity.
- The C-C sandwich beam with V and H-type porosities portrays maximum and minimum loss factors for a given porosity volume fraction. The loss factor of V-type porosity is 12.42% and 17.54% high compared to H- type porosity for the power law (*p*) 0.5 and 3 at β=0.3.

Some of the important observations from the static buckling and free vibration study of FG sandwich beams in a thermal environment are listed as follows:

- Critical buckling temperature (CBT) changes with viscoelastic boundary conditions (VBCs). The support which provides high stiffness shows higher CBT. For the present problem, the CBT of the C-C beam is the maximum among the four VBCs (C-C, C-P, P-P, and P-R).
- The existence of porosity reduces the thermal stress induced in the beam, which intern enhances the CBT. The C-C beam having H-porosity shows high CBT (941.85^0C) for the $\Delta T=50^0$C, which is 27.42%, 22.40%, and 19.80% higher than V, X, and O-porosities.
- The CBT of porous sandwich beams reduces with an increase in the power law index (*p*). An increase in the *p*-value results in higher metal content in FG stiff layers, which reduces the beam's stiffness.
- The natural frequency decreases with an increase in temperature and becomes zero at CBT, whereas the loss factor increases with an increase in temperature and becomes infinity at CBT.
- The natural frequency of the C-C sandwich beam with H-porosity is 661.09 Hz for the $\Delta T=10^0$C, which is 4.99%, 2.01%, and 0.0031% higher than V, X, and O-porosities, respectively. The loss factor of the beam with X-porosity is 0.115% for the $\Delta T=10^0$C, which is 18.26%, 5.22%, and 4.34% than V, X, and H-porosities, respectively.
- The increase in VBCs damping enhances the overall damping of the sandwich beam. X-porosity exhibits maximum damping (0.1032% to 0.2197%), and H-porosity exhibits minimum damping (0.0853% to 0.1806%) for the variation of VBCs loss factor (η_{sp}) from 0 to 2.

6.2.2 Studies on disc brake pad with Al-Al_2O_3 functionally graded back plate and brake insulator of a disc brake system

Free and forced vibration studies of disc brake pads with Al-Al_2O_3 functionally graded back plates and brake insulators are carried out.

The whole study is carried out for two cases. In the first case, up to 40% ceramic-rich Al-Al_2O_3 functionally graded back plate with brake insulator is considered as a sandwich beam. In the second case, a complete brake pad includes up to 100% ceramic-rich Al-Al_2O_3 back plate, brake insulator, and friction material. The conclusions of both studies are listed as follows:

6.2.2.1 *Al-Al_2O_3 back plate with brake insulator (sandwich beam)*

Sandwich beams resemble the back plate and brake insulator assembly are considered for vibration studies with different material combinations such as Steel-Acrylic-Steel, FGM-Acrylic-Steel, FGM-Acrylic-Aluminium, and Steel-Acrylic-Aluminium.

- Free vibration affirms that the back plate's natural frequency and loss factor with brake insulator can be improved by around 26% and 82%, respectively, by replacing the steel back plate with Al-Al_2O_3 FGM.
- Even though the magnitude of the real part of transverse deflection is 10% higher in FGM-Acrylic-Steel, the respective imaginary part is improved by 150%.
- The imaginary axial strain and stress of FGM-Acrylic-Steel are 240% and 54% higher than Steel-Acrylic-Steel. This implies the damping capacity of FGM-Acrylic-Steel is more compared to Steel-Acrylic-Steel.
- Functionally graded Al_2O_3 offers excellent wear resistance and withstands high temperatures due to frictional heat generation during braking. Al_2O_3 is gradually graded with Aluminium rich layers to compromise for brittleness of Al_2O_3.

6.2.2.2 *Complete Brake pad with Al-Al_2O_3 back plate, brake insulator, and friction material (sandwich plate)*

A comparison study is carried out between brake pads with Al-Al_2O_3 FG back plates and conventional steel back plates.

- Free vibration study brings out that the natural frequency and loss factor of the brake pad associated is ameliorated by 21.21% and 4.7% in the first mode of vibration, respectively, by replacing the steel back plate with Al-Al_2O_3 FGM.
- Al-Al_2O_3 FG back plate with 0 to 100% ceramic gradation is as stiff as steel back plate and withstands transverse load (brake load) as effectively as steel.

- FG back plate with power law index *p*=3 to 5 yields higher loss factors, implying the damping capacity of FG back plate with power law index *p*=3 to 5 ceramic gradations is higher.
- The transient results show that the vibration amplitude is reduced by 98.45% and 84.43% in 0.2 sec for FG and steel back plates, respectively, which means energy dissipation will be more if steel is replaced with an FG back plate.

6.3 SCOPE FOR FUTURE STUDIES

The present work focuses on theoretical studies on the bending, buckling, and vibration behavior of FG sandwich beams with viscoelastic boundary conditions (VBCs) in the thermal environment using a FE model. The scope for future studies is listed as follows:

- The bending, buckling, and vibration studies with VBCs can be extended to various FG sandwich structures, such as sandwich plates, shells, and circular and annular discs.
- Studies on geometric nonlinearity due to thermal stresses and the effect of geometric nonlinearity on the bending, buckling, and vibration characteristics of various structures (sandwich plates, shells, and circular discs) can be studied.
- Experimental investigation of FG sandwich structure bending, buckling, and vibration behavior can be conducted.
- Thermo-mechanical investigation can be performed on brake pad with FG back plate with brake insulator.

REFERENCE

Abdullah, M. A., Rahim, E. A., Bakar, A. R. A., and Akop, M. Z. (2017). "Numerical analysis of the effectiveness of brake insulator in decreasing the brake squeal noise." *J. Mech. Eng. Technol.*, 9(1), 87–102.

Al-Maharma, A. Y., Patil, S. P., and Markert, B. (2020). "Effects of porosity on the mechanical properties of additively manufactured components: a critical review." *Mater. Res. Express*, 7.

Arikoglu, A., and Ozkol, I. (2010). "Vibration analysis of composite sandwich beams with viscoelastic core by using differential transform method." *Compos. Struct.*, 92(12), 3031–3039.

Azar, J. J. (1968). "Bending theory for multilayer orthotropic sandwich plates." *AIAA J.*, 6(11), 2166–2169.

Bathe K. (2016). *Finite Element Procedures*. United States of America: Prentice Hall, Pearson Education, Inc.

Bhangale, R. K., and Ganesan, N. (2006). "Thermoelastic buckling and vibration behavior of a functionally graded sandwich beam with constrained viscoelastic core." *J. Sound Vib.*, 295(1–2), 294–316.

Daikh, A. A., and Zenkour, A. M. (2019). "Effect of porosity on the bending analysis of various functionally graded sandwich plates." *Mater. Res. Express*, 6(6), 65703.

Demir, C., and Oz, F. E. (2014). "Free vibration analysis of a functionally graded viscoelastic supported beam." *J. Vib. Control*, 20(16), 2464–2486.

DiTaranto, R. A. (1965). "Theory of vibratory bending for elastic and viscoelastic layered finite-length beams." *J. Appl. Mech.*, 32(4), 881.

DiTaranto, R., and Blasingame, W. (1967). "Composite damping of vibrating sandwich beams." *J. Manuf. Sci. Eng.*, 89(4), 633–638.

Fazzolari, F. A. (2018). "Generalized exponential, polynomial and trigonometric theories for vibration and stability analysis of porous FG sandwich beams resting on elastic foundations." *Compos. Part B Eng.*, 136, 254–271.

Festjens, H., Gaël, C., Franck, R., Jean-Luc, D., and Remy, L. (2012). "Effectiveness of multilayer viscoelastic insulators to prevent occurrences of brake squeal: A numerical study." *Appl. Acoust.*, 73(11), 1121–1128.

Galucio, A. C., De, J.-F., and Ohayon, R. (2004). "Finite element formulation of viscoelastic sandwich beams using fractional derivative operators." *Comput. Mech.*, 33(4), 282–291.

Galuppi, L., and Royer-Carfagni, G. (2012). "Laminated beams with viscoelastic interlayer." *Int. J. Solids Struct.*, 49(18), 2637–2645.

Ganesan, N., and Pradeep, V. (2005). "Buckling and vibration of sandwich beams with viscoelastic core under thermal environments." *J. Sound Vib.*, 286(4–5), 1067–1074.

Gao, J. X., and Liao, W. H. (2005). "Vibration analysis of simply supported beams with enhanced self-sensing active constrained layer damping treatments." *J. Sound Vib.*, 280(1–2), 329–357.

Glisovic, J., and Miloradovic, D. (2010). "Eliminating brake noise problem." *Mobil. &Vehicle Mech.*, (3), 37.

Hadji, L., and Avcar, M. (2021). "Free Vibration Analysis of FG Porous Sandwich Plates under Various Boundary Conditions." *J. Appl. Comput. Mech.*, 7(2), 505–519.

Han, D., Wang, J., Smith, E. C., and Lesieutre, G. A. (2013). "Transient loads control of a variable speed rotor during lagwise resonance crossing." *AIAA J.*, 51(1), 20–29.

Huang, Z., Qin, Z., and Chu, F. (2016). "Vibration and damping characteristics of sandwich plates with viscoelastic core." *J. Vib. Control*, 22(7), 1876–1888.

Jeyaraj, P., Padmanabhan, C., and Ganesan, N. (2011). "Vibro-acoustic behavior of a multilayered viscoelastic sandwich plate under a thermal environment." *J. Sandw. Struct. Mater.*, 13(5), 509–537.

Johnson, C. D., and Kienholz, D. A. (1982). "Finite element prediction of damping in structures with constrained viscoelastic layers." *AIAA J.*, 20(9), 1284–1290.

Joseph, S. V., and Mohanty, S. C. (2019). “Temperature effects on buckling and vibration characteristics of sandwich plate with viscoelastic core and functionally graded material constraining layer.” *J. Sandw. Struct. Mater.*, 21(4), 1557–1577.

Kao, J. (1968). “Bending of Multilayer Sandwich Beams.” *AIAA J.*, (August), 1583–1585.

Khatua, T. P., and Cheung, Y. K. (1973). “Bending and vibration of multilayer sandwich beams and plates.” *Int. J. Numer. Methods Eng.*, 6(1), 11–24.

Kung, S.-W., and Singh, R. (1998). “Vibration analysis of beams with multiple constrained layer damping patches.” *J. Sound Vib.*, 212(5), 781–805.

Lakes, R. (2009). *Viscoelastic materials*. Cambridge university press.

Lall, A. K., Asnani, N. T., and Nakra, B. C. (1988). “Damping analysis of partially covered sandwich beams.” *J. Sound Vib.*, 123(2), 247–259.

Li, J., Zheng, B., Yang, Q., and Hu, X. (2014). “Analysis on time-dependent behavior of laminated functionally graded beams with viscoelastic interlayer.” *Compos. Struct.*, 107(1), 30–35.

Li, Q., Iu, V. P., and Kou, K. P. (2008). “Three-dimensional vibration analysis of functionally graded material sandwich plates.” *J. Sound Vib.*, 311(1–2), 498–515.

Liaw and Little. (1967). “Theory of bending multilayer sandwich plates.” *AIAA J.*, 5(2), 301–304.

Lin, Y. K. (1962). “Free vibrations of a continuous beam on elastic supports.” *Int. J. Mech. Sci.*, 4(5), 409–423.

Liu, M., Cheng, Y., and Liu, J. (2015). “High-order free vibration analysis of sandwich plates with both functionally graded face sheets and functionally graded flexible core.” *Compos. Part B Eng.*, 72, 97–107.

Liu, L., Jia, D., Luo, Y., and Guo, B. (2006). “Preparation, structure and properties of nitrile–butadiene rubber–organoclay nanocomposites by reactive mixing intercalation method.” *J Appl Polym Sci*, 100(3), 1905–1913.

Mahamood, R. M., Akinlabi, E. T., Shukla, M., and Pityana, S. (2012). "Functionally graded material: an overview." *World Congr. Eng.*, London, UK: International Association of Engineers (IAENG), 1593–1597.

McDaniel, J. G., Li, X., Elvenkemper, A., Wegmann, E., Wang, A., Chen, S.-E., and Flint, J. (2005). "Simulating the Effect of Insulators in Reducing Disc Brake Squeele." *SAE Transactions*, 114, 3091–3097.

Mead, D. J., and Markus, S. (1969). "The forced vibration of a three-layer, damped sandwich beam with arbitrary boundary conditions." *J. Sound Vib.*, 10(2), 163–175.

Mead, D. J., and Markus, S. (1970). "Loss factors and resonant frequencies of encastre damped sandwich beams." *J. Sound Vib.*, 12(1), 99–112.

Miyamoto, Y., Kaysser, W. A., Rabin, B. H., Kawasaki, A., and Ford, R. G. (2013). *Functionally graded materials: design, processing and applications*. Springer Science & Business Media.

Moita, J. S., Araújo, A. L., Soares, C. M. M., and Soares, C. A. M. (2018). "Vibration analysis of functionally graded material sandwich structures with passive damping." *Compos. Struct.*, 183, 407–415.

Nouby, M., and Srinivasan, K. (2011). "Simulation of the structural modifications of a disc brake system to reduce brake squeal." Proceedings of the Institution of Mechanical Engineers, Part D: Journal of Automobile Engineering, 225(5), 653–672.

Patil, R., Joladarashi, S., and Kadoli, R. (2020). "Studies on free and forced vibration of functionally graded back plate with brake insulator of a disc brake system." *Arch. Appl. Mech.*, 90(12), 2693–2714.

Pompe, W., Worch, H., Epple, M., Friess, W., Gelinsky, M., Greil, P., Hempel, U., Scharnweber, D., and Schulte, K. (2003). "Functionally graded materials for biomedical applications." *Mater. Sci. Eng. A*, 362(1–2), 40–60.

Sayyad, A. S., and Ghugal, Y. M. (2019). "Modeling and analysis of functionally graded sandwich beams: A review." *Mech. Adv. Mater. Struct.*, 26(21), 1776–1795.

Sharnappa, Ganesan, N., and Sethuraman, R. (2007). “Dynamic modeling of active constrained layer damping of composite beam under thermal environment.” *J. Sound Vib.*, 305(4), 728–749.

Singh, K. V., Oliver, D., and Ling, X. (2015). “Continuous Structures With Viscoelastic Supports: Tuning of Material Parameters and Support Location.” *ASME 2015 Dyn. Syst. Control Conf.*

Tang, S.-J., and Lumsdaine, A. (2008). “Analysis of constrained damping layers, including normal-strain effects.” *AIAA J.*, 46(12), 2998–3011.

Triches Jr, M., Gerges, S. N. Y., and Jordan, R. (2004). “Reduction of squeal noise from disc brake systems using constrained layer damping.” *J. Brazilian Soc. Mech. Sci. Eng.*, 26(3), 340–348.

Vangipuram, P., and Ganesan, N. (2007). “Buckling and vibration of rectangular composite viscoelastic sandwich plates under thermal loads.” *Compos. Struct.*, 77(4), 419–429.

Vynnycky, M. (2020). “On the formation of centreline shrinkage porosity in the continuous casting of steel.” *J. Math. Ind.*, 10(1), 1–26.

Wang G., Veeramani S., W. N. (2000). “Analysis of Sandwich Plates with Isotropic Face Plates and a Viscoelastic Core.” *J. Vib. Acoust.*, 122, 305–312.

Wang, J., Zhang, Y. H., Yu, T., and Han, Q. K. (2018). “Dynamic characteristics of blade with viscoelastic damping block based on complex eigenvalue method.” *Shock Vib.*, 2018.

Wang, X., John, S., and Ren, H. (2011). “A Study of Squeal Noise in Vehicle Brake System.” *ASME 2011 Int. Mech. Eng. Congr. Expo.*, 711–716.

Wattanasakulpong, N., and Ungbhakorn, V. (2014). “Linear and nonlinear vibration analysis of elastically restrained ends FGM beams with porosities.” *Aerosp. Sci. Technol.*, 32(1), 111–120.

Wu, C., Wei, C., Guo, W., and Wu, C. (2008). “Dynamic mechanical properties of acrylic rubber blended with phenolic resin.” *J. Appl. Polym. Sci.*, 109(4), 2065–2070.

Xu, Z., Wang, X., and Jiang, M. (2017). “Investigation on improvement of center porosity with heavy reduction in continuously cast thick slabs.” *steel Res. Int.*, 88(2), 1600061.

Yang, W.-P., Chen, L.-W., and Wang, C.-C. (2005). “Vibration and dynamic stability of a traveling sandwich beam.” *J. Sound Vib.*, 285(3), 597–614.

Zhang, Y., Jin, G., Chen, M., Ye, T., Yang, C., and Yin, Y. (2020). “Free vibration and damping analysis of porous functionally graded sandwich plates with a viscoelastic core.” *Compos. Struct.*, 244, 112298.

CURRICULUM VITAE

1. Name: **RAKESH PATIL**
2. Date of Birth: 31/07/1993
3. Permanent Address: Basava Chetana Nilaya, 6th Cross Kadasiddeshwara colony, Jamakhandi-587301
4. Mobile Number: 7795561604
5. Email ID: rakeshpatil185@yahoo.com
   rakeshpatil31793@gmail.com
6. Education Qualification: B.E. M.Tech., Ph.D.

2015 **Bachelor of Engineering**

Institution: GM Institute of Technology (Aff. VTU).
Davanagere, Karnataka, India.
Specialization: Mechanical Engineering

2017 **Master of Engineering**

Institution: The National Institute of Engineering (Autonomous).
Mysuru, Karnataka, India.
Specialization: Machine Design

2023 **Doctor of Philosophy**

Institution: National Institute of Technology Karnataka, Surathkal, Karnataka, India.
Registration Date: 13/07/2017
Thesis Submission Date: 06/01/2023
Viva-Voice Date: 19/05/2023

LIST OF PUBLICATIONS BASED ON THESIS

International Journals

1. Patil, R., Joladarashi, S., and Kadoli, R. (2020). “Studies on free and forced vibration of functionally graded back plate with brake insulator of a disc brake system.” Arch. Appl. Mech., 90(12), 2693–2714.
2. Patil, R., Joladarashi, S., and Kadoli, R. (2022). “Bending and vibration studies of FG porous sandwich beam with viscoelastic boundary conditions: FE approach.” Mech. Adv. Mater. Struct., 1–20.
3. Patil, R., Joladarashi, S., and Kadoli, R. (2023). “Effect of porosity and viscoelastic boundary conditions on FG sandwich beams in thermal environment: buckling and vibration studies” Struct. (Revision submitted).
4. Patil, R., Joladarashi, S., and Kadoli, R. (2023). “Influence of Al-Al_2O_3 functionally graded back plate on vibration and damping aspects of disc brake pad with brake shim” J. Vib. Eng. Technol. (Revision submitted).

International Conferences

1. Patil, R., Joladarashi, S., and Kadoli, R. (2023). “Finite Element Formulation for Static and Time Dependent Transverse Deflection of Functionally Graded Sandwich Beams with Viscoelastic Core” *In: Manik, G., Kalia, S., Verma, O.P., Sharma, T.K. (eds) Recent Advances in Mechanical Engineering. Lecture Notes in Mechanical Engineering. Springer, Singapore,* 391-400.